Hindawi Publishing Corporation
ISRN Condensed Matter Physics
Volume 2013, Article ID 497073, 43 pages
http://dx.doi.org/10.1155/2013/497073

Review Article

Hexagonal Manganites—($RMnO_3$): Class (I) Multiferroics with Strong Coupling of Magnetism and Ferroelectricity

Bernd Lorenz

Texas Center for Superconductivity and Department of Physics, University of Houston, Houston, TX 77204-5002, USA

Correspondence should be addressed to Bernd Lorenz; blorenz@uh.edu

Received 15 October 2012; Accepted 2 November 2012

Academic Editors: I. Galanakis, M. Higuchi, and V. Kochereshko

Hexagonal manganites belong to an exciting class of materials exhibiting strong interactions between a highly frustrated magnetic system, the ferroelectric polarization, and the lattice. The existence and mutual interaction of different magnetic ions (Mn and rare earth) results in complex magnetic phase diagrams and novel physical phenomena. A summary and discussion of the various properties, underlying physical mechanisms, the role of the rare earth ions, and the complex interactions in multiferroic hexagonal manganites, are presented in this paper.

1. Introduction and Brief History

Since the discovery of the intimate relations between electric and magnetic phenomena by Oersted, Ampère, Faraday, and others, which ultimately led James Clerk Maxwell to formulate the unified theory of electromagnetism, the mutual interaction between magnetic (electric) properties and electric (magnetic) fields has been in the focus of interest for more than a century. Wilhelm Conrad Röntgen discovered in 1888 that a dielectric became magnetized when moving in a uniform electric field [1]. His study was motivated by the following reasoning: when a dielectric sheet, polarized in the external electric field, is moved in the direction perpendicular to the field lines, the motion of negative and positive charges, separated through the induced polarization, becomes equivalent to two electrical currents moving into opposite directions on either side of the sheet. Those currents generate a magnetic field, that is, the dielectric becomes magnetized. The experimental setup to prove the magnetoelectric effect did involve a fast rotating dielectric disc between two horizontal capacitor plates. In the same communication, Röntgen also conjectured that the inverse effect should exist, namely the change of the polarization of a moving dielectric induced by an external magnetic field, which was indeed experimentally shown by Wilson in 1905 [2].

The possibility of a magnetoelectric effect in (nonmoving) materials was later discussed by P. Curie from a symmetry point of view [3]. It took, however, many more years to understand the importance of the violation of time reversal symmetry (either by moving the dielectric, by external magnetic fields, or by magnetic orders) for the magnetoelectric coupling to become effective. The realization of the magnetoelectric effect in the antiferromagnetic phase of Cr_2O_3, predicted by Dzyaloshinskii [4] on symmetry grounds, was experimentally verified through the demonstration that an electric field did induce a magnetization [5–7] as well as the reverse effect, the magnetic field induced electrical polarization [8]. It should be noted that the observed magnetoelectric effect in Cr_2O_3 is linear, that is, the induced magnetization (polarization) increases linearly with the electric (magnetic) field, in agreement with the lowest order of the magnetoelectric part of the thermodynamic potential, derived by Dzyaloshinskii [4]:

$$4\pi\Phi_{\mathrm{me}} = -\alpha_{\parallel}E_zH_z - \alpha_{\perp}\left(E_xH_x + E_yH_y\right). \quad (1)$$

$\alpha_{\parallel}$ and $\alpha_{\perp}$ are the diagonal elements of the linear magnetoelectric tensor α parallel and perpendicular to the z-axis, respectively. In an attempt to search for the microscopic origin of the magnetoelectric effect in Cr_2O_3, Rado linked the

linear magnetoelectric coefficient α to the sublattice magnetization of the antiferromagnetic order and emphasized already on the important role of the spin orbit interaction [9].

In the following years, many more magnetoelectric materials have been discovered. In 1972, Hornreich listed about twenty magnetoelectric materials [10]. A more recent list of compounds showing a linear magnetoelectric effect can be found in the article by Schmid [11]. It should be noted that the linear magnetoelectric coefficient is relatively small because it is limited by the dielectric (χ^e) and magnetic (χ^m) susceptibilities according to the relation [12–14].

$$\alpha_{ij}^2 < \chi_{ii}^e \cdot \chi_{jj}^m. \tag{2}$$

The largest coefficient was found in the antiferromagnetic state of $TbPO_4$ at $T = 1.5$ K, $\alpha_{aa} = 735$ ps/m [11, 15, 16]. This coefficient is about 180 times larger than α_{zz} of Cr_2O_3, however, the field-induced electrical polarization of 58 μC/m^2 measured at a field of 1 kOe [16] (or 585 μC/m^2 if extrapolated to a field of 10 kOe) is relatively small. Furthermore, the linear magnetoelectric effect is often forbidden by symmetry, or it breaks down at larger field values. For example, in $TbPO_4$ the antiferromagnetic order and the magnetoelectric effect are destroyed in fields above 8 kOe [17]. The allowed tensor elements of α_{ij} in different magnetic point groups are listed and discussed in [11, 18].

Under the limitations for the linear magnetoelectric effect discussed above, the higher order coupling terms in the free energy may be important and of interest, particularly at larger magnetic fields. They are derived from the expansion of the free energy density with respect to electric and magnetic fields (in SI units) [19, 20]:

$$\begin{aligned} -g\left(T, \vec{E}, \vec{H}\right) = & -g^0(T) + P_i^s E_i + M_i^s H_i + \frac{1}{2}\varepsilon_0 \varepsilon_{ij} E_i E_j \\ & + \frac{1}{2}\mu_0 \mu_{ij} H_i H_j + \alpha_{ij} E_i H_j + \frac{1}{2}\beta_{ijk} E_i H_j H_k \\ & + \frac{1}{2}\gamma_{ijk} H_i E_j E_k + \cdots. \end{aligned} \tag{3}$$

We use the convention of summation over pairs of equal indices in (3). The first term, g^0, is the free energy in the absence of magnetic or electric fields, the next two terms represent the energy gain due to the interaction of a spontaneous polarization (magnetization) with the electric (magnetic) field, for example, in a ferroelectric (ferromagnetic) state. The following two terms in (3) are due to the interaction of the field-induced polarization (magnetization) with the corresponding electric (magnetic) fields. ε_0 (μ_0) and ε_{ij} (μ_{ij}) are the absolute and relative dielectric permitivities (magnetic permeabilities), respectively. ε_{ij} and μ_{ij} are symmetric second rank tensors. All terms in (3) represent sums over the three respective indices i, j, and k, representing the three spatial directions.

The mixed field terms in line two of (3) start with the linear magnetoelectric energy with the second rank magnetoelectric tensor α_{ij}, followed by the next higher order terms coupling electric and magnetic fields. The third rank tensors β_{ijk} and γ_{ijk} are also called the coefficients of the bilinear (quadratic) magnetoelectric effect [11]. This are the terms that may result in a magnetic field-induced polarization (or an electric field-induced magnetization), even if the linear magnetoelectric effect is forbidden by symmetry ($\alpha_{ij} = 0$). From (3) the magnetic field-induced polarization change in the absence of an electric field can be calculated:

$$\Delta P_i\left(\vec{H}\right) = \alpha_{ij} H_j + \frac{1}{2}\beta_{ijk} H_j H_k. \tag{4}$$

A similar expression is obtained for the change in magnetization due to external electric fields in the absence of a magnetic field:

$$\Delta M_i\left(\vec{E}\right) = \alpha_{ji} E_j + \frac{1}{2}\gamma_{ijk} E_j E_k. \tag{5}$$

Bilinear magnetoelectric effects have indeed been measured in different compounds in the 1960's [21, 22] and the superposition of contributions from both, the linear and the bilinear magnetoelectric effects have been reported for a member of the boracite family of compounds [23] and very recently in the antiferromagnetic state of $LiFeP_2O_7$ [24]. In the boracites, the bilinear magnetoelectric effect turned out to reduce the field-induced polarization from the linear coupling and only moderate values of less than 2 μC/m^2 have been achieved in fields up to 10 kOe. In the search for materials with large magnetoelectric effect, the focus was recently directed toward the rare earth iron borate compounds, $RFe_3(BO_3)_4$ (R: rare earth) (for a review see [25]). Field-induced polarization values of up to 500 μC/m^2 have been reported in $SmFe_3(BO_3)_4$ at 10 kOe [26] and $NdFe_3(BO_3)_4$ [27]. Replacing the transition metal iron by nonmagnetic aluminium, even larger bilinear magnetoelectric effects have been discovered recently in the rare earth aluminum borate, $RAl_3(BO_3)_4$, with polarization values up to 3600 μC/m^2 in $HoAl_3(BO_3)_4$ at the maximum field of 70 kOe [28]. This seems to be the largest magnetic field-induced polarization change reported so far. It was further shown that the polarization in fields up to 10 kOe scaled perfectly with H^2, that is, these compounds exhibit exclusively the bilinear magnetoelectric coupling [29].

The thermodynamic condition (2), limiting the linear magnetoelectric effect, has guided researchers to study materials with large dielectric and magnetic susceptibilities. χ^e and χ^m are large in materials exhibiting ferroic (ferroelectric or ferromagnetic) long range orders, at least near the respective transition temperatures. It has been argued that materials showing ferroelectric and ferromagnetic orders in one and the same phase are rare because the d-electrons of transition metals favoring magnetism are detrimental to the off-center distortions needed to sustain ferroelectricity [30]. However, as early as 1966, Ascher et al. [31] reported the discovery of ferroelectricity arising simultaneously with weak ferromagnetism at 64 K in $Ni_3B_7O_{13}I$. A sizable magnetoelectric effect and the reversal of the polarization in an external magnetic field was also observed in the coexistence region of both ferroic orders. This work was preceded by the report

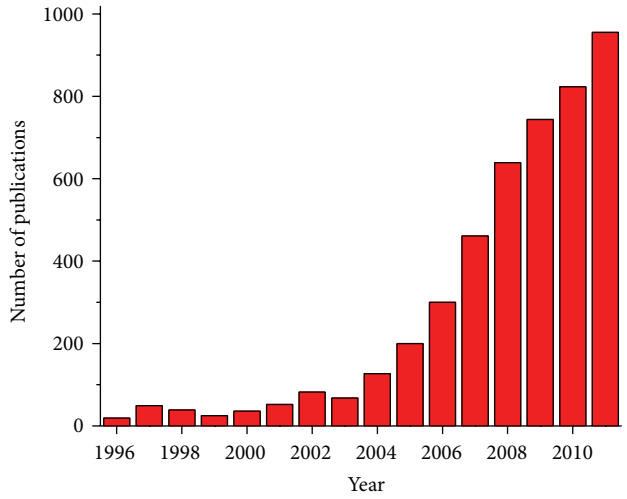

Figure 1: Annual number of publications with "magnetoelectric" or "multiferroic" in their topic (source: Web of Science).

of the coexistence of ferroelectricity and antiferromagnetism in the perovskite $Pb(Fe_{2/3}W_{1/3})O_3$ [32, 33] with significantly different transition temperatures for the two ordered states.

The coexistence and mutual interaction of magnetic (including antiferromagnetic) and ferroelectric orders in matter have attracted increasing attention since then. Many additional materials, originally called ferroelectromagnets, have been studied in the following years, predominantly by groups in the former Soviet Union. An early review by Smolenskii and Chupis (published in 1982, [34]) lists more than 50 compounds showing the coexistence of ferroelectricity and magnetic order in some range of temperature. Among them are more members of the boracite family of compounds, $M_3B_7O_{13}X$ (M = Cr, Mn, Fe, Co, Ni, Cu and X = Cl, Br, I), the hexagonal manganites, $RMnO_3$ (R = Sc, Y, Dy, Ho, Er, Tm, Yb, Lu), compounds with perovskite structure (e.g., $BiFeO_3$), members of the polar $BaMF_4$ (M: transition metal) family, and others.

The term "multiferroic", describing materials in which at least two of three ferroic properties (ferroelectricity, ferromagnetism, or ferroelasticity) occur in the same phase, was introduced by Schmid in 1994 [35]. The definition was later extended to include also antiferroic orders, like antiferromagnetism. A significant number of multiferroic materials known today combine ferroelectricity with antiferromagnetic orders. The continuously increasing interest in the study of multiferroic materials is reflected in the number of scientific papers published annually. Figure 1 shows the annual number of publications with "multiferroic" or "magnetoelectric" in their topic (an extension of a graph originally shown by Manfred Fiebig in a review of the magnetoelectric effect [36]). The graph covers the last 15 years of research, from 1996 to 2011, and it proves the yet growing interest in the field. The number of publications did reach nearly 1000 in 2011 and the tendency is still up. It is also remarkable that a strong increase of research activities is visible past the year 2003, after the magnetic order induced ferroelectric state was discovered in the rare earth manganite $TbMnO_3$ [37].

In general terms, multiferroic compounds can be separated into two classes depending on whether the magnetic order and the ferroelectric state arise independently (and at very different temperatures) or the magnetic order breaks the inversion symmetry and induces a ferroelectric state (due to electronic or ionic displacements). In the first class of multiferroics, the ferroelectricity is usually established at much higher temperature (often above room temperature) and the magnetic order appears at low temperatures. In the second class, the transition into the magnetic and ferroelectric states happen at the same temperature. Examples for class one (I) multiferroics are the rare earth manganites $RMnO_3$ (R: rare earth, Y, Sc) with hexagonal structure [38–41]. While the ferroelectric transition temperature, T_C, is of the order of 900 K [42], the antiferromagnetic order sets in at T_N typically below 100 K. The first signature of a coupling between both orders had been observed in $YMnO_3$ [43]. Another compound family of interest are polar crystals with strongly interacting magnetic ions and a magnetically ordered phase at low-temperature. Although those crystals may not exhibit a ferroelectric phase transition below their melting point, the fact that they crystallize in a structure with a finite lattice polarization makes them an interesting candidate to study the coupling of the magnetic order parameter below T_N with the existing polarization, as shown very recently in $LiFeP_2O_7$ [24].

The second class (II) of multiferroics includes all materials with a magnetically ordered structure that breaks the spatial inversion symmetry and induces simultaneously a ferroelectric state. Different types of magnetic structures which can stabilize a ferroelectric state have been revealed within the last decade of research. Among them are the transverse spin spiral (realized, e.g., in $TbMnO_3$ [37], $Ni_3V_2O_8$ [44], $MnWO_4$ [45–47], $LiCu_2O_2$ [48], $CuFeO_2$ [49], $CoCr_2O_4$ [50], and others), the exchange striction mediated displacement of spins and the associated charges [51] (found in $Ca_3Co_{2-x}Mn_xO_6$ [52] and in the RMn_2O_5 compounds [53, 54]), and the E-type magnetic structures in orthorhombic $RMnO_3$ (R = Ho to Lu) [55, 56]. The origin of the aforementioned inversion symmetry breaking magnetic orders was found in strong frustration of the magnetic system due to geometric constraints or competing magnetic exchange interactions. Therefore, different magnetic orders are close in energy and compete for the ground state. This circumstance explains the extreme sensitivity of class (II) multiferroics with respect to small perturbations in form of external magnetic or electric fields [46, 57–60], physical pressure [61–64], and ionic substitutions [65–69]. This sensitivity is an essential ingredient for the development of prospective applications of multiferroic materials as magnetoelectric sensor or a new type of memory elements. Several good reviews of class (II) multiferroics can be found in a number of recent publications [36, 51, 70–74]. It should also be mentioned that ferroelectricity can be induced by charge order. A recent review was devoted to multiferroics with different types of charge order [75].

In the following sections, we will discuss novel phenomena, complex magnetic and multiferroic phase diagrams, and the effects of magnetic fields on the multiferroic properties of

class (I) multiferroics. The physics of hexagonal manganites, as representatives of class (I) multiferroics, will be reviewed in detail in Section 2 and a brief summary is presented in Section 3.

2. The Hexagonal Manganites: Class (I) Multiferroics

2.1. Structure, Ferroelectricity, and Magnetism. Ferroelectricity in hexagonal manganites $RMnO_3$, with R = Y, Dy, Ho, Er, Tm, Yb, Lu, or Sc, was discovered as early as 1963 by Bertaut et al. [38]. The structure refinement at ambient temperature revealed the crystal structure described by the polar space group $P6_3cm$ (no. 185) with an unusual five- and sevenfold coordination polyhedra about the Mn and R ions, respectively [39]. A sketch of the structure is shown in Figure 2. The origin of ferroelectricity in hexagonal $RMnO_3$ has been a matter of discussion. It should be noted that the manganites do not fulfil the condition of "d^0-ness" which leads to an off center displacement in common perovskite ferroelectrics (like $BaTiO_3$) due to the hybridization of empty transition metal orbitals with the oxygen 2p states and the associated second-order Jahn-Teller effect [76]. They also do not possess a "lone pair" (s^2) set of electrons which may cause the loss of inversion symmetry through a mixing with an excited (s^1)(p^1) state [77] as, for example, realized in $BiMnO_3$ [78]. The lattice distortion in $RMnO_3$ resulting in a noncentrosymmetric and polar structure has to be sought in other physical mechanisms.

Extensive studies of the structure over a large temperature range and the ferroelectric properties have been conducted for $YMnO_3$, some of the results will be discussed in the following. Based on first principle calculations, Van Aken et al. [79] have concluded that the ferroelectricity in $YMnO_3$ is due to electrostatic and size effects. The structural distortion involves mainly the rotation of the MnO_5 bipyramids which displaces the oxygen atoms from their centrosymmetric positions and a displacement of Y atoms along the *c*-axis forming a buckled triangular lattice in the ferroelectric state. The resulting huge Y-O displacements along the *c*-axis create large local electric dipoles which are antiparallel (but of different magnitude) for the two inequivalent yttrium ions of the structure. Therefore, the polar state of $YMnO_3$ (and all hexagonal $RMnO_3$) is ferrielectric.

The centrosymmetric high temperature phase of $YMnO_3$ is stable above $T_S \simeq 1270$ K [80–84]. The space group was determined as $P6_3/mmc$ (no. 195). The transition temperature T_C into the ferroelectric $P6_3cm$ phase was reported to be about 300 K lower and the possible existence of an intermediate phase (space group $P6_3/mcm$) between T_C and T_S was suggested [81, 85]. The symmetry analysis of different modes explaining the possible distortions which lead from the high-temperature $P6_3/mmc$ to the low-temperature $P6_3cm$ structure are discussed for example, in [86]. However, recent neutron scattering experiments have shown that the best refinement below T_S could only be achieved for the $P6_3cm$ space group, indicating a direct transition from $P6_3/mcm$ to $P6_3cm$ with a tripling of the unit cell and no intermediate symmetry phase [84]. Anomalies observed by different authors near 900 K were attributed to an isosymmetric transition within the same space group, $P6_3cm$.

Table 1: Lattice parameters and magnetic ordering temperatures of hexagonal $RMnO_3$.

	a (Å)	c (Å)	T_N (K)	References
$InMnO_3$	5.869	11.47	120	[89]
$ScMnO_3$	5.833	11.17	130	[88, 90]
$YMnO_3$	6.148	11.44	72	[90, 91]
$DyMnO_3$	6.182	11.45	57	[92]
$HoMnO_3$	6.142	11.42	76	[41, 88]
$ErMnO_3$	6.112	11.40	79–81	[41, 88]
$TmMnO_3$	6.092	11.37	84–86	[41, 93]
$YbMnO_3$	6.062	11.36	87–89	[41, 94]
$LuMnO_3$	6.046	11.41	90	[90, 91]

The magnetism in hexagonal $RMnO_3$ and the details of the long range order of Mn spins have been studied in the early 1960's by Bertaut and Mercier [87] and Koehler et al. [88] All hexagonal manganites show antiferromagnetic (AFM) order of the Mn^{3+} spins below their respective Néel temperatures, T_N. Table 1 shows the lattice constants and the Néel temperatures of nine hexagonal $RMnO_3$ (R = In, Sc, Y, Dy to Lu). The AFM transition happens below 100 K (except for $ScMnO_3$ and $InMnO_3$).

The understanding of the magnetic order compatible with the hexagonal symmetry requires a closer inspection of the lattice structure, mainly the sublattice of the magnetic Mn^{3+} ions. Figure 3 shows a projection of the Mn sublattice along the hexagonal *c*-axis. The Mn^{3+} ions form layers of triangular structure stacked along *c*. Two subsequent layers of Mn are distinguished by color in Figure 3. The R ions (not shown in the figure) are located in the open spaces between the Mn layers. The magnetic interactions of the Mn spins are antiferromagnetic (AFM) super exchange interactions. The spins on a triangular lattice with AFM interactions between nearest neighbors are highly frustrated and the corresponding magnetic structure, compatible with the hexagonal symmetry, is characterized by a non collinear spin arrangement where the three spins on a triangle form an angle of 120° with one another.

There are two possibilities to arrange the relative spin orientation between neighboring Mn layers, depending on the relative orientation of the pairs of spins (belonging to two layers) along the edges of the magnetic unit cell (and the pair of two spins in the center): in the α model the spins of a so defined pair are parallel (shown in Figure 3(a)) whereas they are antiparallel in the β model (Figure 3(b)). The angle Φ of the spins with the hexagonal axis determines the details of the magnetic space group. Two preferred values of Φ, 0° and 90°, define the magnetic orders corresponding to the four one-dimensional irreducible representations, Γ_1 to Γ_4, of the little group $G_{\mathbf{k}}$ ($\mathbf{k} = 0$) which is identical to the crystal's space group $P6_3cm$. A complete group theoretical analysis of the little group $G_{\mathbf{k}}$ was presented by Muñoz et al. [95]. Two of the possible magnetic symmetries (assigned to the α and

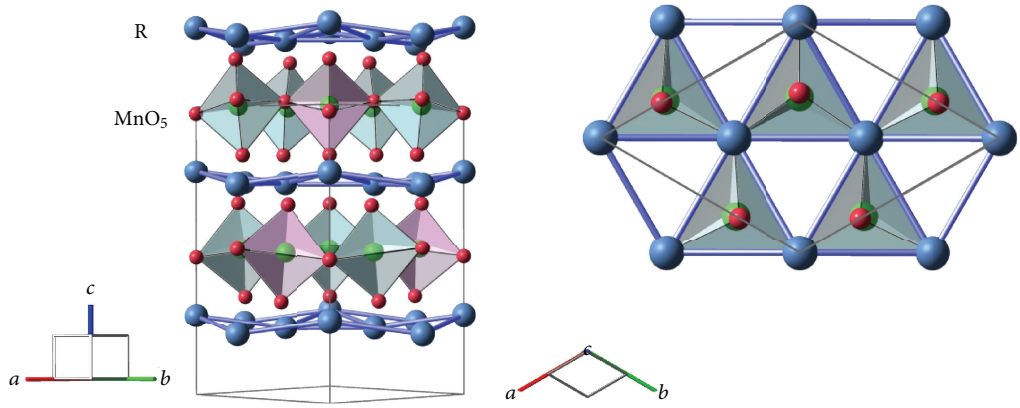

Figure 2: Structure of hexagonal rare earth manganites, $RMnO_3$. (a) View along (110) and (b) view along the c-axis showing only a single layer of MnO_5 trigonal bipyramids. The next layer of MnO_5 fits above or underneath the voids shown in (b).

Table 2: Magnetic symmetries of the Mn^{3+} spins in hexagonal manganites, according to [93, 95].

Irrep.	Model	Angle Φ	Space group	Example
Γ_1	β_2	90°	$P6_3cm$	
Γ_2	β_1	0°	$P6_3\underline{cm}$	
Γ_3	α_1	0°	$P\underline{6}_3\underline{cm}$	$YMnO_3$
Γ_4	α_2	90°	$P\underline{6}_3\underline{cm}$	$ErMnO_3$
$\Gamma_2 \leftrightarrow \Gamma_1$	$\beta_1 \leftrightarrow \beta_2$	$0^\circ < \Phi < 90^\circ$	$P6_3$	
$\Gamma_3 \leftrightarrow \Gamma_4$	$\alpha_1 \leftrightarrow \alpha_2$	$0^\circ < \Phi < 90^\circ$	$P\underline{6}_3$	$LuMnO_3$
$\Gamma_2 \leftrightarrow \Gamma_4$	$\beta_1 \leftrightarrow \alpha_2$	$0^\circ < \Phi < 90^\circ$	$P3\underline{c}$	
$\Gamma_3 \leftrightarrow \Gamma_1$	$\alpha_1 \leftrightarrow \beta_2$	$0^\circ < \Phi < 90^\circ$	$P3c$	

β models) had been considered for $YMnO_3$ by Bertaut and Mercier based on the results of powder neutron scattering experiments [87], however, a definite conclusion of whether the α or β model describes the magnetic order best could not be drawn.

The four magnetic space groups associated with the Γ_1 to Γ_4 irreducible representations are listed in Table 2 and their characteristic spin order is visualized in Figure 4. Besides the one-dimensional representations Γ_1 to Γ_4, there exist two more two-dimensional irreducible representations, Γ_5 and Γ_6, as discussed in [95]. According to the irreducible representations listed in Table 2, the original models proposed for $YMnO_3$ in [87] are described by the Γ_1 (β model) and Γ_3 (α model) representations. Muñoz et al. have conducted extensive powder neutron studies of $YMnO_3$ and concluded that the favored magnetic symmetry is described by the Γ_1 representation (β model, $\Phi = 90^\circ$) [95]. However, more recent powder neutron scattering experiments could not distinguish between the originally suggested Γ_1 and Γ_3 representations [96]. It should also be noted that combinations of different irreducible representations are possible and they describe a magnetic structure with an angle Φ between 0° and 90°. A total of four intermediate ($0^\circ < \Phi < 90^\circ$) magnetic structures can be visualized if the spins on the two sublattices are allowed to rotate by an angle Φ either in the same or in opposite directions, leading to transitions within or between the α and β models. Their magnetic space groups are $P6_3$, $P\underline{6}_3$, $P3\underline{c}$, and $P3c$ [93]. The four intermediate structures, which may be important to understand spin rotation transitions and new phases induced by magnetic fields, are included in Table 2.

The problem with powder neutron scattering experiments in determining complex magnetic orders is the limited resolution in fitting different magnetic structures to the scattering spectra. Therefore, alternative methods, preferentially working with single crystals, need to be used for a precise magnetic structure determination. Due to the non centrosymmetric structure of hexagonal manganites, nonlinear optical methods can be employed [97, 98]. It was shown that the second harmonic generation (SHG) provides a very sensitive probe of magnetic symmetries since the second order susceptibility tensor obeys selection rules that are characteristic for different magnetic structures. This method was first used by Fröhlich et al. to study the magnetic and ferroelectric orders in $YMnO_3$ [99]. Fiebig et al. developed the SHG method further and applied it to the extensive study of the magnetic symmetry of hexagonal manganites [100]. The non-linear susceptibility tensors describing the second harmonic generation experiments have been derived for the hexagonal manganites in [101] and it was shown that they can be used to distinguish different magnetic structures. The results for most of the hexagonal $RMnO_3$ are shown

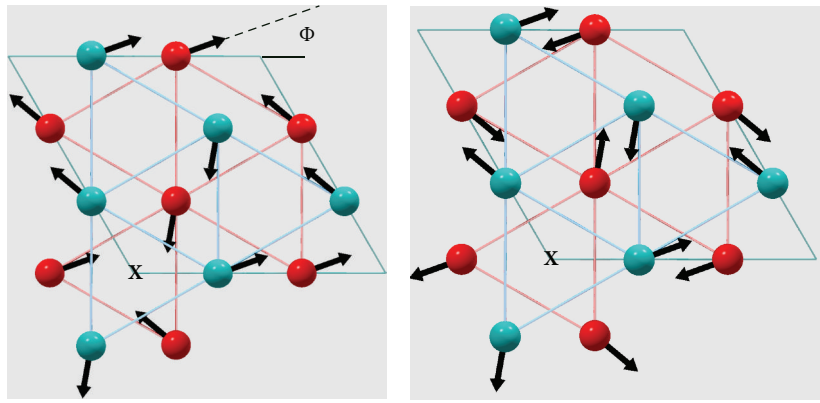

Figure 3: Triangular sublattices of Mn ions of hexagonal $RMnO_3$, viewed along the c-axis. The two subsequent Mn layers in the unit cell are distinguished by blue and red color. The magnetic unit cell is shown (origin at **X**) and the black arrows indicate the Mn spin order in the (a) α model and (b) β model. The angle Φ determines different magnetic symmetries, as discussed in the text.

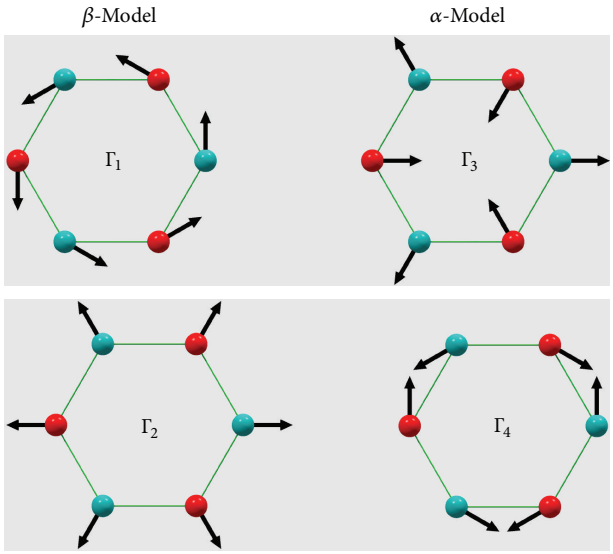

Figure 4: Characteristic spin structures according to the onedimensional irreducible representations of the little group $G_{\mathbf{k}}$ of $\mathbf{k} = 0$. The right and left columns correspond to the α and β models, respectively. The six Mn^{3+} ions shown represent the three ions of each layer around the origin of the magnetic unit cell, marked by "**X**" in Figure 3.

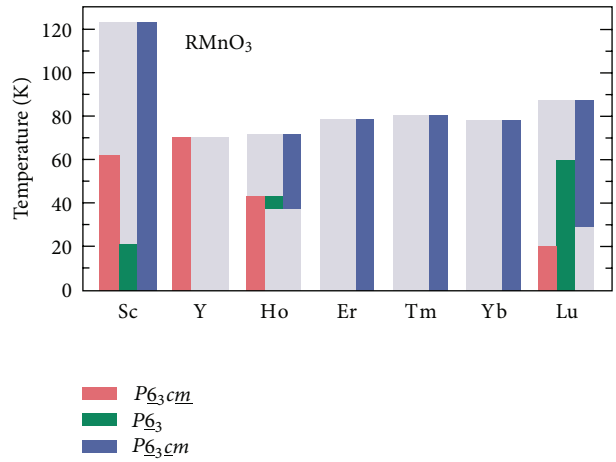

Figure 5: Magnetic symmetries realized in hexagonal $RMnO_3$, R = Sc, Y, Ho, Er, Tm, Yb, Lu. Reprinted with permission from [100].

in Figure 5. The symmetry of the ordered phase of $YMnO_3$ has been uniquely identified as $P\underline{6}_3c\underline{m}$ (Γ_3). It is interesting that $ScMnO_3$ and $LuMnO_3$ appear to show the coexistence of different magnetic symmetries in some temperature range and $HoMnO_3$ experiences a sudden spin rotation from $P\underline{6}_3c\underline{m}$ (Γ_4) to $P\underline{6}_3c\underline{m}$ (Γ_3) upon decreasing temperature (the spins rotate by an angle of 90°). The spin rotation in $HoMnO_3$ was already proposed by Koehler et al. in their early neutron scattering experiments of hexagonal $RMnO_3$ compounds [88].

The above discussion of the magnetic orders in the $RMnO_3$ system focusses only on the Mn^{3+} spins; however, most rare earth ions carry their own magnetic moment oriented along the c-axis due to a strong uniaxial anisotropy. The interaction of the rare earth moments may cause another magnetic phase transition at low temperature involving mainly the rare earth moments with a possible effect on the Mn^{3+} spins. The rare earth moment order was indeed observed in $ErMnO_3$ below 2.5, . . . , 5 K, in $YbMnO_3$ below 4 K, and in $HoMnO_3$ below 5.4 K [41, 94, 102, 103]. The complex phase diagrams of various $RMnO_3$ will be discussed in the following sections.

2.2. Magnetoelectric Coupling and the Complex Phase Diagram of Hexagonal $HoMnO_3$. The coexistence of ferroelectric and magnetic orders below the Néel temperature raises the question of how the two order parameters mutually interact with one another and how different physical properties might be affected by their coupling. Symmetry does not allow for a linear coupling of the AFM order parameter

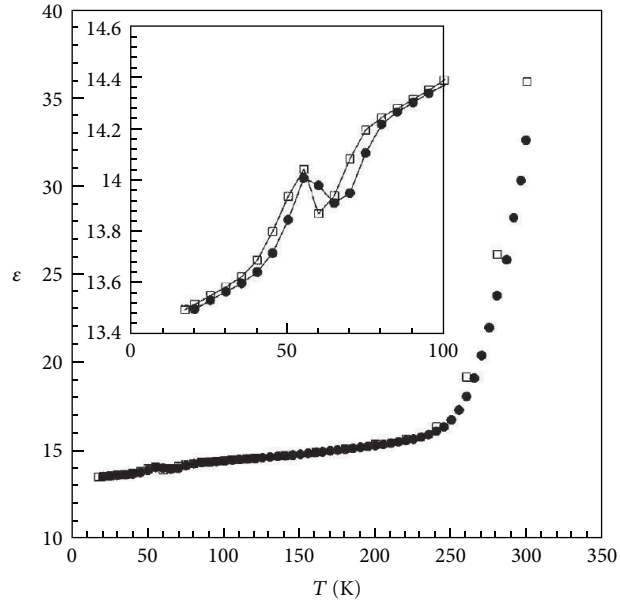

Figure 6: Dielectric anomaly at the magnetic phase transition of $YMnO_3$. Open symbols: $H = 0$ kOe, bold symbols: $H = 50$ kOe. Reprinted with permission from [43].

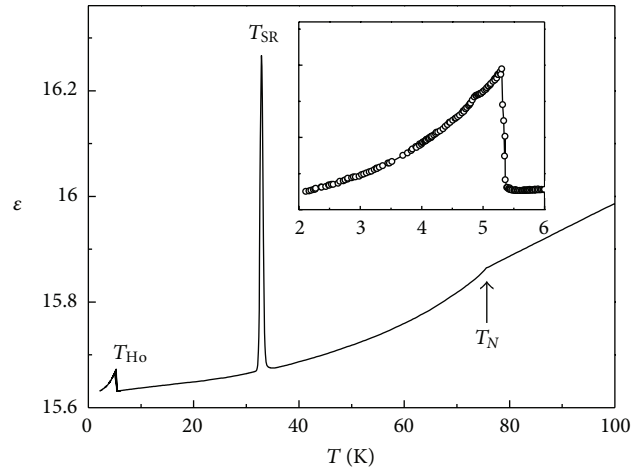

Figure 7: Dielectric anomalies at three magnetic phase transitions of $HoMnO_3$. The inset shows the low-T transition on an enlarged scale.

and the c-axis ferroelectric polarization. However, higher order couplings mediated through the strong spin-lattice interaction may result in sizable anomalies, for example, of dielectric quantities at the magnetic phase transitions.

The first signature of a coupling between the magnetic order and dielectric properties in hexagonal manganites was observed in $YMnO_3$ [43]. A distinct anomaly of the dielectric constant and the loss factor at the Néel temperature provides clear evidence for a strong correlation between magnetic and ferroelectric orders in this class of compounds, as shown in Figure 6. A magnetic field of 5 T caused a small shift of the anomaly to higher temperature which could be an effect of the field on T_N. While the early measurements had been conducted on polycrystalline samples of $YMnO_3$, later studies on single crystals of various $RMnO_3$ have confirmed the existence of a clear, kink-like dielectric anomaly at the magnetic transition temperature [90, 104, 105].

2.2.1. Magnetic Order and Dielectric and Thermodynamic Properties of $HoMnO_3$ in the Absence of Magnetic Fields. The most pronounced anomalies of the dielectric constant at magnetic phase transitions had been reported in hexagonal $HoMnO_3$. Upon decreasing temperature, three distinct and sharp anomalies could be observed at $T_N = 76$ K, $T_{SR} = 32.8$ K, and $T_{Ho} = 5.4$ K (Figure 7). The kink of $\varepsilon(T)$ at T_N is the typical signature of the onset of frustrated magnetic order in the hexagonal manganites. The sharp peak at T_{SR}, however, is unusual and has only be seen this sharp in $HoMnO_3$. The transition at T_{SR} was attributed to the rotation of the Mn^{3+} spins by 90° [88]. With regard to the exact magnetic symmetries above and below T_{SR}, contradicting results have been reported. Muñoz et al. [106] proposed a transition from $P6_3\underline{cm}$ (Γ_2) to $P6_3cm$ (Γ_1) upon decreasing temperature. However, subsequent neutron scattering [103, 107, 108] and optical experiments [109, 110] have shown that the transition at T_{SR} is most likely from $P\underline{6}_3\underline{c}m$ (Γ_4) to $P\underline{6}_3c\underline{m}$ (Γ_3) and the $P6_3cm$ magnetic structure (Γ_1) is only realized after the second transition at T_{Ho} below 5 K. The two magnetic orders of the Mn^{3+} spins above and below T_{SR} are included as Γ_3 and Γ_4 structures, respectively, in Figure 4. A partial magnetic polarization of the Ho^{3+} moments below T_{SR}, with moments aligned antiferromagnetically along the hexagonal c-axis, was detected in neutron [103] and magnetic X-ray scattering experiments [111]. Based on symmetry arguments and a theoretical calculation, the origin of the magnetic coupling between Mn^{3+} and Ho^{3+} and the magnetic polarization of Ho moments below T_{SR} was attributed to a trigonal anisotropy term [112]. The increasing magnetic fluctuations of the subsystem of Ho^{3+} moments upon decreasing temperature and their coupling to the Mn spins may be considered as the possible origin of the Mn^{3+} spin rotation.

Notably, at much lower temperatures, there is a sharp increase of $\varepsilon(T)$ indicating another change in the magnetic structure of the Mn^{3+} and Ho^{3+} moments (see inset in Figure 7). This transition at T_{Ho} was identified as a second 90° Mn spin rotation transition to $P6_3cm$ symmetry (β model, Γ_1 in Figure 4) with a significant increase of both, the Mn- and Ho-sublattice magnetizations [103, 108, 111]. Whereas below T_{SR} the Ho^{3+} moments in both Wyckoff positions occupied by Ho (2a and 4b) show AFM order, the $P6_3cm$ symmetry does not allow magnetic order of the Ho in 2a position. It should be noted that all three phase transitions observed in $HoMnO_3$ are extremely sharp when high quality single crystals are studied. From the dielectric data of Figure 7 the transition widths are all found close to the experimental resolution. The slope change (kink) of $\varepsilon(T)$ at T_N happens within less than 0.7 K, the peak of the dielectric constant at T_{SR} is 0.5 K wide, and the sudden increase of $\varepsilon(T)$ at T_{Ho} has a width of 0.07 K [113, 114]. The sharp dielectric anomalies of $HoMnO_3$ have been confirmed by different research groups [115–120].

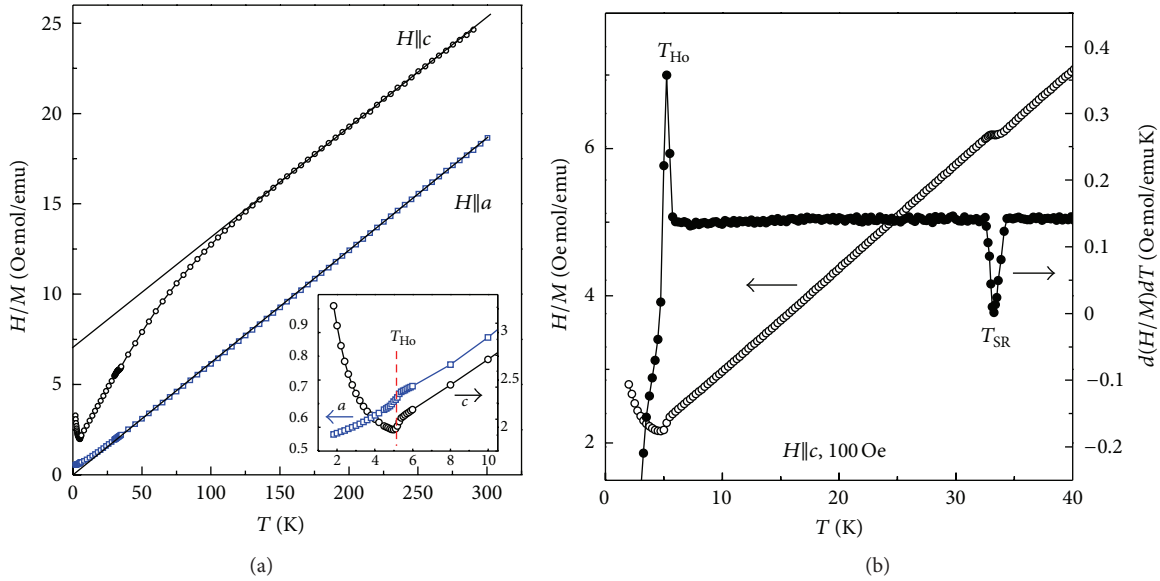

FIGURE 8: (a) Inverse magnetization of $HoMnO_3$. The anomalies at T_{Ho}, shown in the inset, are clearly detected in the low-temperature range. (b) The derivative of χ_c^{-1} shows the sharp transitions at $T_{SR} = 32.8$ K and $T_{Ho} = 5.2$ K, respectively.

The three magnetic transitions in $HoMnO_3$ are also reflected in sharp anomalies of other physical quantities [121]. The magnetization in the hexagonal plane and along the c-axis is shown in Figure 8. The magnetization is moderately anisotropic with the in-plane magnetization slightly larger than the c-axis values. Similar data have been obtained by [122]. The Curie-Weiss fit to the high temperature part of χ^{-1} yields an effective magnetic moment of 11.43 μ_B which is in reasonably good agreement with the value of 12.14 μ_B which is expected for the sum of the free ion values of Mn^{3+} (5.92 μ_B) and Ho^{3+} (10.6 μ_B). The deviation of χ_c^{-1} from the Curie-Weiss line sets in below 130 K indicating the onset of magnetic fluctuations and short range correlations between the Mn-spins. The Néel transition at 76 K is barely detectable in the magnetization data since the large Ho moment dominates the magnetic response. However, a clear magnetization drop at T_{SR} indicates the Mn spin rotation transition and the onset of AFM Ho moment order with orientation along the c-axis. At T_{Ho}, the magnetization shows a sudden increase followed by a continuous decrease toward lower temperatures due to the increasing Ho moment order.

All transitions are also accompanied by distinct anomalies of the heat capacity, as shown in Figure 9 [121]. The three sharp anomalies in $C_p(T)$ have been verified by different groups [117, 119, 123–125]. Near the Néel temperature, $C_p(T)$ exhibits a λ-shaped peak characteristic for a second order phase transition. The critical magnetic fluctuations at T_N have been studied recently [126] and the critical exponents were found close to those of the three dimensional Heisenberg universality class. The critical scaling properties prove the second order nature of the transition.

The spin rotation at T_{SR} is revealed by a small, but sharp peak of $C_p(T)$ (lower inset in Figure 9). The narrow peak suggests that this transition is first order in nature.

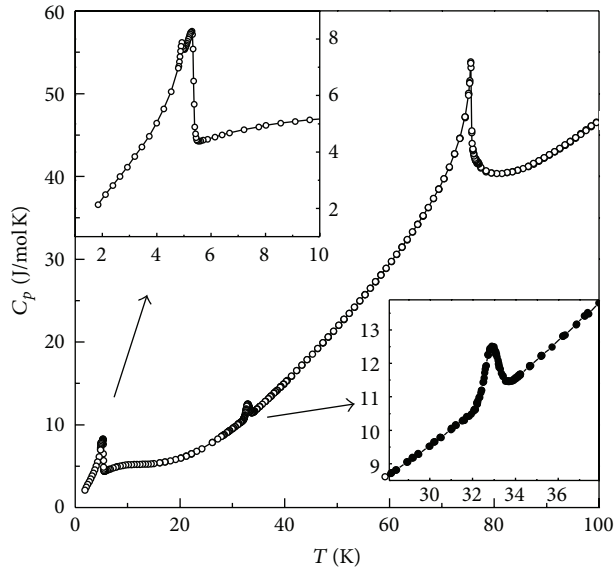

FIGURE 9: Heat capacity of $HoMnO_3$. The anomalies at T_{SR} and T_{Ho} are shown in the lower and upper insets, respectively, on an enlarged scale.

The entropy change across the spin rotation transition, as estimated from the integral over the peak area, is relatively small, $\Delta S = 0.04$ J/(mol K). A careful entropy analysis showed that the value of ΔS is consistent with the changes of volume and magnetization across the transition and the Clausius-Clapeyron equation, valid at first order transitions, is fulfilled [127]. It appears conceivable that the rotation of the Mn-spin system by 90° does not contribute significantly to the entropy

change at T_{SR} but the onset of AFM Ho^{3+} moment order is the main cause of ΔS.

At the second spin rotation transition temperature, T_{Ho}, the specific heat shows a sharp increase followed by a decrease towards lower temperatures. A closer inspection reveals a two-peak structure of C_p at this transition (upper inset in Figure 9) which could indicate that the Mn^{3+} spin rotation and the low-temperature order of the Ho^{3+} moments happen at slightly different temperatures. It should be noted that the two transitions near 5.3 K and 4.9 K, respectively, are also resolved in the dielectric constant data (a small kink is clearly visible in the inset of Figure 7) and in the c-axis magnetization (χ_c increases sharply at 5.3 K and drops suddenly at 4.9 K). In magnetic fields (see below), both anomalies actually split apart and define different phases in the phase diagram.

The sharp anomalies of the dielectric constant (Figure 7) at all three magnetic phase transitions reveal a sizable magnetoelectric effect mediated by strong interaction of the magnetic moments with the lattice. The experimental evidence for strong spin-lattice coupling was first found in distinct anomalies of the thermal expansion coefficients [127]. The hexagonal a-axis shrinks with decreasing temperature and exhibits a clear anomaly at the onset temperature of magnetic order, T_N. In contrast, the c-axis expands and shows a similar anomaly at T_N, but with opposite sign. The strong 2D spin fluctuations in the frustrated magnetic system of Mn^{3+} spins on the triangular lattice are responsible for the anisotropic response of the lattice. The gain of magnetic exchange energy apparently causes the in-plane contraction, particularly near T_N, and the expansion of the c-axis is mediated through the elastic forces of the lattice. The thermal expansivities, $\alpha_i(T) = d \ln L/dT$, are shown in the inset of Figure 10. The λ-type anomalies of α_a and α_c reflect the second order nature of the Néel transition in agreement with the specific heat anomaly (Figure 9). It is worth noting that the spin rotation transition at T_{SR} is also accompanied by a sudden change of the lattice constants, as shown by the sharp peaks of α_a and α_c (lower inset in Figure 10). The thermal expansion measurements and the observed anomalies at the magnetic transitions provide unambiguous evidence for extraordinarily strong spin-lattice interaction in the hexagonal rare earth manganites.

Further signatures for the strong coupling of the magnetic order to the lattice or phonons was derived from Raman experiments showing an enhancement of the phonon frequencies of two modes, which modulate the Mn-Mn interaction, below the Néel temperature of $HoMnO_3$ [128]. A similar phonon enhancement had also been reported for hexagonal $LuMnO_3$ near T_N [129]. The thermal conductivity of $HoMnO_3$ and other hexagonal $RMnO_3$ is suppressed in the paramagnetic state, but it experiences a sudden increase with the onset of magnetic ordering, suggestive of a strong dynamic coupling between acoustic phonons and low-energy spin fluctuations [115]. High resolution neutron scattering experiments have revealed the atomic displacements of the Mn^{3+} ions in passing from the paramagnetic to different magnetically ordered states and their effect on the spin wave excitations [130]. The local structure and the Mn-Mn, Mn-Ho, and the Mn-O bond distances have been studied through

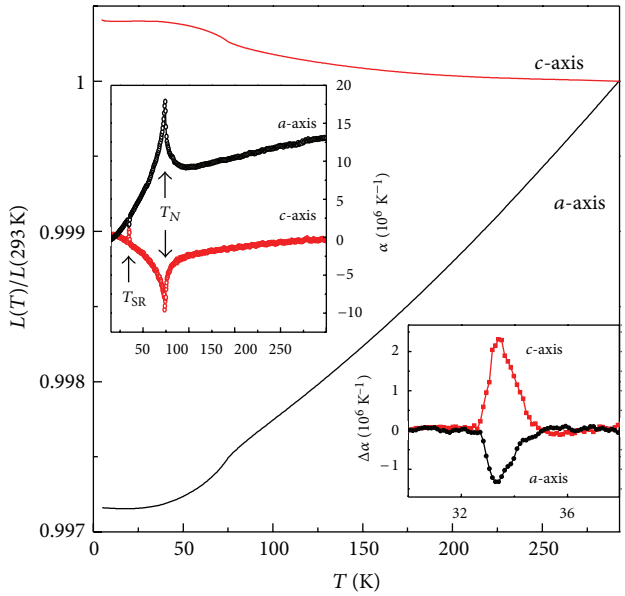

FIGURE 10: Thermal expansion parameters of $HoMnO_3$. The relative length changes of the hexagonal a- and c-axes are shown in the main panel. The upper inset displays the thermal expansivities $\alpha(T)$ and the lower inset shows the change of $\alpha(T)$ at the first spin rotation transition.

X-ray absorption spectroscopy [131]. The results show that different displacements of ion pairs happen at the three magnetic phase transaitions of $HoMnO_3$. The structural distortion at T_N is dominated by the change of in-plane distances between Mn ions, the first spin rotation transition causes a change of Mn-Mn and nearest neighbor Mn-Ho distances, and the low-temperature transition involves a structural distortion of all ions, including Ho-Ho pairs. The enhanced magnetoelastic effects in $HoMnO_3$ have finally be studied with ultrasonic techniques [132]. The sudden change of the elastic moduli at T_N and T_{SR} are further indications for the importance of the spin-lattice coupling in hexagonal manganites.

The structural changes at the magnetic transitions of $HoMnO_3$ and the distinct dielectric anomalies observed raise the question about the response of the ferroelectric polarization to the magnetic order. It is conceivable to expect significant changes of $P_c(T)$, the c-axis polarization, due to the strong coupling of the magnetic system to the lattice. The polarization changes below 100 K have recently been investigated through pyroelectric measurements [120]. Figure 11 shows $\Delta P_c(T) = P_c(T) - P_c(100\,\mathrm{K})$ as function of temperature. At T_N, a minute kink of $P_c(T)$ indicates the entrance into the magnetically ordered phase. The sharp drop near T_{SR} and the increase of $P_c(T)$ at T_{Ho} correlate well with the anomalies of the dielectric constant (as shown in Figure 7).

2.2.2. The Magnetic Phase Diagram of $HoMnO_3$: Dielectric Measurements. Based on second harmonic generation optical experiments, Fiebig et al. have proposed a complex field-temperature phase diagram for $HoMnO_3$ [93, 109]. With

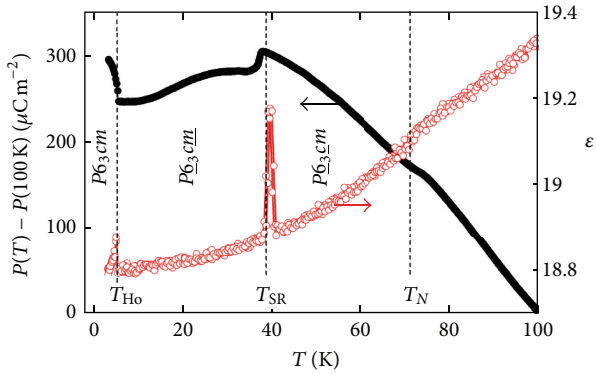

FIGURE 11: Change of ferroelectric polarization of $HoMnO_3$ below 100 K. The anomalies at T_N, T_{SR}, and T_{Ho} are consistent with sharp anomalies of the dielectric constant and other quantities. Reprinted with permission from [120].

the external field oriented along the c-axis, four different magnetic structures according to the 1D irreducible representations (Γ_1 to Γ_4, Table 2) had been proposed. Besides the three phases at zero field, a high-field phase of $P6_3\underline{cm}$ symmetry was detected, stable above 20 kOe and below 10 K.

The sharp anomalies shown in the dielectric constant at all magnetic transitions, which are strongly correlated with the magnetic and thermodynamic anomalies, and the high sensitivity of state of the art capacitance meters makes the dielectric constant an extremely sensitive probe of phase transitions in the $RMnO_3$ compound system. Therefore, the dielectric measurements shown in Figure 7 (at zero magnetic field) have been extended to study the complete magnetic phase diagram of $HoMnO_3$ in external fields along the hexagonal c-axis [113, 114]. It turns out that the magnetic phase diagram is far more complex than originally suggested [109].

The signature of the spin rotation (T_{SR}) and the low temperature (T_{Ho}) transitions are sharp peaks of the dielectric constant at zero field (Figure 7). With applied c-axis magnetic field, the peak at T_{SR} broadens into a plateau-like structure while moving to lower temperatures. At the same time, the sharp increase of $\varepsilon(T)$ at T_{Ho} moves higher in T, forms a second plateau which finally merges with the high-temperature plateau at about 34 kOe. Between 34 kOe and 40 kOe only one plateau-like enhancement of $\varepsilon(T)$, centered at about 18 K, exists. Above 40 kOe, no anomaly of the dielectric constant exists between 6 K and T_N. This is shown in detail in Figure 12(a). Additional anomalies like sharp steps and peaks of $\varepsilon(T)$ at very low temperatures will be discussed separately below.

The data shown in Figure 12(a) suggest that the plateau-like enhancements of $\varepsilon(T)$, evolving with magnetic fields from T_{SR} and T_{Ho}, are the signature of one and the same phase. The phase diagram, constructed from the rapid increase/ decrease of $\varepsilon(T)$ at the edges of the high- and low-temperature plateaus, is shown in Figure 13 (note that the low-temperature part of the phase diagram will be discussed later). In contrast to earlier studies [109], the transition between the $P\underline{6_3}cm$ to $P\underline{6_3}c\underline{m}$ magnetic structures in higher magnetic fields is not instantaneous (as in zero field), but it passes through a well defined intermediate phase, characterized by an enhanced dielectric constant. The magnetic symmetry group of this phase is most likely $P\underline{6_3}$, that is, the angle Φ of the Mn^{3+} spins with the a-axis is intermediate between 0° ($P\underline{6_3}c\underline{m}$) and 90° ($P\underline{6_3}\underline{c}m$). The two transition temperatures are tentatively labeled T_1 ($P\underline{6_3}\underline{c}m \leftrightarrow P\underline{6_3}$) and T_2 ($P\underline{6_3} \leftrightarrow P\underline{6_3}c\underline{m}$). The plateau-like enhancement of ε in the $P\underline{6_3}$ phase is further confirmed by isothermal $\varepsilon(H_c)$ measurements shown in Figure 12(b).

It appears conceivable that Φ is continuously changing between the to limiting values and that it has a well defined value at any given temperature and field. This makes the intermediate phase a true thermodynamic phase, in contrast to a possible coexistence of the bordering $P\underline{6_3}c\underline{m}$ and $P\underline{6_3}\underline{c}m$ magnetic phases. However, since the low-frequency dielectric measurements could be sensitive to domain boundaries, possibly formed by a coexistence of the two major magnetic structures ($P\underline{6_3}\underline{c}m$ and $P\underline{6_3}c\underline{m}$), further evidence is needed to prove the existence of a new $P\underline{6_3}$ phase. The increased value of the dielectric susceptibility in the $P\underline{6_3}$ phase could be an expression of the softness of the magnetic system and the strong coupling to the lattice, as discussed below. An alternative explanation of the plateau like increase of $\varepsilon(T, H)$ was given by Lottermoser and Fiebig [133]. In a careful study of the magnetic domain structure in the $P\underline{6_3}$ phase it was concluded that domain walls separating two magnetic domains with spin rotation angles of Φ and $-\Phi$, respectively, may result in a lowering of the local symmetry within the domain walls and a magnetoelectric effect which modifies (enhances) the dielectric function. The strong coupling between magnetic and ferroelectric domain walls was also proposed from the study of local magnetism and magnetoelectricity by muon-spin relaxation measurements [134].

The magnetic susceptibility is another bulk property and its changes in the different magnetic phases of $HoMnO_3$ are discussed in the following. The c-axis magnetic susceptibility was measured at different magnetic fields between 100 Oe and 45 kOe. The low-field data of the inverse susceptibility shown in Figure 8(b) indicate that $1/\chi_c(T)$ is strictly linear between T_{Ho} and T_N with a kink-like anomaly at T_{SR}. The derivative $d(H/M)/dT$ suits best to visualize the changes of the inverse magnetization in the intermediate $P\underline{6_3}$ phase. The $d(H/M)/dT$ data at different fields are shown in Figure 14 (note that data in Figure 14(a) are vertically offset for better clarity). It is obvious that the derivative plotted in Figure 14 clearly deviates from the constant in the $P\underline{6_3}$ phase. This deviation is negative above 20 K and positive below.

According to the phase diagram (Figure 13), at 33 kOe the sequence of phases upon decreasing temperature is $P\underline{6_3}\underline{c}m \rightarrow P\underline{6_3} \rightarrow P\underline{6_3}c\underline{m} \rightarrow P\underline{6_3} \rightarrow P\underline{6_3}\underline{c}m$, that is, the system passes twice through the intermediate $P\underline{6_3}$ phase. The corresponding transitions and critical temperatures T_1 and T_2 are indicated in Figure 14(a). At slightly higher fields, 35 kOe and 38 kOe, the magnetic system does not pass into the $P\underline{6_3}c\underline{m}$ phase and the sequence is $P\underline{6_3}\underline{c}m \rightarrow P\underline{6_3} \rightarrow P\underline{6_3}\underline{c}m$, as indicated by the continuous and linear increase of $d(H/M)/dT$ between the two phase transitions. Above 40 kOe no transition could

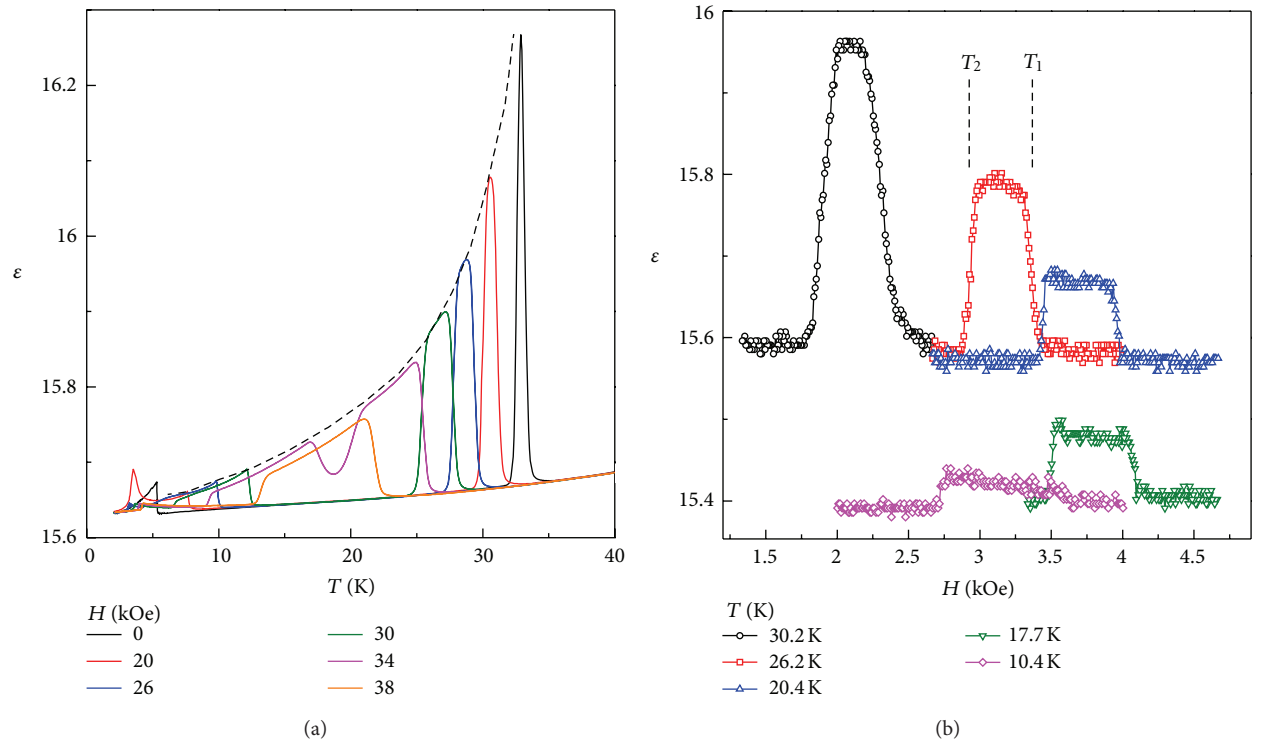

FIGURE 12: (a) Temperature dependence of the dielectric constant $\varepsilon(T)$ of $HoMnO_3$ at different magnetic fields oriented along the c-axis. The dashed line represents the increase of $\varepsilon(T)$ in the intermediate $P\underline{6}_3$ phase. (b) Field dependence of ε at selected temperatures. The two sets of data are vertically offset for better clarity. The two transition temperatures labeled T_1 and T_2 are shown for the 26 K data.

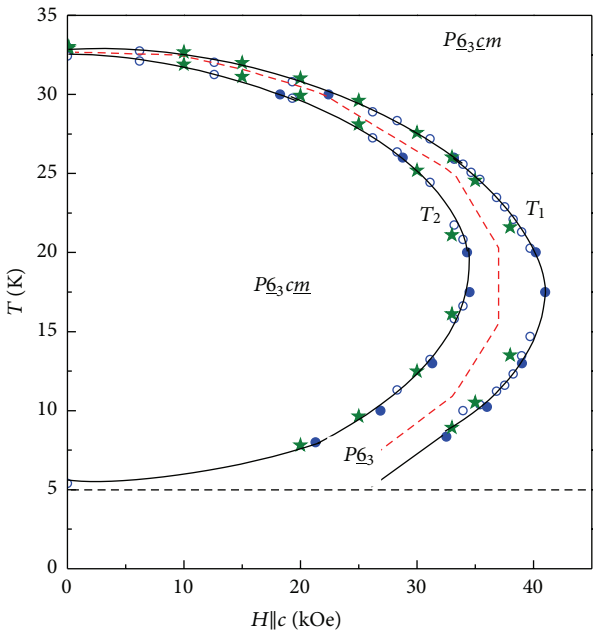

FIGURE 13: Magnetic phase diagram of $HoMnO_3$ between T_{SR} and T_{Ho}. Blue open and solid circles are phase boundaries derived from $\varepsilon(T)$ and $\varepsilon(H)$ scans, respectively. Solid stars are derived from anomalies of the c-axis magnetization. The red dashed line is the phase boundary from [109]. The low-temperature ($T < 5$ K) section of the phase diagram will be discussed separately.

be observed above 5 K, in agreement with the phase diagram of Figure 13.

If all data of Figure 14(a) are plotted without any offset on the same scale (Figure 14(b)), it becomes obvious that the values of $d(H/M)/dT$ within the $P\underline{6}_3$ phase are well defined and follow the dashed line in Figure 14(b). This can be considered as further evidence that the intermediate phase is not a mixture of coexisting $P\underline{6}_3cm$ and $P\underline{6}_3c\underline{m}$ phases, but instead it is a uniform phase determined by the spin angle Φ in the $P\underline{6}_3$ magnetic structure. It should also be noted that no signature of a large temperature or field hysteresis had been observed at T_1 or T_2 in all measurements, although small hysteretic effects cannot be completely excluded.

At $H_c \rightarrow 0$, the two phase boundaries with transition temperatures T_1 and T_2 merge into a single transition at T_{SR}. The temperature range of stability of the $P\underline{6}_3$ phase shrinks to zero and the transition at T_{SR} ($H_c = 0$) is characterized by an instantaneous rotation of the Mn^{3+} spins by 90° from the $P\underline{6}_3cm$ to the $P\underline{6}_3c\underline{m}$ magnetic structure. It is interesting, that the dielectric constant of the $P\underline{6}_3$ phase (the envelop to the plateaus of $\varepsilon(T)$, as shown by the dashed line in Figure 12(a)) appears to diverge in approaching the critical point $H_c \rightarrow 0$, $T \rightarrow T_{SR}$.

On the low temperature side, $T < 6$ K, the phase diagram of $HoMnO_3$ exhibits an unprecedented complexity [114]. Starting from a detailed analysis of the temperature and field dependence of the dielectric constant, a series of distinct anomalies define the extension of the phase boundaries at T_1

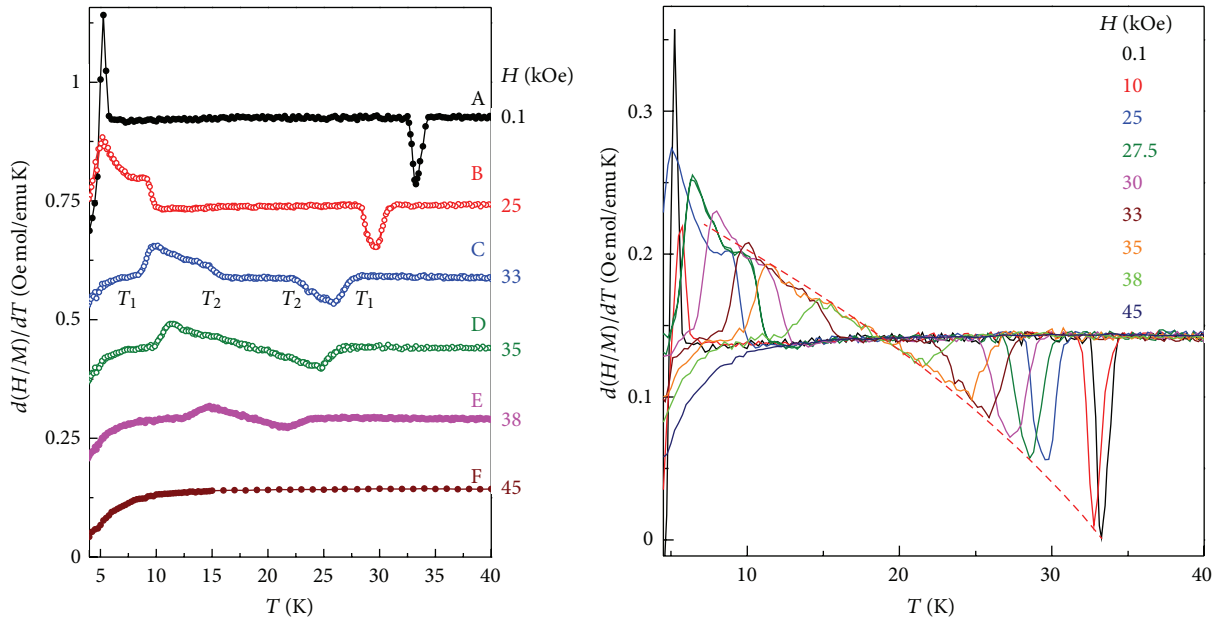

FIGURE 14: Derivative of the inverse magnetic susceptibility, $d(H/M)/dT$, of $HoMnO_3$ at different high magnetic fields. In (a) different curves are vertically offset for better clarity. In (b) all data are shown at the same scale. The dashed line indicates the T-dependence of the derivative in the intermediate $P6_3$ phase.

and T_2, as well as new phase transitions. The low temperature data of $\varepsilon(T, H_c)$ are summarized in Figure 15. The two phase boundaries separating the three high temperature phases, T_1 and T_2, can be traced to lower temperature. The inner phase boundary of the $P6_3$ phase, T_2, is characterized by a sharp increase of $\varepsilon(T)$, as indicated in Figures 15(a), 15(b), and 15(c). It can be traced to the zero field T_{Ho}, as discussed above. The outer phase boundary of the $P6_3$ phase T_1, however, decreases to zero near a critical field of about 20 kOe, as shown in Figure 15(c). The derived phase diagram below 9 K is shown in Figure 16. Additional sharp anomalies of $\varepsilon(T, H)$ are labeled T_3 to T_5. At about 6 kOe, the dielectric constant develops a sharp step (Figure 15(a)) at low temperature (denoted T_3). T_3 increases first up to 3.3 K with increasing H_c and decreases again to zero at 20 kOe. The corresponding phase boundary is shown by the red squares in Figure 16. Above 20 kOe, another step-like increase of $\varepsilon(T)$ develops at T_4 from low temperatures. With increasing field, T_4 rises to 4.5 K and drops to zero at about 80 kOe, as shown in Figures 15(c) and 15(d). This phase boundary is included in Figure 16 as blue triangles. At 12 kOe, another anomaly of $\varepsilon(T)$ splits off from the step at T_2 (c.f. 12 kOe data in Figure 15(b)). This anomaly, labeled T_5 in Figures 15 and 16, shifts to lower temperature and merges with the T_3 phase boundary, as shown by the pink squares in the phase diagram of Figure 16.

The assignment of the different magnetic structures was made based on the results from second harmonic generation optical experiments [93, 109, 110] and neutron scattering measurements [103, 106, 108, 130]. The phase boundary T_5 apparently separates the low-field $P6_3cm$ phase from the high-field $P6_3$ phase. It should be noted that a significant thermal hysteresis is observed in crossing T_5 (see Figure 15(b)) which shows the strong first order character of this transition. In addition to the sharp phase boundaries T_1 to T_5, other subtle anomalies of $\varepsilon(T, H)$ are observed and indicated by $\tilde{T}_1$ and $\tilde{T}_2$ in Figure 15. Of particular interest is the sharp peak of ε developing at T_1 below 5 K and 22 kOe, with a maximum height near 2.8 K and 19 kOe. It is remarkable that this low-temperature peak of ε appears near a point in the phase diagram where three phase boundaries, T_1, T_3, and T_4, come very close and, possibly, form a multicritical point. The ε-peak indicates a softness of the dielectric system in approaching the critical point. The magnetic structures of the two low-temperature phases labeled LT1 and LT2 in Figure 16 have yet to be explored.

The multitude of phase boundaries as revealed by the temperature dependent dielectric measurements at low temperatures is shown in more detail in isothermal measurements of $\varepsilon(H_c)$ as a function of field in Figure 17. At 9 K (Figure 17(a)), a sharp increase followed by a drop of $\varepsilon(H)$ defines the range of the $P6_3$ phase, that is, T_2 and T_1. T_2 can be traced to lower temperature until it ends at $H_c = 0$ as T_{Ho} defined in the zero field measurements (Figure 7). At about 7 K, a peak of $\varepsilon(H)$ develops at $\tilde{T}_1$ and it sharpens significantly to lower temperatures. This peak and $\tilde{T}_1$ can be traced to 2.6 K when it meets the T_3 phase boundary of the LT1 phase (Figures 17(a), 17(b), and 17(c)).

The phase boundary between the $P6_3cm$ and $P6_3$ phases, T_5, splits off from T_2 between 5.5 and 6 K. It's characteristics is a small step and a sizable field hysteresis, as shown in

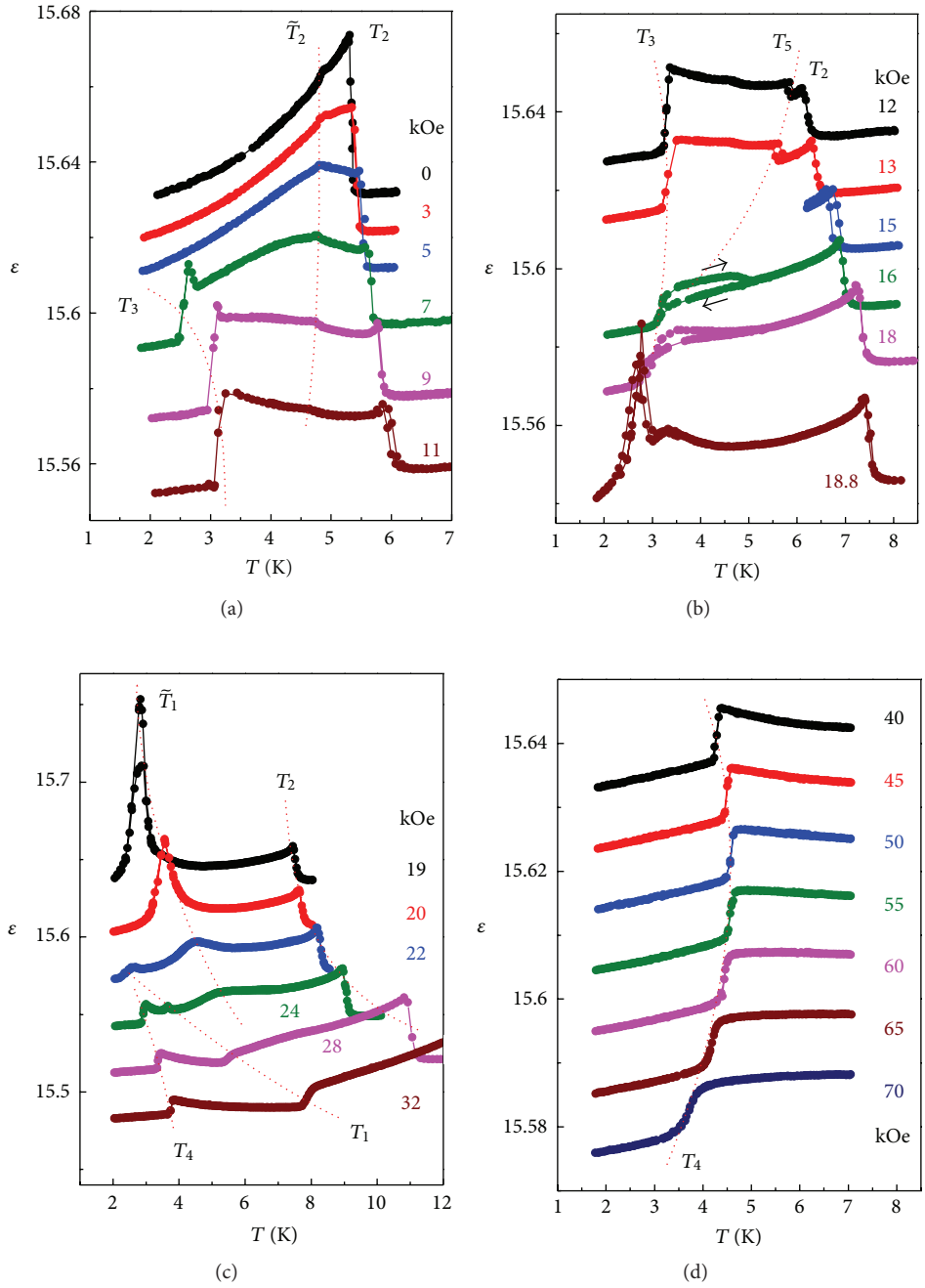

FIGURE 15: Dielectric constant $\varepsilon(T, H_c)$ of $HoMnO_3$. Four different field ranges are shown in (a) to (d). Different curves are vertically offset for better clarity. Anomalies of ε indicating phase boundaries are highlighted by dotted lines and labeled with temperature symbols $T_1, \ldots, T_5$.

Figure 17(a) (5.5 K data). The decrease of T_5 towards the T_3 boundary of the LT1 dome is demonstrated in Figure 17(b). Several phase boundaries merge smoothly in the phase diagram of Figure 16. Those deserve a more careful study. T_1 and T_4 approach one another upon decreasing temperature (Figure 17(b)) and they finally merge at about 2 K (Figure 17(c)). The T_4 phase boundary defines the second low-temperature phase, LT2. The LT2 phase emerges below 4.7 K and it is characterized by another valley of $\varepsilon(H)$ (shown in Figures 17(d) and 17(f)), similar to the LT1 phase. The two low-temperature phases, LT1 and LT2, appear to share one phase boundary at very low temperature. As shown in Figure 17(e), the two corresponding phase boundaries T_3 and T_4 merge at 1.4 K. The dielectric data at 1.4 K (Figures 17(e) and 17(f)) reveal a direct transition from LT1 to LT2 without any signature of an intermediate phase with enhanced ε. The step of $\varepsilon(H)$ at 1.4 K and 76 kOe (Figure 17(f)) designates the approximate upper field limit of the LT2 phase. No

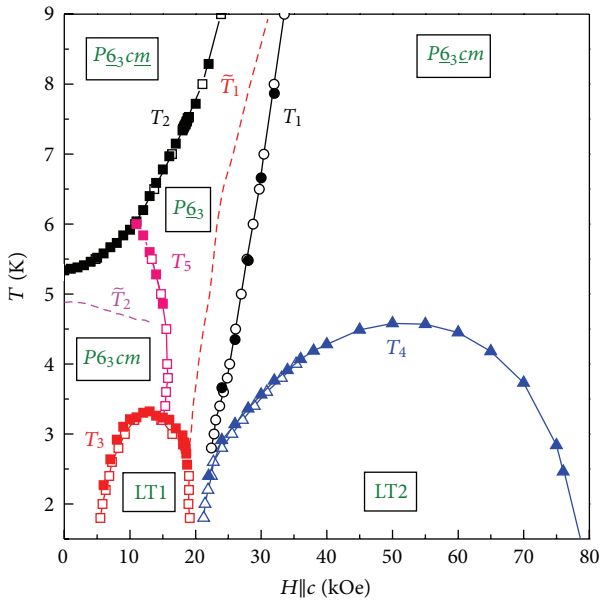

FIGURE 16: Low temperature phase diagram of $HoMnO_3$. Phase boundaries T_1 to T_5 are derived from distinct anomalies of the dielectric constant, the magnetic susceptibility, the specific heat, and magnetostriction data. The dashed lines labeled $\tilde{T}_1$ and $\tilde{T}_2$ denote the location of the peak of the dielectric and magnetic susceptibilities and the weak anomaly of the dielectric constant, respectively.

further phase transition could be detected above 80 kOe, as demonstrated by the ε-data shown in Figure 17(e) up to 130 kOe.

2.2.3. Magnetic Properties and Heat Capacity in the Phase Diagram of $HoMnO_3$. The subtle anomalies of the dielectric constant have to be related to corresponding changes of the magnetic order and should be reflected also in anomalies of the magnetic properties of $HoMnO_3$. This is best verified by measuring the ac magnetic susceptibility as function of a dc bias field along the hexagonal c-axis. Figure 18 shows the results in two different temperature ranges, $25\,\mathrm{K} \leq T \leq 5.7\,\mathrm{K}$ (a) and $5\,\mathrm{K} \leq T \leq 1.8\,\mathrm{K}$ (b). In the high-temperature range (Figure 18(a)), the real part $\chi'_{ac}(H_c)$ shows a significant enhancement in the stability range of the $P6_3$ intermediate phase. This increased susceptibility indicates a softness of the magnetic system with respect to the external field. The softness results from the fact that the angle Φ of the Mn^{3+} spins is not locked in at 0° or 90° as in the $P6_3cm$ and $P6_3cm$ phases, respectively. The two boundary angles apparently increase the stiffness of the magnetic system resulting in a reduced susceptibility with respect to the external magnetic field. The dielectric constant is also enhanced in the $P6_3$ phase due to the strong spin-lattice interaction, as shown in Figure 12(b). The change of the ferroelectric polarization $P_c(H)$ was measured by Hur et al. [120] and they found a sizable increase of P_c in the $P6_3$ phase with increasing H_c.

In the low-temperature region (Figure 18(b)), several peaks and anomalies of $\chi'_{ac}(H)$ can be distinguished. The sharp drop at the high-field end corresponds to the T_1 phase boundary. On the low-field side, for temperatures below 3.2 K, a sharp peak of χ'_{ac} develops between 5 and 10 kOe. This peak coincides with the sharp drop of the dielectric constant (Figure 17(c)) and determines the T_3 phase boundary between the $P6_3cm$ and the LT1 phases. Most remarkably, a broad maximum of χ'_{ac} below 5 K becomes a sharp peak near 3 K and 20 kOe before it is cut off by the entrance into the LT3 phase by crossing the T_3 phase boundary. The sharp peak of χ'_{ac} in this temperature-field range and the equivalent peak of the dielectric constant (Figures 17(b) and 17(c), marked as $\tilde{T}_1$ in the phase diagram of Figure 16) may suggest that the magnetic system is heading towards an instability at zero temperature. The increase of the peak maximum of both, the magnetic (χ'_{ac}) and dielectric (ε) susceptibilities are shown in Figure 19. The singular increase is interrupted by the T_3 phase boundary, indicated by the vertical dotted line. One may speculate about the possible existence of a quantum critical point which is hidden in the emerging LT1 phase. The linear extrapolation of the peak position to zero temperature would locate this critical point near $H_c \simeq 15$ kOe.

The complex phase diagram of Figure 16 was quantitatively confirmed by other groups reporting the results of a microwave study of $HoMnO_3$ single crystals [135] and an investigation of the magnetoelastic coupling through the temperature and field dependence of elastic moduli [132]. Neutron scattering experiments have revealed characteristic changes of the peak intensities measured along different scattering geometries [108, 136]. While the observed anomalies are consistent with the phase boundaries drawn in Figure 16, the results of the neutron study had been interpreted differently in the low-temperature section ($T < 5$ K) of the phase diagram. Vajk et al. [108] derived from their data an extension of the T_5 phase boundary into the dome-shaped LT1 phase and the corresponding phase diagram is shown in Figure 20. The major difference are the phase boundaries drawn below 5 K, merging in a pentacritical point near 6 K and 13 kOe. A slightly revised low-temperature phase diagram of $HoMnO_3$ was presented recently based on dielectric constant and polarization measurements [120].

Comparing the low-temperature part of the phase diagram of [108, 120, 136] with Figure 16 and those proposed in [132, 135], there arises the question whether the LT1 phase forms the dome shaped stability region defined by the T_3 phase boundary. Heat capacity ($C_p(T, H)$) experiments have been chosen to define the thermodynamic phase boundaries of $HoMnO_3$ [121]. The data shown in Figure 21 clearly define the T_3 phase boundary of the LT1 phase by a sharp peak of $C_p(T)$ starting at $H_c = 5$ kOe. The peak rises in magnitude when the field increases to 12 kOe at $T_3 = 3.33$ K and it traces back to lower temperature with further increasing field, eventually disappearing at the upper limiting field of about 20 kOe. This smooth and continuous development and shift of the C_p-peak supports the interpretation of the dielectric and magnetic data and it defines unambiguously the dome shaped LT1 phase and its T_3 boundary, as shown in Figure 16. Whether or not the T_5 transition line extends into the LT1 phase to zero temperature, as suggested in [108, 120, 136], is not clear. No anomaly of the dielectric constant or the

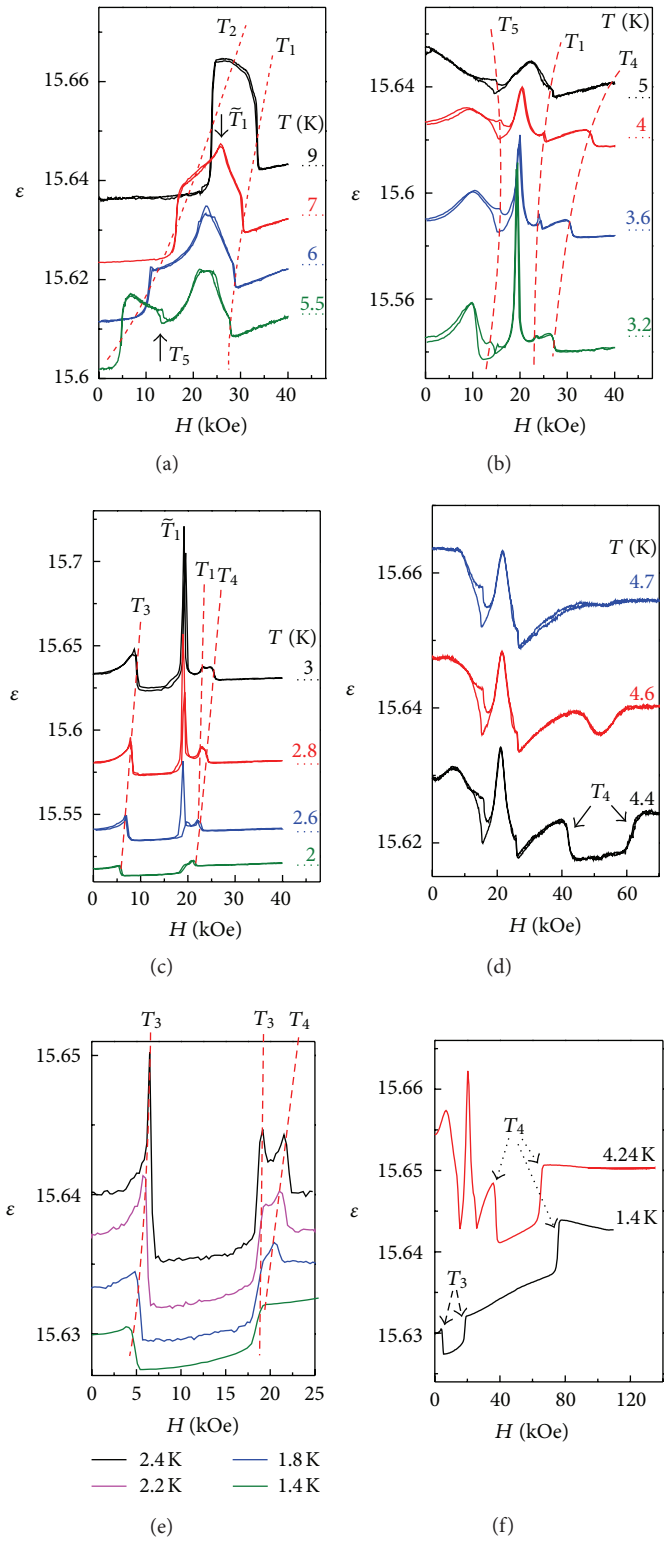

Figure 17: Isothermal field scans of the dielectric constant $\varepsilon(H_c)$ at different temperatures. Different curves are vertically offset for better clarity. Phase boundaries T_1 to T_5 and the ε-peak at $\tilde{T}_1$ are marked by dashed lines. (a) to (c) show $\varepsilon(H_c)$ curves between 9 K and 2 K up to 40 kOe. (d) shows the emergence of the LT2 phase. (e) displays the valley-like anomaly of ε in the LT1 phase and the merging T_3 and T_4 phase boundaries. (f) highlights the upper field boundary of the LT2 phase in $\varepsilon(H_c)$ data extending to 130 kOe.

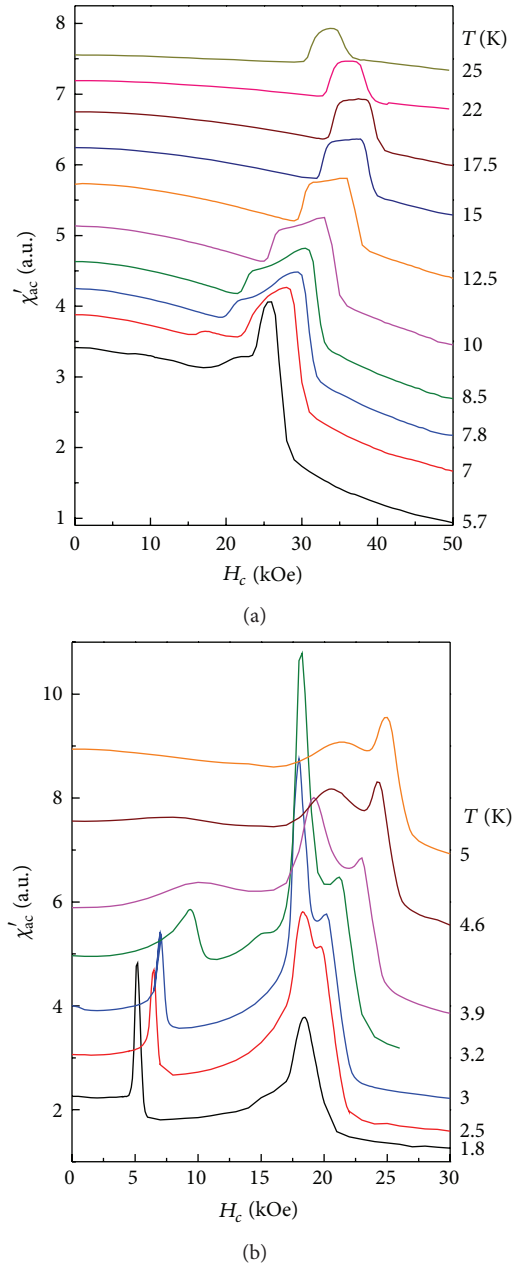

FIGURE 18: Isothermal field scans of the dielectric constant $\varepsilon(H_c)$ at different temperatures. Different curves are vertically offset for better clarity.

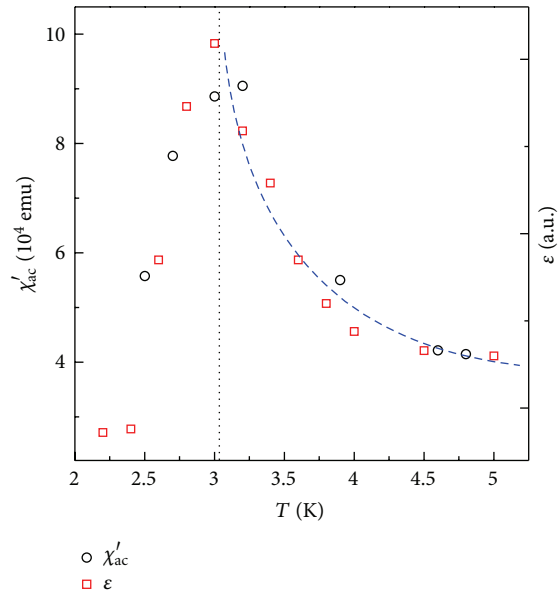

FIGURE 19: Increase of the peak magnetic and dielectric susceptibilities along the $\tilde{T}_1$ line indicating a possible instability at low temperatures. The dashed line is a guide to the eye. The vertical dotted line is the T_3 phase boundary of the LT1 phase.

ac magnetic susceptibility, that could be associated with such extension of T_5, was detected in temperature or field dependent data discussed above.

The phase boundary T_2 is defined by a sharp increase of $C_p(T)$ upon decreasing temperature. T_2 and T_3 are highlighted by the dashed lines in Figure 21. At magnetic fields above 20 kOe, the heat capacity develops another sharp peak at low temperature, indicating the transition into the LT2 phase across T_4, as shown in Figure 22. At the high temperature end, the heat capacity peak at the spin rotation transition temperature T_{SR} shifts to lower temperature and broadens with increasing H_c (Figure 23). Above about 40 kOe, the heat capacity peak cannot be discerned anymore indicating that the only magnetic phase transition below T_N is the transition into the LT2 phase at about 4 K, in agreement with the phase diagram of Figures 13 and 16. The heat capacity data thus confirm the major phase transitions in $HoMnO_3$ in the magnetic field oriented along the c-axis.

2.2.4. Magnetoelastic Effects as Evidence for Strong Spin-Lattice Coupling in $HoMnO_3$. The large effects of the magnetic order on the ferroelectricity, as revealed in the pyroelectric measurements by Hur et al. [120] (Figure 7), can only be explained by the presence of strong spin-lattice interactions. Direct evidence for magnetoelastic effects was found in sizable anomalies of the lattice constants at the magnetic phase transitions. Figure 10 shows the temperature dependence of the a- and c-axis lattice constants of $HoMnO_3$ as determined through thermal expansion measurements [127]. Interestingly, the c-axis displays a negative expansion coefficient over the whole temperature range, that is, c is expanding upon decreasing temperature. With the onset of magnetic order at T_N, both axes experience a sharp anomaly, the c-axis expanding more and the a-axis shrinking to lower temperatures.

The thermal expansivities, shown in the left inset of Figure 10, exhibit a pronounced λ-shaped peak anomaly, similar to the heat capacity (Figure 9), as expected at a second order phase transition. Based on a systematic study of the heat capacity, Oleaga et al. [126] concluded that the critical properties of the hexagonal manganites near T_N fit best to the 3D-Heisenberg universality class. At the spin rotation transition, the thermal expansivities show a narrow peak with

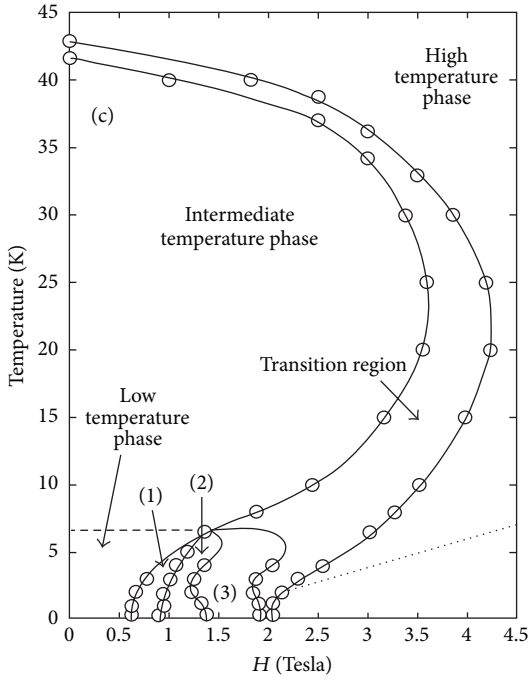

FIGURE 20: Magnetic phase diagram of $HoMnO_3$ as derived from neutron scattering experiments. Note the different phase boundaries at low temperatures merging in a pentacritical point. Reprinted with permission from [136].

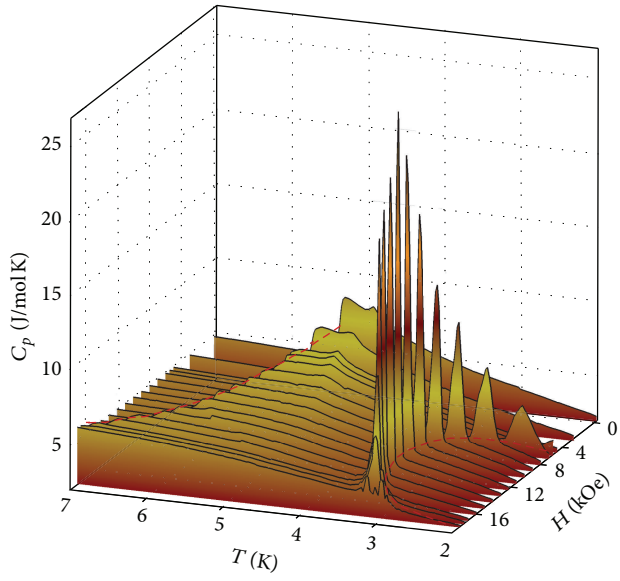

FIGURE 21: Heat capacity $C_p(T, H)$ of $HoMnO_3$. The two most prominent phase boundaries T_2 and T_3 are shown as dashed lines.

opposite sign for the a- and c-axes. This peak is enlarged in the lower right inset to Figure 10. The sharpness of this peak reveals a sudden step-like change of c (decreasing) and a (increasing) resulting in a decrease of the relative volume upon cooling by $\Delta V/V = 0.6 \cdot 10^{-6}$. Other relevant physical quantities showing step-like changes at T_{SR} are the

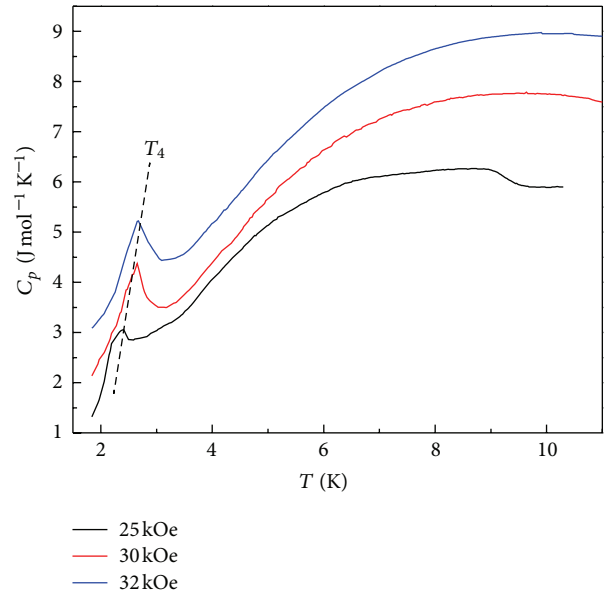

FIGURE 22: Heat capacity $C_p(T, H)$ of $HoMnO_3$ in the high-field range. The transition into the LT2 phase is marked by the sharp peak at T_4.

magnetization and the entropy. The sudden changes suggest that the spin rotation transition in $HoMnO_3$ is of first order. This could be proven by calculating the entropy change at T_{SR} which can be expressed by the Clausius-Clapeyron equation:

$$\Delta S = \Delta V \frac{dp}{dT_{SR}} - \frac{1}{2}\frac{\Delta M}{B}\frac{d\left(B^2\right)}{dT_{SR}}. \quad (6)$$

p and B denote the external pressure and magnetic field, respectively. ΔV and ΔM are the measured changes of the volume and the magnetization across the transition and the entropy change ΔS can be derived by integrating the peak of the heat capacity at T_{SR}. The pressure and field dependencies of T_{SR} had been determined and (6) was shown to be valid, proving the first order nature of the transition [127]. This is also consistent with the sudden 90° flop of the Mn^{3+} spins and the symmetry change from $P6_3cm$ to $P6_3cm$ at T_{SR}.

The negative thermal expansion of the c-axis over a large temperature range appears unusual at first and it could be associated with strong magnetic correlations among the quasi-2D manganese spin system, resulting in an enhanced contraction of the in-plane distances and an expansion of the c-axis through elastic forces upon decreasing temperature. A similar negative expansivity was also reported for the related compound, $YMnO_3$, below room temperature [96, 137, 138]. High-temperature studies of the structure of $YMnO_3$ have shown that the expansivity of the c-axis becomes negative below 1260 K, the transition temperature from the centrosymmetric $P6_3/mmc$ structure to the polar $P6_3cm$ phase [82–84, 91]. Therefore, the negative c-axis expansivity appears to be more related to the properties of the ferroelectric phase.

Longitudinal magnetostriction measurements along the hexagonal c-axis of $HoMnO_3$ confirm the strong magnetoelastic effects suggested by the thermal expansion anomalies

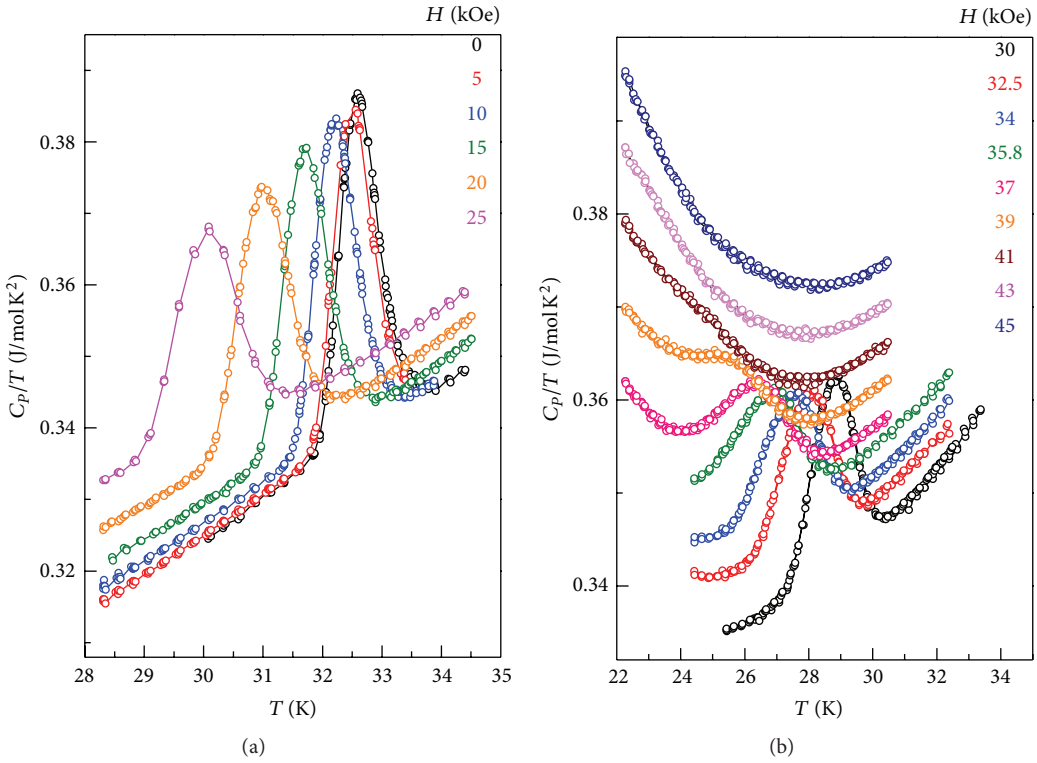

FIGURE 23: Magnetic field dependence of the heat capacity peak near the spin rotation transition temperature, T_{SR}. Above H_c = 40 kOe, no phase transition can be detected.

at zero magnetic field [41]. In the high-temperature range, the c-axis length increases nonlinearly in the $P\underline{6}_3c\underline{m}$ phase with increasing magnetic field, as shown in Figure 24(a). At the T_2 phase boundary, $c(H_c)$ suddenly changes slope and increases at a steeper pace in the intermediate $P\underline{6}_3$ phase, until $c(H_c)$ experiences another sudden decrease of slope with the entrance into the $P\underline{6}_3\underline{c}m$ magnetic structure at T_1. In the high-field $P\underline{6}_3\underline{c}m$ phase $c(H_c)$ appears to change linearly with further increasing field. The sharper increase of c with H_c in the intermediate $P\underline{6}_3$ phase reflects a remarkably strong response of the lattice to the Mn^{3+} spin rotation from $\Phi = 0^\circ$ to $\Phi = 90^\circ$, resulting in an increased expansion of the c-axis.

At lower temperature, several of the phase boundaries shown in Figure 16 are reflected in distinct magnetostriction anomalies of the c-axis. The low-temperature data are summarized in Figure 24(b). At 5 K, the only transition that is clearly resolved in $c(H_c)$ is from $P\underline{6}_3$ to $P\underline{6}_3\underline{c}m$ across the T_1 phase boundary. The sharp increase of c just below this transition coincides with the peaks of the dielectric (Figure 17) and magnetic (Figure 18) susceptibilities, again proving the softness of the magnetic, dielectric, and elastic properties. At lower temperature, the entrance into and exit from the LT1 phase by crossing the T_3 phase boundary twice is accompanied by a sudden increase and decrease of the c-axis, respectively. This is clearly seen in the first two peaks of the derivative of the 3 K data, shown in the inset to Figure 24(b). The next sharp peak is associated with the $\widetilde{T}_1$-line and the last peak above 20 kOe signals the entrance into the LT2 phase (note that the T_1 and T_4 phase boundaries merge at this point, see Figure 16).

At the lowest temperature of this study (1.43 K), only two sharp anomalies of $c(H_c)$ can be distinguished. Both result in a step-like increase of c in crossing from the $P6_3cm$ phase into the LT1 phase and eventually into the LT2 phase. It is interesting to note that no magnetostrictive anomaly of the c-axis was detected at the T_5 phase boundary although magnetic as well as dielectric properties exhibit distinct anomalies with a strong field and temperature hysteresis.

The thermal expansion and magnetostriction measurements discussed above have revealed the macroscopic length changes of for example, the c-axis with an extraordinary resolution that can only be obtained by the high-precision capacitance dilatometer employed for the studies. This makes the measurements significantly more sensitive than any structural characterization using scattering methods. However, the dilatometry cannot resolve the microscopic distortions within one unit cell which should be studied for a more fundamental understanding of the magnetoelectric coupling in multiferroics.

Recent high-resolution neutron diffraction experiments on different $RMnO_3$ have proposed a correlation between the magnetic structure according to Table 2 and the position of the Mn^{3+} ion in the primitive cell [130]. In the $P6_3cm$ structure, the relative position of the Mn ion is defined by one

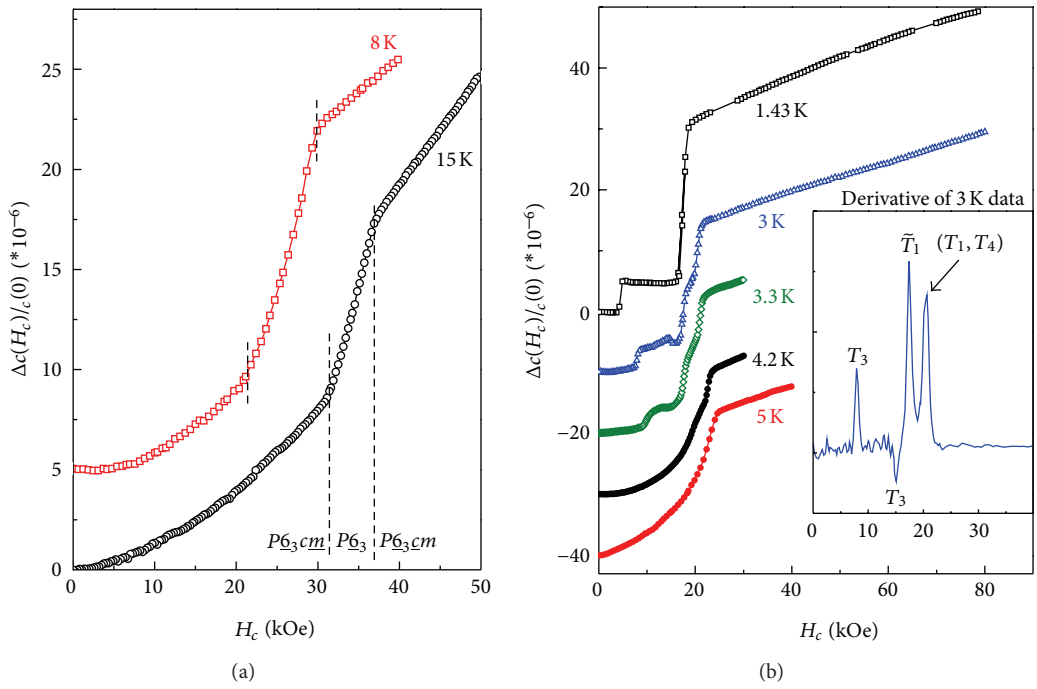

FIGURE 24: Magnetostriction of the c-axis of $HoMnO_3$ in longitudinal magnetic fields, H_c. Note that different curves are vertically offset for better clarity. (a) High-temperature range. The vertical dashed lines mark the two phase transitions from $P6_3cm$ to $P6_3$ and to $P6_3cm$. (b) Low-temperature range. The inset to (b) shows the derivative at 3 K which clearly reveals 4 successive phase transitions.

free parameter x_{Mn} which varies between different rare earth ions in the $RMnO_3$ compounds and also with temperature and magnetic orders. In $HoMnO_3$, x_{Mn} increases from 0.325 above T_N to 0.335 below T_{SR}. Since the super exchange interactions between the Mn^{3+} spins within the *ab*-planes as well as along the *c*-axis depend on the crucial parameter x_{Mn}, it was proposed that the different magnetic orders realized in $HoMnO_3$ and in other hexagonal manganites (e.g., $ScMnO_3$, $YbMnO_3$) are strictly correlated with x_{Mn} [130].

The local structure of $HoMnO_3$ was studied using X-ray absorption spectroscopy [131]. The bond distances between different Mn- and Ho-ions were extracted from the atomic distribution functions and it was shown that different interatomic distances experience sudden changes at the three magnetic phase transitions. The onset of magnetic order at T_N did mainly affect the inplane Mn-Mn bond distances. At the spin rotation transition temperature, T_{SR}, the Mn-Mn as well as Ho-Mn bonds show distinct anomalies. At the lowest transition temperature, T_{Ho}, all bonds are distorted, including the nearest and next nearest neighbor Ho-Mn and the Ho-Ho distances. A model calculation based on the local spin density approximation was carried out to study the correlated spin-lattice system and the role of different magnetic exchange interactions (Mn-Mn, Ho-Mn, Ho-Ho) in driving the three observed magnetic phase transitions was determined [131].

The important role of the Ho-Mn magnetic interactions was also derived from an investigation of the magnetoelastic coupling in $HoMnO_3$ through measurements of the elastic moduli [132]. An elastic softening was observed over a wide temperature range, with pronounced anomalies at T_{SR} and T_{Ho}, and it was attributed to spin fluctuations induced by the Ho-Mn interactions. It should also be noted that magnetic ordering effects below T_N result in a sizable hardening of phonon modes that modulate the Mn-Mn interactions which is further evidence of the strong spin-lattice coupling in $HoMnO_3$ [128].

2.2.5. The Role of the Ho^{3+} Magnetic Moment in $HoMnO_3$. As already discussed in the previous section, the involvement of the Ho^{3+} magnetic moment is essential to understand the complex sequence of magnetic phase transitions in $HoMnO_3$. The Ho^{3+} moments interact with the Mn^{3+} spins and, at lower temperature, with one another. They also participate in the magnetic ordering in certain temperature and field ranges. There are two crystallographically inequivalent sites for the Ho ions: Ho(1) and Ho(2) occupying the 2a and 4b positions, respectively, and six formula units per primitive cell, including two Ho(1) and four Ho(2). The complete group theoretical representation of the structure was given by Muñoz et al. [106]. Above the spin rotation transition temperature, the $P6_3cm$ magnetic symmetry would only allow the Ho(2) moments to order, however, neutron scattering experiments have not found any indication of a Ho^{3+} moment order above the spin rotation transition temperature T_{SR}. A gradual increase of the Ho sublattice magnetization below about 30 K is an indication of a polarization and the onset of the Ho magnetic order at T_{SR} [106].

Below T_{SR} and above T_{Ho}, the moments of both Ho(1) and Ho(2) are allowed to order antiferromagnetically. Thereby, the moments of Ho(1) within one hexagonal *ab*-plane form ferromagnetically aligned planes which are antiferromagnetically oriented between to neighboring planes. The Ho(2) moments form similar ferromagnetic planes but they are opposite in direction to the Ho(1) within each plane, as shown in Figure 25(a). The magnetic moments of Ho(1) and Ho(2) within one plane do not completely compensate so that a ferrimagnetic moment remains in each plane forming an antiferromagnetic alignment along the hexagonal *c*-axis. Various experimental data are consistent with this order [103, 107, 111, 133].

Below T_{Ho}, only the antiferromagnetic order of the Ho(2) moments is allowed by the $P6_3cm$ (Γ_1) magnetic space group and the Ho(1) are paramagnetic. The transition into the $P6_3cm$ phase is accompanied by a large increase of the Ho(2) sublattice magnetization and a sudden jump of the Mn ordered magnetic moment. The AFM order of the Ho(2) below T_{Ho} is schematically shown in Figure 25(b). It should be noted that, although the phase transition at T_{Ho} is well established through magnetic, dielectric, and thermodynamic measurements (see previous sections), and neutron scattering [103, 108, 130], second harmonic generation [93, 133], and X-ray resonant magnetic scattering experiments [111] support the $P6_3cm$ magnetic symmetry below T_{Ho}, a recent report did not find a change of the magnetic order of the Ho moments below T_{Ho} [107]. The origin of the discrepancy is not clear at this point.

In magnetic fields along the *c* axis, the Ho moments can be expected to become systematically aligned with the field (note that the Mn spins are in the *ab* plane and are less susceptible to the field H_c). A ferromagnetic alignment of the Ho moments along the *c* axis is allowed by symmetry, for example, in the $P6_3\underline{cm}$ magnetic space group, corresponding to the Γ_2 irreducible representation (Figure 4). It was suggested that this phase is realized in $HoMnO_3$ at low-temperatures and high magnetic fields ($H_c > 20$ kOe) [93, 139]. However, according to the phase diagram of Figure 16, there are at least to successive phase transitions as a function of increasing field below 3 K, the first transition into the LT1 phase at 5 kOe and a second transition into the LT2 phase at 20 kOe. It is likely that at high enough magnetic fields the magnetic structure turns into the $P6_3\underline{cm}$ symmetry, but the details of the the magnetic orders in the LT1 and LT2 phases remain a puzzle. The symmetry change with increasing field from $P6_3cm$ to $P6_3\underline{cm}$ allows all Ho moments to order and it is accompanied by another 90° rotation of the Mn spins resulting in the Γ_2 magnetic structure shown in Figure 4.

The symmetry allowed magnetic orders of the Ho(1) and Ho(2) ions in the unit cell and the linear magnetoelectric effect are summarized in Table 1 of [139]. It is particularly interesting that the linear magnetoelectric coupling along the *c* axis is allowed only in $P6_3\underline{cm}$ symmetry, that is, the system can gain magnetoelectric energy through a coupling of the electrical polarization with the magnetization of the Ho ions, $H_{me} = \alpha_{zz} P_z S_z^{Ho}$ (α_{zz} is the longitudinal magnetoelectric tensor element along the *c* axis, P_z is the ferroelectric polarization, and S_z^{Ho} is the *c* axis component of the Ho magnetization). This coupling may result in an electric field effect on the magnetization of the Ho moments. Lottermoser et al. [139] indeed found that an applied electric field did quench the second harmonic generation signal at all temperatures below T_N indicating a major change of the Mn spin magnetic order. The response of the Ho sublattice moment was derived from a change of the Faraday rotation in electric fields applied with different polarities. The observed results indicate that the electric field did induce a macroscopic magnetization attributed to the ferromagnetic order of the Ho moments. The results of the optical study of [139] are shown in Figure 26.

The thermodynamic origin of the electric field effects on the magnetic order in $HoMnO_3$, as discussed in [110], is found in the gain of magnetoelectric energy through the linear magnetoelectric coupling of magnetization and polarization. Since the linear magnetoelectric effect with the *c*-axis electrical polarization is only allowed in the $P6_3\underline{cm}$ magnetic structure, the external electric field stabilizes this symmetry through the control of the electrical polarization with the consequence of a ferromagnetic alignment of the Ho moments and a 90° rotation of the Mn spins. The magnetoelectric energy gain competes with the change of the magnetic anisotropy and superexchange energy. Fiebig et al. [110] have shown that the different ferroelectric displacements of the Ho(1) and Ho(2) ions as well as the finite sublattice magnetization of the Mn spins are essential for a macroscopic magnetoelectric effect in the case of $P6_3\underline{cm}$ symmetry.

Other groups have searched for the electric-field induced magnetic moment in $HoMnO_3$ and the symmetry allowed linear magnetoelectric effect at low temperatures and high fields. In field-dependent polarization measurements below 3 K and magnetic fields above 30 kOe, Hur et al. could not detect a linear magnetoelectric effect within their experimental resolution [120]. Using X-ray resonant magnetic scattering, Nandi et al. have elucidated the role of Ho^{3+} ions and studied the magnetic order of the Ho moments [111]. The results confirm the onset of Ho moment order at T_{SR} and a change of the order at T_{Ho}. However, measurements in high electric fields were found to be identical to the results of zero field experiments and the suggested change of the Ho moment order in electric fields could not be confirmed. Small angle neutron scattering experiments conducted on single crystals of $HoMnO_3$ in magnetic and electric fields have indicated that the ferromagnetic moment in electric fields possibly arises from uncompensated spins in the antiferromagnetic domain walls rather then from bulk magnetism of the Ho moments [140]. This issue is still not decided and more studies have to be conducted.

2.3. Magnetoelectric Effects in Hexagonal Manganites without Rare Earth Moments

2.3.1. Ferroelectricity, Magnetic Order, and Magnetoelectric Coupling in $YMnO_3$. $YMnO_3$ was in the focus of interest because of the absence of the rare earth moment which dominates the magnetic response in other hexagonal manganites. Structurally, $YMnO_3$ is quite similar to $HoMnO_3$ because of

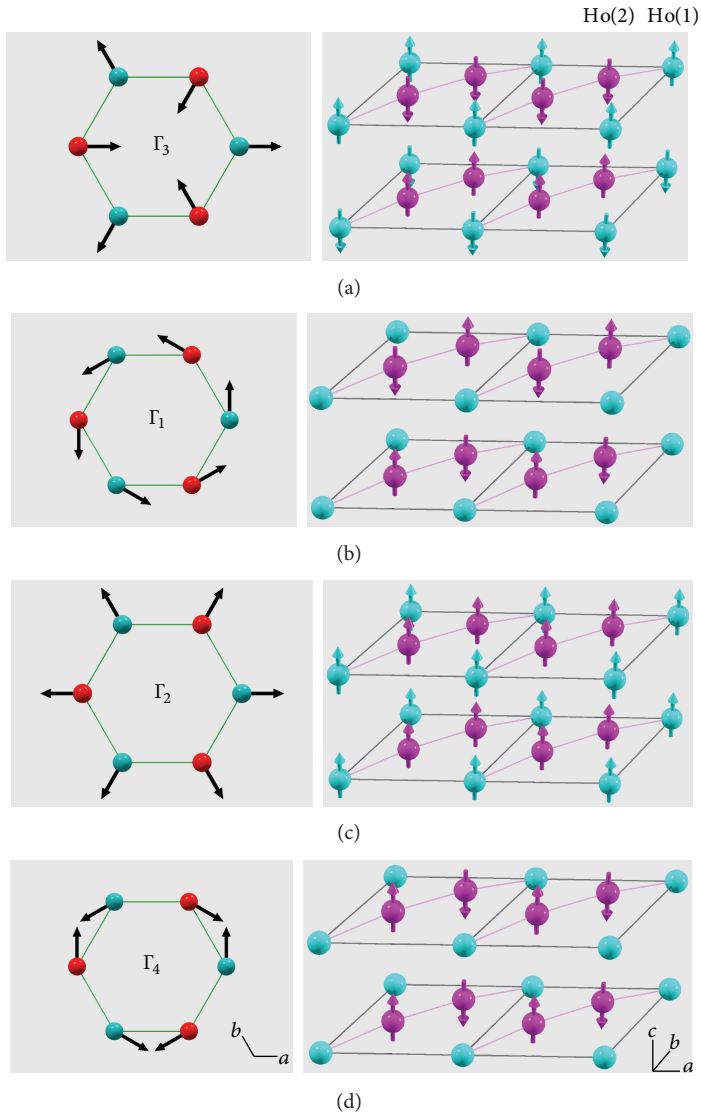

FIGURE 25: Schematic order of the Mn spins (left) and Ho magnetic moments (right) in different magnetic phases of $HoMnO_3$. (a) $P6_3cm$, $T_{Ho} < T < T_{SR}$ in zero magnetic field, (b) $P6_3cm$, $T < T_{Ho}$ in zero magnetic field, (c) $P6_3cm$, (suspected high-field symmetry, the relative alignment of the FM sublattices of Ho 2a and 4b can also be antiferromagnetic resulting in a ferrimagnetic state, possibly at lower magnetic fields), and (d) $P6_3cm$, for $T_{SR} < T < T_N$ in zero magnetic field. Note that (d) allows for a magnetic order of the Ho^{3+} moments on 4b sites, but it was not observed experimentally. The Ho ions and their magnetic moments in two neighboring unit cells are shown.

the very similar size of the Y^{3+} and Ho^{3+} ions, however, the magnetic system appears to be simpler and the only magnetic ion is the Mn^{3+}. Therefore, $YMnO_3$ has been studied extensively and compared to $HoMnO_3$ and other hexagonal manganites. While there is no complete consensus about the high-temperature structures and phase transitions in $YMnO_3$ [82–85], most studies confirm the onset of ferroelectricity near 1200 K with the change of structure to the $P6_3cm$ phase. After the discovery of ferroelectricity in $YMnO_3$ [38], Smolenskii and Bokov revealed the coexistence of the ferroelectric state with antiferromagnetism at low temperatures [42].

The origin of ferroelectricity was attributed to the buckling of the MnO_5 polyhedra which is accompanied by displacements of the O^{2-} and Y^{3+} ions along the c-axis, away from a centrosymmetric position. The distortions in the ferroelectric phase are schematically shown in Figure 27. The Y^{3+} ions in different Wyckoff positions are displaced along the c-axis in opposite directions creating local dipolar moments of different sign. The local moments are not completely compensated and, in combination with the displacements of the oxygen ions, generate the macroscopic polarization. Theoretical calculations of the bonding and the Born effective charges (Z^*) come to different conclusions. Van Aken et al. found the Z^* values for all ions close to the formal ionic charges suggesting that there is no significant rehybridization and charge transfer with the entrance into the ferroelectric phase [79]. The macroscopic polarization arises mainly from the Y-O_p displacements along the c-axis. The origin of the

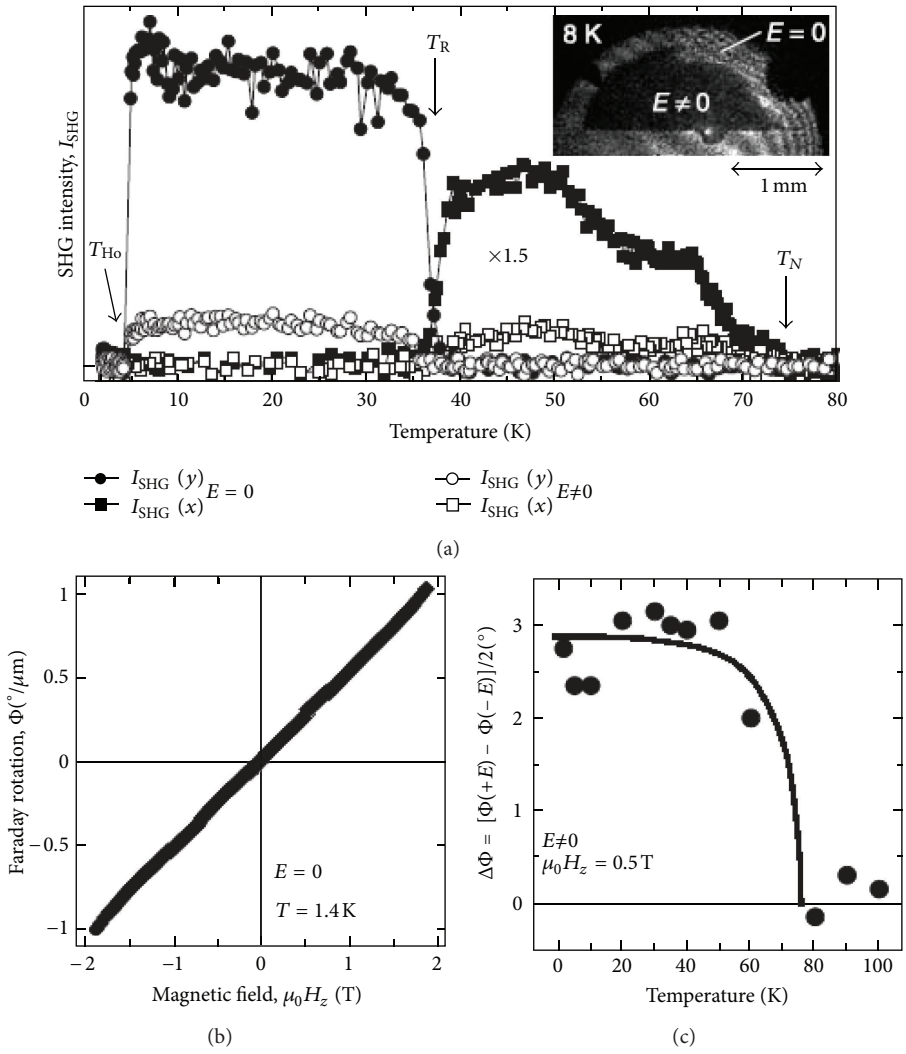

FIGURE 26: (a) Suppression of second harmonic generation intensities in $HoMnO_3$ by external electric fields, indicating a major change of the Mn spin order. (b) Faraday rotation in the absence of electric fields. (c) Change of the Faraday rotation angle in electric fields of opposite polarities. Reprinted with permission from [139].

instability is apparently a strong coupling of a zone boundary instability with the polarization resulting in an improper ferroelectric state [141, 142]. However, recent polarization dependent X-ray absorption measurements have suggested the existence of strong anisotropic hybridization of the Y 4*d*-O 2*p* bonds which creates the off-center displacements of Y^{3+} and the resulting large anomalies in the Born effective charges as the possible cause of the ferroelectric instability [143].

The details of the magnetic order below $T_N = 72$ K in $YMnO_3$ has been explored through bulk magnetization, neutron scattering, and second harmonic generation optical experiments. Unlike in $HoMnO_3$, where the large Ho moment dominates the magnetic susceptibility and makes the Néel transition of the Mn spins almost invisible (see Figure 8(a)), a clear change of slope of the T-dependent magnetic susceptibility signals the onset of magnetic order in $YMnO_3$, as shown in Figure 28 for a floating zone grown single crystal. The sharp slope change is consistent with earlier reports for single crystals [144–146]. However, the magnetic signature at T_N may be less clear in powder samples, possibly due to sample quality or grain size problems [43, 90, 95, 147–150].

The first neutron study of $YMnO_3$ by Bertaut and Mercier [87] proposed two possible magnetic structures, $P\underline{6}_3c\underline{m}$ (Γ_3, α-model) or $P6_3cm$ (Γ_1, β-model), according to Table 2. Later, the same authors favored the $P\underline{6}_3c\underline{m}$ magnetic symmetry [151]. Subsequent neutron studies found it difficult to distinguish between the two magnetic symmetries (Γ_1 and Γ_3) since both did describe the spectra equally well [96, 152], but other data have been interpreted in favor of the $P6_3cm$ (Γ_1) symmetry [95, 153, 154]. Recent neutron diffraction and polarimetric studies have suggested the lower $P\underline{6}_3$ magnetic symmetry with a spin tilt angle of $\Phi = 11^\circ$ with reference to the $P\underline{6}_3c\underline{m}$ structure [107]. Second harmonic genaration optical spectra are sensitive to the details of the magnetic order in hexagonal manganites [99]. For $YMnO_3$, the results

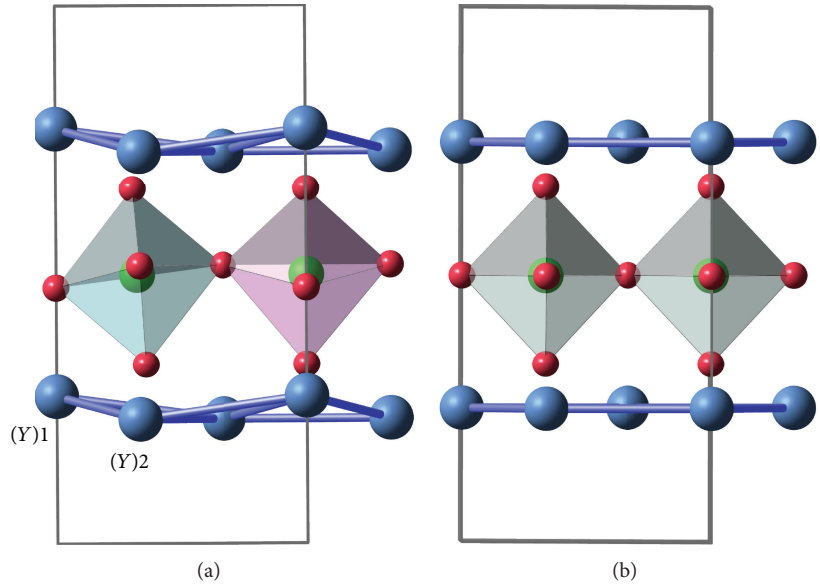

FIGURE 27: (a) Distorted structure of $YMnO_3$ in the ferroelectric state. (b) Structure without distortions with ions in centrosymmetric positions.

of SHG experiments suggest the $P6_3cm$ (Γ_3) magnetic symmetry, the same symmetry as in $HoMnO_3$ below the spin rotation transition [99, 100].

The discussion about the magnetic symmetry of $YMnO_3$ below the Néel temperature is even more complicated after signatures of diffuse scattering as well as unconventional short range spin fluctuations have been reported above T_N as well as in the ordered phase [147, 148, 155–157]. The results seem to be consistent with a quasi two-dimensional frustrated magnetic system with weak interplane coupling and a spin liquid phase above T_N which extends into the magnetically ordered phase below T_N. Thermal conductivity measurements show an unusual suppression in a large temperature range, stretching from T_N to nearly room temperature, which was attributed to strong spin fluctuations as a result of the 2D character of the Mn magnetic sublattice and geometric frustration [115]. Furthermore, a large deviation of the low-temperature ($T < T_N$) heat capacity from the phonon contribution seems to indicate the presence of a residual magnetic C_p, possibly due to a magnetic glassy state coexisting with the ordered antiferromagnetism in some $RMnO_3$ (R = Y, Lu, Sc) [90, 144]. In contrast, a recent study of the heat capacity of $YMnO_3$ and the critical scaling near the Néel transition has argued that the deviation of the low-temperature C_p from the Debye law, previously attributed to an abnormal magnetic contribution, can be accommodated by an additional Einstein contribution and the critical exponents derived are well within the range of a 3D Heisenberg model, thus not supporting 2D or chiral models for the magnetic system [126, 158]. It appears that the true nature of the magnetic order and the spin fluctuations below and above T_N has yet to be revealed.

The magnetoelectric coupling between the ferroelectric polarization (oriented along the hexagonal c-axis) and the

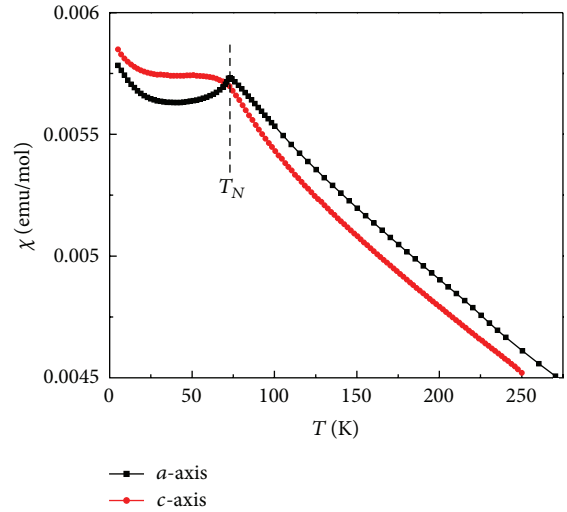

FIGURE 28: Magnetic susceptibility of $YMnO_3$ along a- and c-axes. The Néel temperature is marked by the dashed line.

Mn^{3+} spin order in the ab plane was first reported in form of a distinct anomaly of the dielectric constant, as shown in Figure 6, by Huang et al. [43]. These results were confirmed for $YMnO_3$, $LuMnO_3$, and $ScMnO_3$ by Tomuta et al. [90]. While those measurements were conducted on polycrystalline ceramic samples, a clearer picture is obtained from single crystals. Katsufuji et al. [144] reported a sudden drop of the dielectric constant ε_{ab} measured with the electric field orientation within the ab-plane in $YMnO_3$ and $LuMnO_3$.

The dielectric response to the magnetic order at T_N suggests a very strong coupling of the Mn^{3+} spins to the lattice. The spin-lattice interaction in $YMnO_3$ is not complicated by

the presence of a rare earth moment with a strong uniaxial anisotropy, as for example in $HoMnO_3$ discussed above. First evidence for the existence of magnetoelastic effects was derived from subtle anomalies of the lattice parameters detected in neutron scattering experiments [96], although the observed anomalies are almost within the resolution of the scattering experiment. Much higher resolution of length measurements can be achieved if a capacitance dilatometer is used. Thermal expansion data for $YMnO_3$ are shown in Figure 29. Similar to $HoMnO_3$, the c-axis shows a negative expansivity at all temperatures below ambient whereas the a-axis contracts with decreasing T. Those results are consistent with data from neutron scattering experiments [95]. At T_N, both axes respond to the onset of magnetic order but with opposite sign, the c-axis expands faster and the inplane distances experience an enhanced contraction. The λ-shaped sharp anomalies of the expansivities (Figure 29(b)) are consistent with the second order nature of the magnetic phase transition and the existence of critical spin fluctuations near T_N. The anomalous T-dependence of the lattice parameters was confirmed by neutron scattering experiments [138, 159].

The details of the ionic distortions in the structure of $YMnO_3$ and $LuMnO_3$ have been investigated through high resolution X-ray diffraction and neutron scattering experiments only very recently [137]. This work mapped out the details of the structural changes at T_N on an atomic scale and showed that all atoms in the unit cell exhibit giant displacements, two orders of magnitude larger than in typical magnetic materials. The coupling between the ferroelectric polarization and the antiferromagnetic order (the internal magnetoelectric effect) was explained by the magnitude and nature of the atomic displacements. The driving mechanism for the huge magnetoelastic effect was proposed to be the displacement of the Mn^{3+} ions from their ideal symmetric position ($x = 1/3$) which results in a coupling to the electric dipole moments [159]. It is interesting to note that the deviation from the $x = 1/3$ position for the Mn^{3+} is of opposite sign in $YMnO_3$ and $LuMnO_3$, resulting in different magnetic structures below T_N. The possible effects of the Mn^{3+} displacements on the magnetic exchange coupling parameters and the resulting magnetic orders was also discussed by Fabrèges et al. [130]. Similar to the internal magnetic order, external magnetic fields have a significant influence on the atomic position in the unit cell. This was demonstrated in neutron scattering experiments in magnetic fields up to 50 kOe [150].

The strong magnetoelastic effects observed in $YMnO_3$ and other hexagonal $RMnO_3$ leave their imprint also on other physical quantities as, for example, the elastic moduli studied in ultrasound measurements [160]. The study of magnetic and lattice excitations using inelastic neutron scattering experiments provided evidence for a strong coupling between magnons and phonons which appear to hybridize in one mixed elementary excitation [154], similar to the electromagnons studied in multiferroic orthorhombic manganites [161, 162]. Raman and infrared absorption investigations of the temperature dependent phonon spectrum of $YMnO_3$ and $LuMnO_3$ have found a kink at T_N and an abnormal hardening in the magnetically ordered phase, indicating strong spin-phonon coupling [163–165]. Similar phonon hardening was also found in compounds with rare earth magnetic moments, $HoMnO_3$ and $ErMnO_3$ [128, 166].

2.3.2. Ferroelectric and Magnetic Domains in $YMnO_3$. Ferroelectric and magnetic domains and the associated domain walls play an essential role in multiferroic compounds. Novel techniques of visualizing and distinguishing those domains had to be developed in order to study the domain physics in detail. One of the more sensitive methods is the second harmonic generation (SHG) spectroscopy and it's power in making domains of magnetic materials (e.g., antiferromagnetic Cr_2O_3) visible has been demonstrated [167, 168]. The SHG technique was later refined to investigate the multiferroic domain structure of hexagonal manganites [169]. Most investigations have focused on $YMnO_3$ to avoid the influence of the rare earth magnetic moments. The principle of the second harmonic generation technique is the sensitivity of the third rank SHG susceptibility tensor with respect to magnetic symmetry and polar structure.

It is the beauty of the nonlinear optical process (SHG) that it allows to distinguish between electric and magnetic 180° domains within one experiment. This technique was successfully applied to the study of ferroelectric and magnetic domains in $YMnO_3$ [170]. The results shown in Figure 30 clearly show different domain pattern of the same area of the crystal's surface, depending on the polarization geometry of the incoming and SHG light. By choosing the appropriate geometry, different domains (ferroelectric, magnetic, or a combination of both) can be made visible through an optical interference technique with an external reference signal [171, 172]. Examples are shown in Figure 30, left panel. The top-left image reveals the ferroelectric domains only, the dark and bright areas corresponding to $P = -1$ and $P = +1$, respectively. The antiferromagnetic domains are made visible in the bottom image, dark and bright areas denoting $L = +1$ and $L = -1$, respectively. The top right image of Figure 30 was taken in a geometry that distinguishes the sign of the product of P and L, the dark area corresponds to $P * L = +1$ and the bright area denotes $P * L = -1$. From combining all images, a complete domain picture can be constructed, as shown in the right panel of Figure 30 [170]. The most interesting result of this study was the observation that ferroelectric domain walls are not forming independently of the antiferromagnetic domains. Instead a "clamping" property was shown to exist between ferroelectric and magnetic domain walls, as illustrated in Figure 30 (right panel). In contrast, some magnetic domain walls do exist within one ferroelectric domain and are not necessarily attached to ferroelectric domain walls. This behavior indicates the strong interaction of ferroelectric and magnetic orders and novel physical phenomena happening in between the different domains.

After the discovery of the clamping feature of ferroelectric and magnetic domain walls in $YMnO_3$, the possible microscopic origin was discussed by Hanamura et al. [173]. The authors considered the isotropic as well as the antisymmetry (Dzyaloshinskii-Moriya) exchange interactions between the

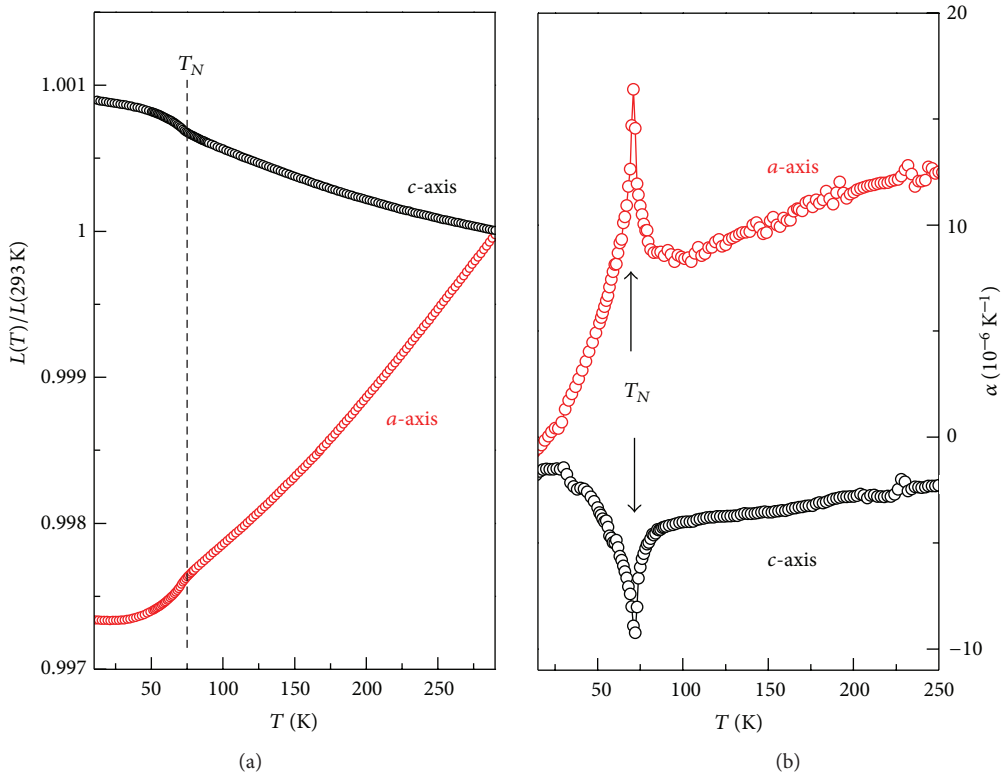

FIGURE 29: (a) Thermal expansion of the a- and c-axes of $YMnO_3$. (b) Thermal expansivities of a and c showing a λ-shaped anomaly at T_N.

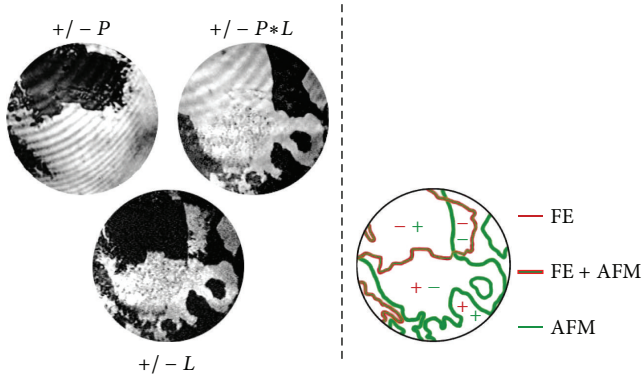

FIGURE 30: Left panel: second harmonic generation images of $YMnO_3$ measured in different polarization of the incoming and SHG light (for details see [170]). The two ferroelectric domains are denoted by $P = \pm 1$ and the two antiferromagnetic domains are labeled $L = \pm 1$, and they are distinguished in contrast, dark or bright. Right panel: domain pattern constructed from the images in the left panel. Note that ferroelectric domain walls always coincide with antiferromagnetic domain walls. Reprinted with permission from [170].

Mn^{3+} spins within the ab-plane of $YMnO_3$ and calculated the energy of the ferroelectric and antiferromagnetic domain boundaries within a continuum approximation. It was shown that the Dzyaloshinskii-Moriya interaction did stabilize the ferroelectric-antiferromagnetic domain boundary and a single ferroelectric domain wall was not a stable solution in the calculations. These calculations highlight the importance of the antisymmetric Dzyaloshinskii-Moriya interactions in hexagonal manganites, at least in the boundaries between different domains.

An alternative explanation of the clamping property of ferroelectric and antiferromagnetic domain walls was proposed by Goltsev et al. [174, 175] based on a microscopic model that includes the in-plane and out-of-plane exchange interactions of the Mn^{3+} spins, their anisotropy, the local distortion at the ferroelectric domain wall, and the piezomagnetic coupling between the local strain and the local magnetic moment. The energy gain achieved through this piezomagnetic effect favors the clamping of magnetic to ferroelectric domain walls at T_N. Since the ferroelectric domains do exist above T_N, the first magnetic domain walls formed in the ordered state coincide with the ferroelectric walls, however, additional magnetic domains may form within one ferroelectric domain. It should be noted that the proposed mechanism does not involve the antisymmetric Dzyaloshinskii-Moriya exchange interaction.

2.3.3. Multiferroic Properties of $LuMnO_3$ and $ScMnO_3$. $LuMnO_3$ and $ScMnO_3$ are of interest since Lu^{3+} and Sc^{3+} both do not carry their own magnetic moment, similar to Y^{3+}, but they are significantly smaller resulting in a compression of the lattice (see Table 1) and stronger magnetic exchange interactions within the ab-plane as well as along the c-axis. As

a consequence, the Néel temperatures increase from $YMnO_3$ (72 K) to $LuMnO_3$ (90 K) and to $ScMnO_3$ (130 K). In addition, the in-plane magnetic anisotropy decreases and is quite small for $ScMnO_3$ making the magnetic orders with the preferred Mn spin angles $\Phi = 0^\circ$ and $\Phi = 90^\circ$ (see Table 2) less favorable.

The crystal structure at high temperatures ($T > 300$ K) had been studied and compared with data for $YMnO_3$ [91]. The *a*-axis lattice parameters show a similar change with temperature, however, there are significant changes with respect to the thermal expansion of the *c*-axis. While $YMnO_3$ exhibits a strongly negative expansivity, similar to $HoMnO_3$ (see also Figures 10 and 29), the *c*-axis is almost temperature independent for $LuMnO_3$ and it shows a "normal" behavior (positive expansivity) in the case of $ScMnO_3$. The differences in the thermal expansion property of the *c*-axis and the negative *c*-axis expansivity of $YMnO_3$ has been attributed to differences of the buckling angle of the MnO_5 bipyramids and it's specific temperature dependence. The *c*-axis length scales with the buckling angle and, for $YMnO_3$, the decrease of this angle with increasing temperature results in the contraction of the *c*-axis, as observed experimentally [91]. For $ScMnO_3$, the buckling angle slightly increases with temperature explaining the normal expansion property of the *c*-axis in this compound.

The transition into the magnetically ordered state of $LuMnO_3$ at 90 K is well documented in anomalies of the bulk magnetic susceptibility and the heat capacity [90, 144, 176]. Measurements of polycrystalline samples show a kink in the magnetic susceptibility which continues to increase below the magnetic transition temperature [90, 177]. However, high-quality single crystals reveal a clear peak of the magnetic susceptibility at T_N, as expected for an antiferromagnetic phase transition [122, 144, 176]. This is similar to data obtained for polycrystalline samples of $YMnO_3$ [90] as compared to single crystals (see Figure 28). The magnetic contribution to the heat capacity of $LuMnO_3$ and $ScMnO_3$ was extracted and it was shown that the entropy change between zero temperature and T_N corresponds to the expected value for spin 2, $R\ln(2S + 1)$, with a significant part of the entropy change shifted to lower temperatures [90].

The magnetic susceptibility of $ScMnO_3$ exhibits a different anomaly at T_N with a field-dependent irreversible behavior (difference between field-cooled and zero field-cooled data) below T_N and an obvious magnetization hysteresis loop at the lowest temperatures [90, 95, 178, 179]. This has been interpreted as a weak ferromagnetic moment associated with the magnetic order below T_N. However, it has been pointed out by Fiebig et al. that the magnetic structure of the Mn^{3+} spins ($P\underline{6}_3c\underline{m}$ or $P\underline{6}_3$), as derived from neutron scattering [179] and SHG experiments [180], is not compatible with a ferromagnetic moment. There arises the question of whether or not the polycrystalline nature of the samples or possible impurity phases (not detectable in X-ray measurements) could have been the source of the irreversibility in the bulk magnetization. A recent study of single crystals and ceramic samples of $HoMnO_3$ has shown magnetic irreversibility in the polycrystalline material [181].

The detailed structure of $LuMnO_3$ at low temperature had been studied by high resolution neutron scattering. Interestingly, the *c*-axis of $LuMnO_3$ experiences a sizable increase with decreasing temperature below 200 K, signaling the onset of magnetic fluctuations [137, 176, 182]. This increase and the related anomaly in $YMnO_3$ (also in $HoMnO_3$) show that the buckling of the MnO_5 units and the related ferroelectric distortion discussed above are not the only mechanism affecting the thermal expansion behavior of the *c*-axis. The origin of the structural distortions in the magnetically ordered phase was suggested to lie in the displacements of the Mn^{3+} ions from their $x = 1/3$ ideal position in the unit cell. Interestingly, the deviation from $x = 1/3$ is opposite for $YMnO_3$ (x increases below T_N) and $LuMnO_3$ (x decreases below T_N) [137, 182]. As pointed out by Fabrèges et al. [130], the deviation from $x = 1/3$ determines the sign of the magnetic coupling between Mn^{3+} spins in adjacent planes and the magnetic structure for different $RMnO_3$.

The magnetic structure of $LuMnO_3$ was discussed based on neutron scattering experiments. The proposed models for the magnetic order vary significantly among different publications. Koehler et al. [88] determined an intermediate angle of $\Phi = 55^\circ$ within the α model (Figure 3) with the magnetic symmetry $P\underline{6}_3$. In contrast, Katsufuji et al. [91] and Kozlenko et al. [152] suggested two possible spin configurations for $LuMnO_3$, $P6_3c\underline{m}$ (β model, $\Phi = 0^\circ$) or $P\underline{6}_3c\underline{m}$ (α model, $\Phi = 90^\circ$). The latter model is supported by the neutron study of Bieringer et al. [183]. The α model magnetic order in $LuMnO_3$ was also derived from SHG optical experiments [100] and it was concluded that $LuMnO_3$ apparently exhibits a spin reorientation from $P\underline{6}_3c\underline{m}$ to $P\underline{6}_3c\underline{m}$ magnetic symmetry with an intermediate phase ($P\underline{6}_3$) coexisting with the two other phases below 60 K. It is not clear why this spin reorientation has not been observed in neutron scattering experiments. The spatial coexistence of phases with different magnetic symmetry can make the correct determination of the Mn^{3+} spin order below T_N quite difficult.

Unlike in $LuMnO_3$, the spin reorientation in $ScMnO_3$ was detected in early neutron scattering experiments [179] and later confirmed by other neutron studies [95, 130]. While all neutron investigations agree about a smooth spin reorientation starting between 60 and 80 K and slowly progressing toward lower temperature, there is no consensus about the specifics of the magnetic order (α or β model). Bieringer et al. [179] assigned the $P\underline{6}_3$ magnetic symmetry with a spin angle of $\Phi = 80^\circ$ (close to $P\underline{6}_3c\underline{m}$) to the high-temperature phase and suggested a spin rotation within the α model to a low-temperature angle of $\Phi = 15^\circ$ (close to $P\underline{6}_3c\underline{m}$), the same type of spin reorientation as reported for $HoMnO_3$. Muñoz et al., however, described the magnetic order within the β model with the spin angle $\Phi = 0^\circ$ ($P6_3c\underline{m}$ symmetry) at high temperatures ($75 < T < 130$ K) and continuously increasing from 17° at 75 K to 54° at 1.8 K. In this model, the symmetry of the low-temperature phase would be $P6_3$. The SHG optical experiments support the α model with $P\underline{6}_3c\underline{m}$ below T_N coexisting with $P\underline{6}_3c\underline{m}$ below 60 K, and all three phases (including $P\underline{6}_3$) coexisting at the lowest temperatures within different regions of the same crystal [93, 100, 184].

It is interesting to note that the spin reorientation in $ScMnO_3$ is realized in a system of exclusively Mn^{3+} spins and no rare earth moment is involved, unlike in the sister compound $HoMnO_3$. Therefore, the change in the in-plane magnetic anisotropy has to be considered as the origin of those phenomena. In $ScMnO_3$, the magnetic anisotropy is less pronounced making this system more susceptible to spin reorientations and phases with intermediate spin angles Φ. The strong spin lattice interaction causes the structural distortions and the change of the Mn position in the unit cell, as reported in recent high resolution neutron studies [130]. The "softness" of $ScMnO_3$ with respect to an in-plane spin rotation is also reflected in the photoinduced control of the average Mn^{3+} spin angle at low temperature [180].

2.4. Multiferroic Properties and Phase Diagrams of $ErMnO_3$, $TmMnO_3$, and $YbMnO_3$. The multiferroic phase diagrams of $ErMnO_3$, $TmMnO_3$, and $YbMnO_3$ in *c*-axis magnetic fields and the associated magnetic orders were first proposed by Fiebig et al. [93, 102], as shown in Figure 31, based on SHG and Faraday rotation optical experiments. It is interesting that in the case of $ErMnO_3$, $TmMnO_3$, and $YbMnO_3$, the high-field phase assumes the $P6_3\underline{cm}$ symmetry which can be understood by the energy gain through the coupling of the external magnetic field to the *c*-axis magnetization [102]. In between the pure $P\underline{6_3}c\underline{m}$ and $P6_3\underline{cm}$ magnetic phases there is a region (grey area in Figure 31) showing hysteretic and irreversible effects resulting in a history dependence of the final state within a certain mode of field and temperature change [93]. The Néel temperatures of $ErMnO_3$, $TmMnO_3$, and $YbMnO_3$ slightly decrease with the external field up to about 40 kOe and than trace back to low temperatures and low fields resulting in the typical "nose" shape of the phase boundaries to the high-field phase (Figure 31).

In contrast to the results of Figure 31, bulk measurements of the magnetization and dielectric constant have shown that the phase boundary to the high-field phase extends to much higher magnetic fields, for example, above 140 kOe for $YbMnO_3$ [41]. A more detailed discussion of the anomalies of bulk physical properties of all three compounds, $ErMnO_3$, $TmMnO_3$, and $YbMnO_3$, is therefore warranted. Bulk measurements such as dc or ac magnetization and heat capacity can be utilized to detect the thermodynamic nature of the phase transitions. The dielectric constant is extremely sensitive to the magnetic transitions because of the strong spin lattice coupling in all hexagonal manganites. This was clearly demonstrated in Section 2.2.2 for $HoMnO_3$. The measurement of $\varepsilon(T, H)$, in combination with other physical quantities, is therefore an ideal tool to study the high-field phase diagrams of other $RMnO_3$.

The zero-field heat capacity of $ErMnO_3$ reveals two distinct peaks at $T_N = 80$ K and $T_{Er} = 2.4$ K, as shown in Figure 32(a). The dc magnetization χ_c measured at 200 Oe is shown in Figure 32(b). A subtle slope change of χ_c at T_N (right inset) and a strong rise at T_{Er} indicate the onset of antiferromagnetic Mn^{3+} spin order and another low-temperature change of the magnetic orders of Mn/Er moments, respectively. The anomaly of the heat capacity at T_N, similar to the one shown in Figure 32(a), was also reported earlier [185]. Sugie et al. [105] found a magnetic hysteresis loop at low temperatures indicative of a possible ferro- or ferrimagnetic moment, however, no such irreversibility could be detected in our *M*-*H* measurements. The dielectric constant of $ErMnO_3$, shown in Figure 32(c), displays the kink-like anomaly at T_N, as reported earlier [105].

The phase diagram of $ErMnO_3$ in external *c*-axis magnetic fields can be derived by tracing the anomalies of magnetization and dielectric constant as functions of temperature and field. The low-temperature region can be studied through magnetization measurements as function of the field (shown in Figure 34(a)). $M(H_c)$ increases sharply at very low fields and experiences a sudden change of slope at 450 Oe (1.85 K) indicating a metamagnetic phase transition. With increasing temperature the critical field for this transition decreases to 270 Oe at 2.3 K, as shown in the inset of Figure 34(a). No transition is observed in the low field range above the critical temperature of 2.4 K (T_{Er}). At higher magnetic fields, a second steep increase of $M(H_c)$ signals a second phase transition (see Figure 34(a)). The critical field of this transition increases quickly with temperature and is already above the maximum field of 50 kOe at about 14 K. Note the curves of $M(H_c)$ shown in Figure 34(a) include data collected with increasing as well as decreasing field and no magnetic hysteresis is observed, unlike in the previous publication by Sugie et al. The absence of any hysteretic behavior upon increasing or decreasing temperature or field was also confirmed in a recent study of the magnetization of $ErMnO_3$ to temperatures as low as 80 mK [186]. Furthermore, the first transition at fields below 1000 Oe (inset of Figure 34(a)) was not reported in [105].

The second phase transition in the high-field region of the phase diagram ($H_c > 7$ kOe) is also manifested in temperature dependent magnetic susceptibility data, shown on a logarithmic scale in Figure 34(b). The Néel temperature T_N, indicated by the dashed vertical line, decreases only very little at higher fields. At low temperatures, however, a clear kink of $\chi_c(T)$ identifies a second phase boundary, labeled $\widetilde{T}_N$ in Figure 34(b). The anomaly at $\widetilde{T}_N$ develops at magnetic fields above 7 kOe and moves quickly to higher temperature with increasing field H_c. The field and temperature dependent data of the magnetic susceptibility recently published [186] are in good agreement with our results shown in Figure 34.

The high-field phase diagram of $ErMnO_3$ is revealed through dielectric constant measurements. Since $\varepsilon(T)$ exhibits a sharp kink at T_N, it is expected that this anomaly can be traced to higher magnetic fields (note that the magnetization measurements in Figure 34 are limited to 50 kOe). Upon closer inspection of $\varepsilon(T, H_c)$, a second anomaly in form of a sharp peak is revealed above a magnetic field of 9 kOe. This peak, shown in the $\varepsilon(H_c)$ data of Figure 34(a), shifts to higher temperature with increasing field and it's position coincides with the anomalies of the magnetization (Figure 34). It therefore is the signature of the dielectric constant in crossing the $\widetilde{T}_N$ phase boundary which can be traced to much higher fields. At lower magnetic fields, $\widetilde{T}_N$ is also defined by the peak of $\varepsilon(T)$ shown in the inset of Figure 34(b). At high magnetic fields, $H_c > 70$ kOe, the two

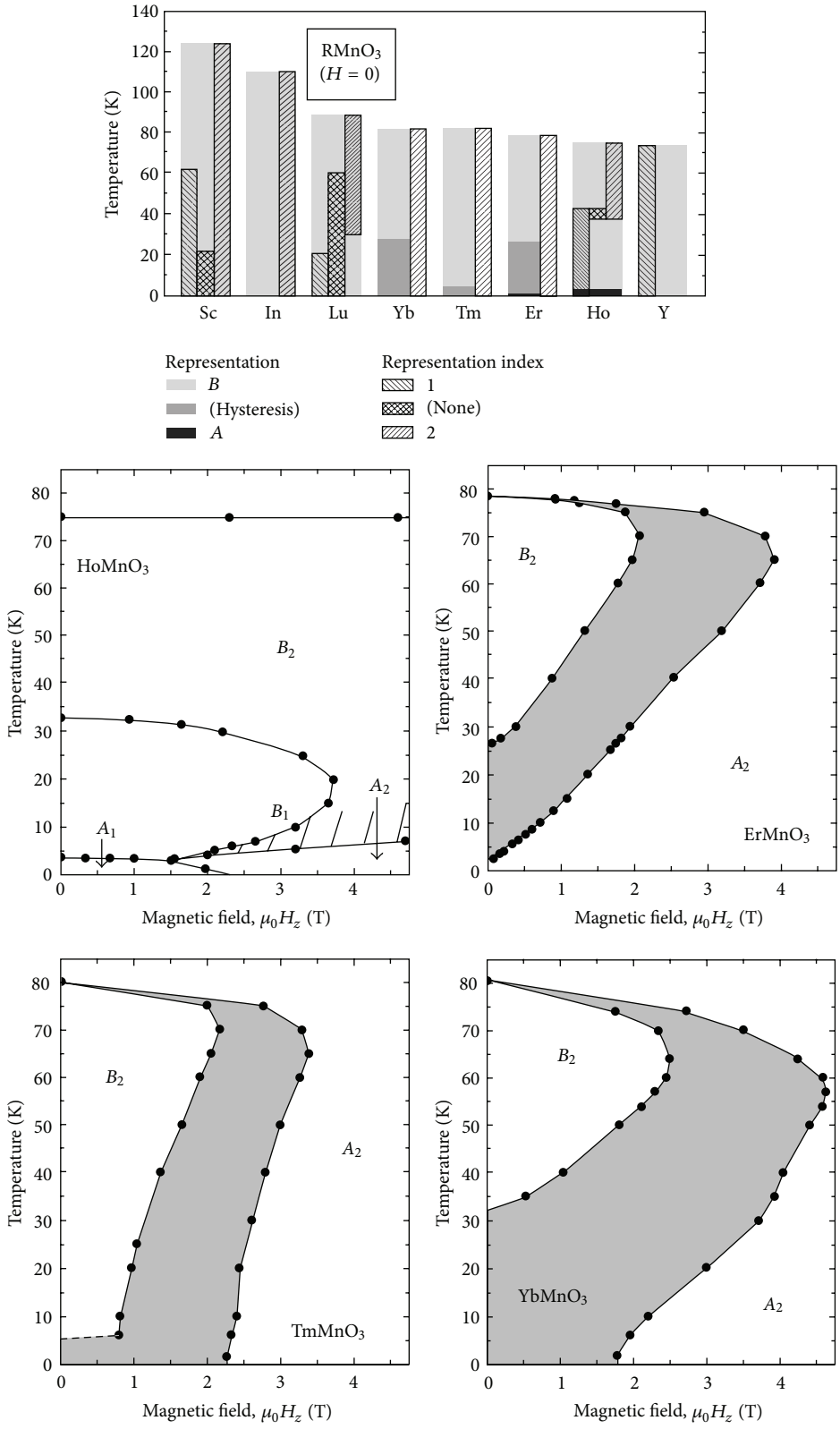

Figure 31: Magnetic phase diagrams and magnetic symmetries of $RMnO_3$ (R = Ho, Er, Tm, Yb) as derived from SHG optical experiments. The symbols A_i and B_i denote the following magnetic space groups: $A_1 = P6_3cm$, $A_2 = P6_3\underline{cm}$, $B_1 = P\underline{6}_3\underline{cm}$, and $B_2 = P\underline{6}_3\underline{c}m$. Reprinted with permission from [93].

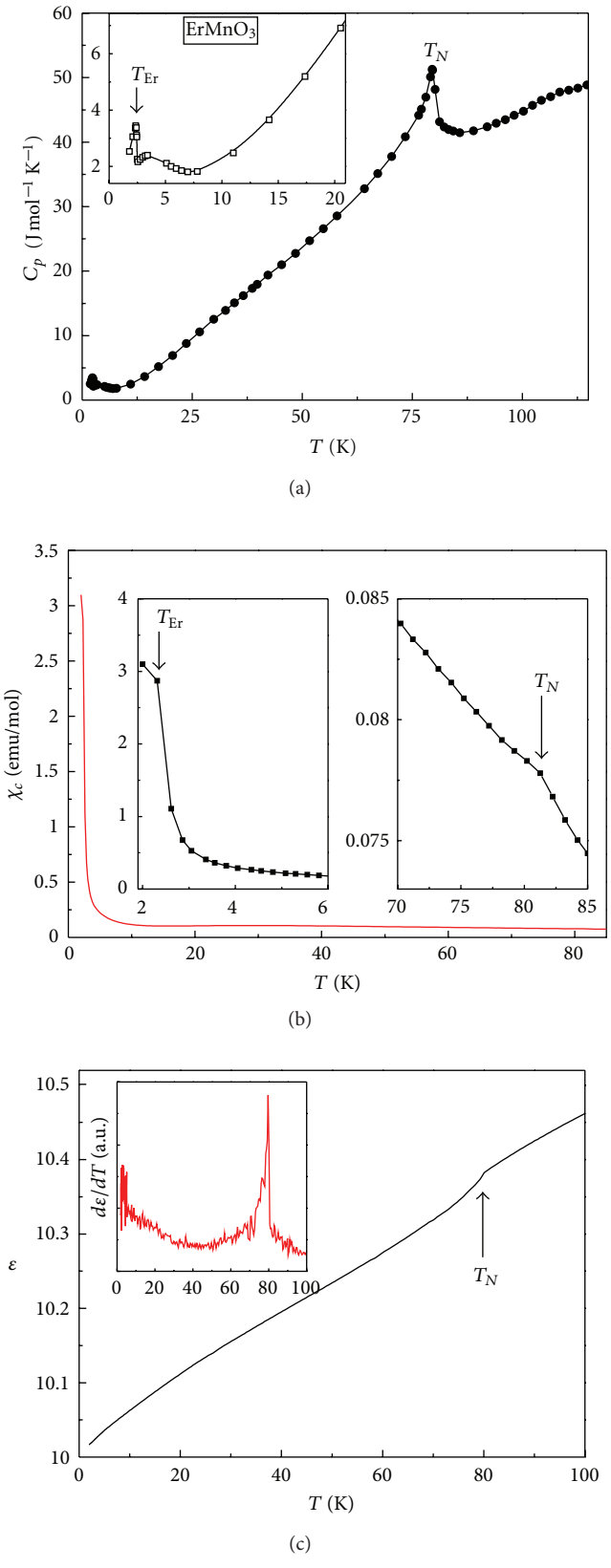

FIGURE 32: (a) Heat capacity at zero magnetic field, (b) magnetization at $H_c = 200$ Oe, and (c) dielectric constant of multiferroic $ErMnO_3$. The two transitions at T_N and T_{Er} are marked by vertical arrows. The inset to (c) shows the derivative, $d\varepsilon/dT$.

transition temperatures T_N and $\widetilde{T}_N$ are detected as small kink-like anomalies of $\varepsilon(T)$ in the main panel of Figure 34(b). With increasing field, T_N decreases while $\widetilde{T}_N$ increases and both temperatures eventually merge above 125 kOe.

The resulting phase diagram is shown in Figure 35. The magnetically ordered phase below T_N exhibits a remarkable stability with respect to the field H_c, at least in the intermediate temperature range, extending up to 130 kOe (unlike earlier reports [102]). The phase boundaries given in Figure 35 have been confirmed in recent studies up to 40 kOe [186]. The low-field and low-temperature section of the phase diagram is dominated by two transitions separating three different magnetic phases and the details are shown on an enlarged scale in the inset of Figure 35. Meier et al. [186] suggested another phase boundary based on the inflection point observed in the temperature dependence of the dc susceptibility $\chi(T)$. This phase boundary is shown as the red dotted line in the inset of Figure 35. While the magnetization data shown in Figure 33(b) indeed show the inflection point of the susceptibility near 4 K, it is not clear whether this feature provides clear evidence for an additional phase transition since the inflection point of $\chi_c(T)$ (minimum of dM/dT) extends to even higher fields at about the same temperature of 4 to 5 K (see 40 kOe and 50 kOe data of dM/dT in the inset of Figure 33(b)). The minimum of dM/dT, as obtained from our magnetization measurements, is shown as the blue dotted line in the high-field region ($H_c > 20$ kOe). Dielectric constant data $\varepsilon(T)$ measured at different magnetic fields between 3 kOe and 40 kOe do not indicate any anomaly at the temperature defined by the inflection point of $\chi_c(T)$. Therefore, it is not clear if the phase boundary proposed by Meier et al. [186], shown as the red dotted line in Figure 35, indicates a real phase transition associated with distinct changes of physical quantities or rather a cross-over with a smooth change of the magnetic structure.

The magnetic orders and symmetries in the various phases of $ErMnO_3$ are still a matter of discussion. Koehler et al. [88] in their early work determined the magnetic structure of the Mn^{3+} spins within the α model with a spin angle to the hexagonal a-axis as 70° and independent of temperature corresponding to the $P6_3$ magnetic symmetry (close to $P6_3cm$). Park et al. [187] found two possible solutions fitting their neutron spectra equally well, $P6_3cm$ (α model) or $P6_3cm$ (β model). Fiebig et al., using optical SHG methods, identified the magnetic space group of $ErMnO_3$ as $P6_3cm$ at all temperatures below T_N [93, 100].

In a recent work [186], the discussion of magnetic symmetries was extended to include the low-temperature phase (below T_{Er}) and the phases induced by c-axis magnetic fields. Based on bulk magnetic measurements, SHG optical, and neutron scattering studies, the following development of magnetic structures with temperature and field was proposed: The magnetic order in zero magnetic field sets in below T_N with the magnetic space group $P6_3cm$, similar to other $RMnO_3$. The interaction with the Er^{3+} f-moments results in the partial AFM order of the Er spins on crystallographic 4b sites whereas the Er moments on 2a sites remain paramagnetic. This is consistent with the magnetic symmetry of the

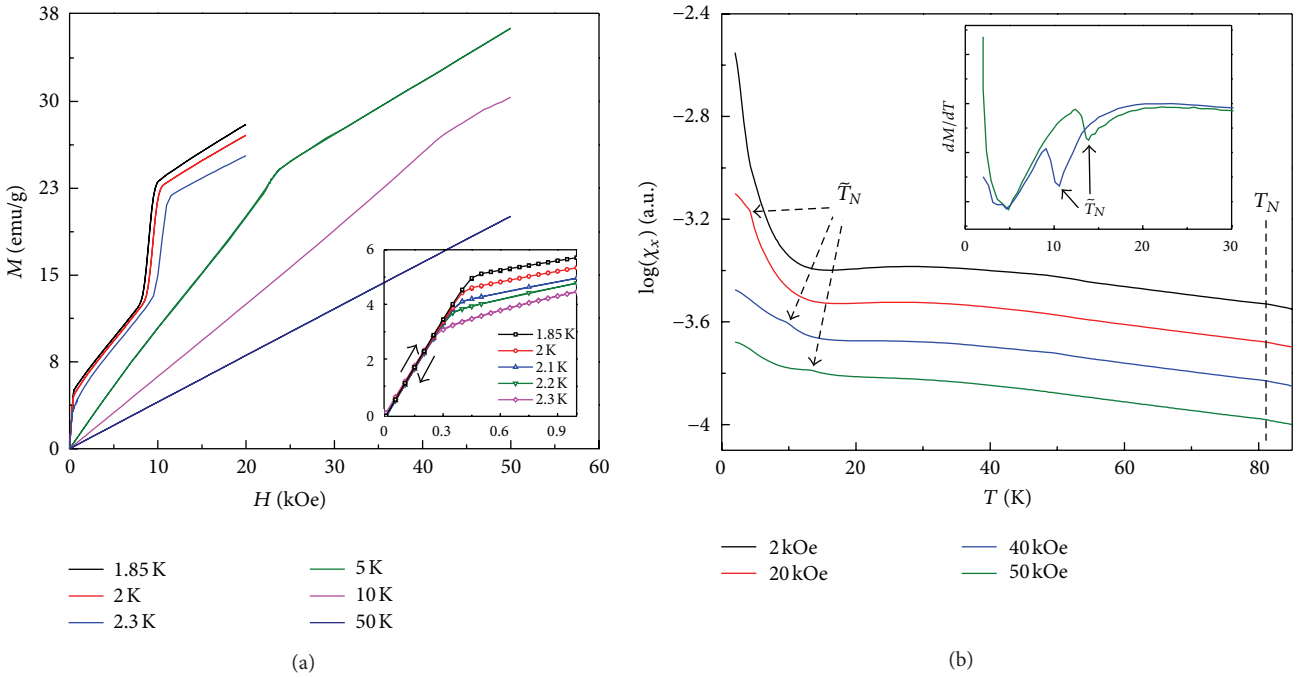

FIGURE 33: Anomalies of the magnetization defining different phase boundaries of $ErMnO_3$ up to a field of 50 kOe. (a) M versus H data at various temperatures and (b) dc susceptibility on a logarithmic scale at various fields. The different curves in (b) coincide above about 50 K, but are vertically offset for better clarity. The inset to (b) shows the derivative dM/dT with sharp minima at $\tilde{T}_N$ and another minimum near 4 to 5 K.

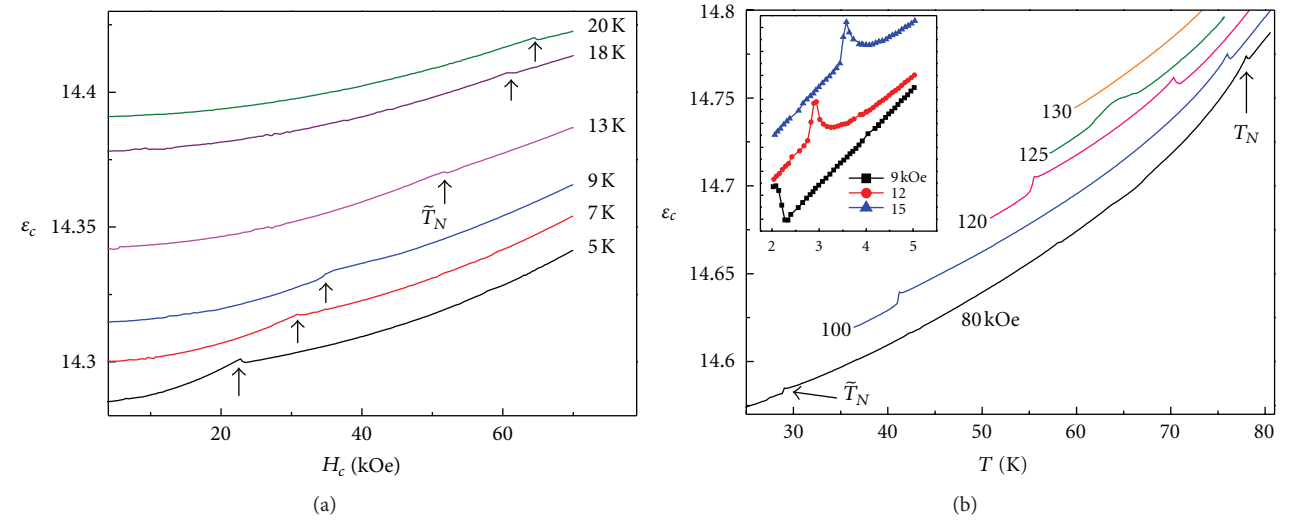

FIGURE 34: (a) Anomalies of the isothermal dielectric constant $\varepsilon(H_c)$ at different temperatures. The arrows show the anomaly at the $\tilde{T}_N$ phase boundary. (b) Dielectric constant $\varepsilon(T)$ at high fields. The two transitions at T_N and $\tilde{T}_N$ are marked for the 80 kOe data. The different curves in (b) are vertically offset for better clarity. The inset to (b) shows the $\varepsilon(T)$ anomaly near $\tilde{T}_N$ at low magnetic fields.

Mn spins. At low temperatures, the 4f exchange interaction of Er^{3+} on 2a sites becomes stronger, resulting in their magnetic order according to the $P6_3\underline{cm}$ magnetic symmetry, triggering a simultaneous spin reorientation of the Mn^{3+} spin system. This could explain the phase transition at T_{Er} into the FIM_1 phase. The FIM_1 phase is ferrimagnetic since the magnetic moments of the Er^{3+} on 2a and 4b sites are counter aligned along the c-axis but they do not completely compensate each other. The transition from the FIM_1 phase to the FIM_2 phase with increasing magnetic fields is considered to be a change from a multi domain (FIM_1) to a single domain state (FIM_2). At higher fields (crossing the phase boundary $\tilde{T}_N$) all Er^{3+} moments are ferromagnetically aligned along the c-axis (FM phase) without any change of the Mn^{3+} spin arrangement.

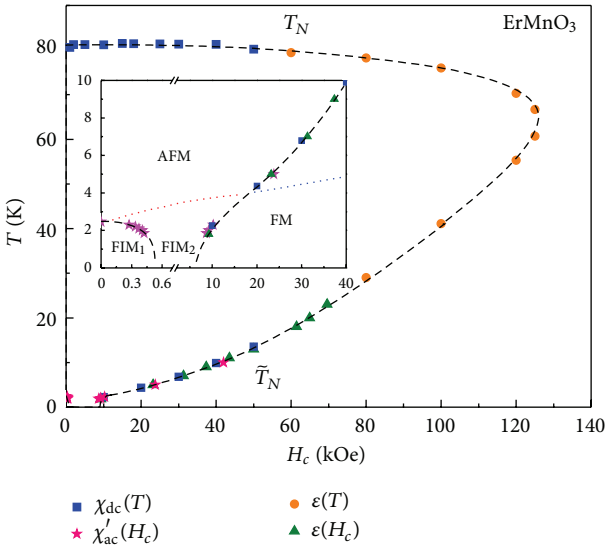

FIGURE 35: Magnetic phase diagram of $ErMnO_3$ in c-axis fields up to 140 kOe. The phase boundaries are defined by distinct anomalies of the magnetic dc and ac susceptibilities, χ_{dc} and χ'_{ac}, as functions of temperature and field, as well as from the kink anomalies of the dielectric constant $\varepsilon(T, H_c)$. The dashed lines are a guide for the eye. The inset shows the low-temperature section on an enlarged scale (note the different scales for the low and high fields). The red dotted line shows the additional phase boundary proposed by Meier et al. [186]. The blue dotted line shows the minimum of dM/dT in the high-field section. The labels for the different phases, AFM, FM, FIM_1, and FIM_2, are the same as used in [186].

Note that the $P6_3\underline{cm}$ magnetic symmetry is compatible with a ferromagnetic moment along the c-axis.

The phase diagram of $ErMnO_3$ at low temperatures is nearly as complex as that of $HoMnO_3$ due to the magnetic exchange between rare earth moments and manganese spins which also have been shown to affect the magnon spectra and crystal field transitions in optical experiments [188]. On the other hand, there is also evidence for strong spin lattice interactions as, for example, shown in the phonon hardening below T_N [166]. This could explain the anomalies of the dielectric constant at the various phase boundaries, similar to other rare earth manganites.

$TmMnO_3$ was less intensively studied in the past. The magnetic order of Mn^{3+} spins sets in at $T_N = 84$ K and the symmetry was determined as $P6_3\underline{c}m$ [93, 100]. The gradual polarization of the Tm^{3+} moments on 4b sites was detected below T_N in ^{169}Tm Mössbauer experiments [189]. The measured temperature dependence of the ^{169}Tm hyperfine field at the 4b site could quantitatively well fitted by a crystal field model with the lowest level split by the molecular field arising from the Mn-Tm exchange interaction. The Néel temperature obtained is consistent with magnetic susceptibility and dielectric measurements [41, 177, 190]. There is no evidence so far of an additional phase transition which could be associated with a possible Tm^{3+} moment order on 2a sites and a Mn^{3+} spin rotation, as observed in $HoMnO_3$, $ErMnO_3$, and $YbMnO_3$. The dielectric constant at zero magnetic field shows the kink at T_N, but no further anomaly at lower temperatures (Figure 36(a)).

With increasing magnetic field oriented along the c-axis, the kink anomaly at T_N shifts minutely to lower temperature. Above 42 kOe, a second step of $\varepsilon(T)$ at low temperatures indicates another phase boundary, similar to the high-field transition in $ErMnO_3$ (Figure 36(a)). The critical temperature, $\tilde{T}_N$, increases with the field and merges with T_N just below 110 kOe and about 65 K. The low-temperature anomaly of $\varepsilon(T, H_c)$ is clearly seen as a sharp step in the field-dependent data of Figure 36(b). The phase diagram, derived from the dielectric data is shown in Figure 37. Similar to $ErMnO_3$, the stability of the magnetic order below T_N extends to much higher fields as earlier proposed [93]. The fact that there is only one transition at the lowest temperatures with increasing magnetic field indicates that the $P6_3\underline{cm}$ magnetic structure with the antiferromagnetic order of Tm(4b) moments is very stable and the order of the Tm(2a) moments with the reorientation of the Mn spin system requires significantly higher fields (>42 kOe) than in $ErMnO_3$.

The bulk magnetic and dielectric properties of $YbMnO_3$ were studied by Sugie et al. [105]. Besides the onset of magnetic order at $T_N = 90$ K, a second phase transition was found below 5 K and at magnetic fields above 30 kOe a metamagnetic transition was detected in field-dependent magnetization data. The details of the magnetic phase diagram, however, have only been revealed through high-field magnetic and dielectric measurements [41]. The temperature dependence of χ_c at low field (100 Oe) indeed shows a sharp increase at 4 K (see inset in Figure 38(a)) indicating a possible ferrimagnetic moment arising from the ytterbium sublattice order, in analogy to $ErMnO_3$. This transition is marked by a sharp peak of the heat capacity, in addition to the λ-shaped peak at T_N (Figure 39). The isothermal magnetization as function of the c-axis field, shown in Figure 38(a), is very similar to the results obtained for $ErMnO_3$. The steep increase of the magnetization for small fields is typical for the FIM_1 phase discussed in [186] for $ErMnO_3$.

The sudden decrease of the $M(H_c)$-slope defines the first phase boundary, T_{Yb}. The step-like increase of $M(H_c)$ above 30 kOe could be understood as the transition to the complete ferromagnetic alignment of the Yb^{3+} moments. The corresponding phase boundary is labeled $\tilde{T}_N$. The two low-temperature transitions are also reflected in distinct anomalies of the magnetization, $M(T)$, shown in Figure 38(b). In the low-field range ($H_c < 1$ kOe), the sharp increase of $M(T)$ near 4 K signals the onset of the ferrimagnetic order of the Yb^{3+} moments. At magnetic fields betyween 1 and 30 kOe, however, no sharp anomaly is detected in $M(T)$. A broad maximum and a smooth drop to lower temperature is the characteristic feature of $M(T)$. At higher field, another sharp increase of $M(T)$ indicates the transition into the ferromagnetic phase with all Yb^{3+} moments aligned with the field. Comparing the magnetic moments of the 40 kOe and 50 kOe data in Figure 38(b), it becomes obvious that saturation is reached at the lowest temperatures. This is consistent with the proposed ferromagnetic state. The fact that no significant difference between field-cooled and

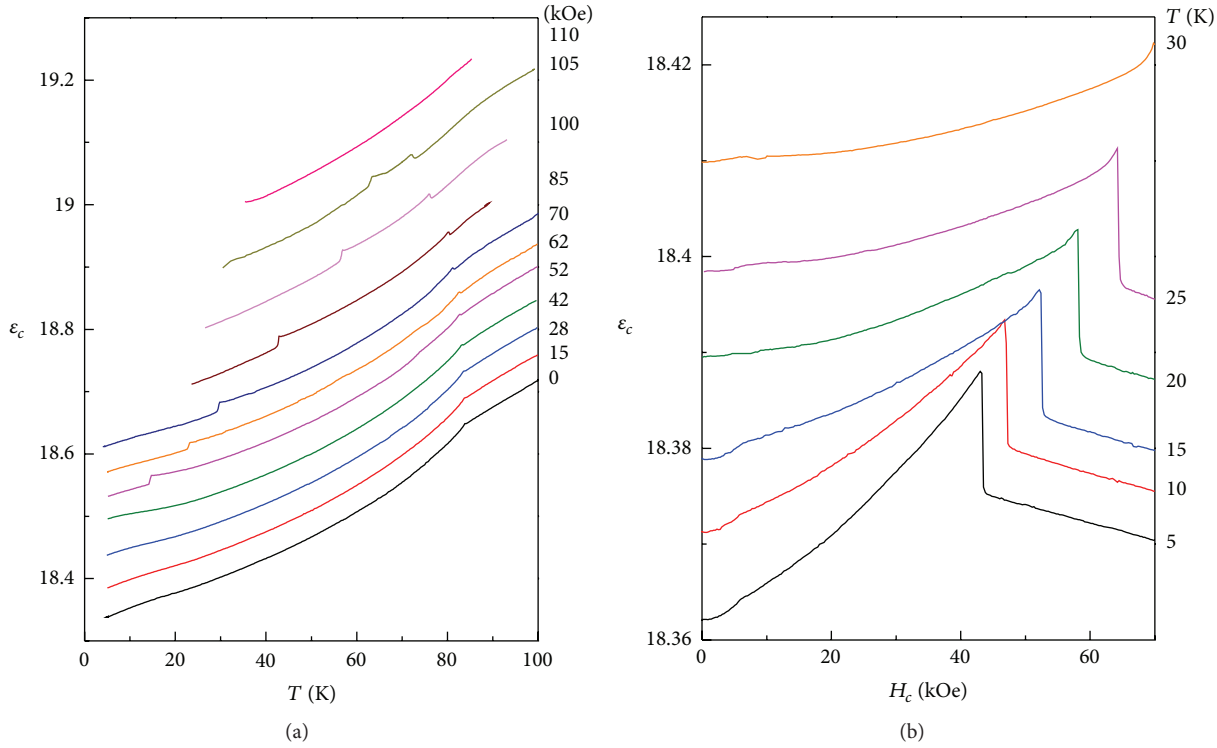

FIGURE 36: Temperature and field dependence of the dielectric constant of $TmMnO_3$. (a) $\varepsilon(T)$ at different fields. (b) Isothermal data $\varepsilon(H_c)$.

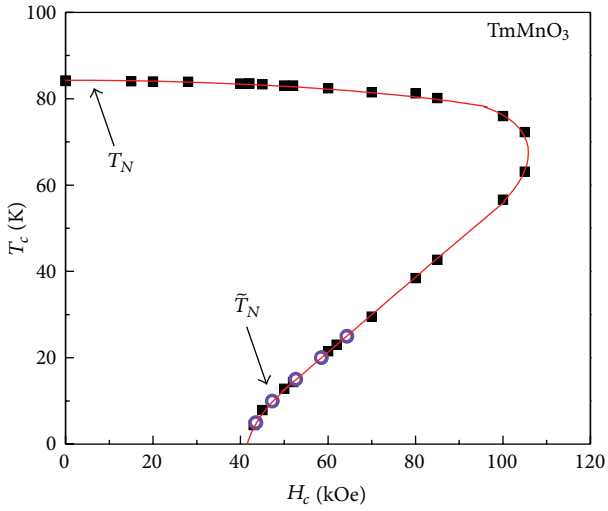

FIGURE 37: Magnetic phase diagram of $TmMnO_3$ in c-axis fields up to 120 kOe. The phase boundaries are defined by distinct anomalies of the dielectric constant $\varepsilon(T, H_c)$, shown in Figure 36. The red lines are a guide for the eye. The closed and open symbols are refer to anomalies of $\varepsilon(T)$ and $\varepsilon(H)$, respectively.

zero field-cooled data was observed in this high-field range indicates that the magnetic field is strong enough to create a single domain state. Some of the results for the temperature and field dependence of the magnetization discussed above have been confirmed in recent studies [94, 124, 191].

The complete phase diagram of $YbMnO_3$ is derived from thermodynamic, magnetic, and dielectric measurements in a similar way as for $ErMnO_3$ and $TmMnO_3$ above and it is shown in Figure 40. The similarity to $ErMnO_3$ is obvious, however, the antiferromagnetic phase extends to much higher fields, beyond the limit of 140 kOe of this investigation. The phase assignment could be similar to $ErMnO_3$. SHG optical measurements favor the $P6_3cm$ magnetic symmetry below T_N. The low-temperature transition almost certainly does involve the order of Yb^{3+} moments. Following the same scenario proposed for $ErMnO_3$ [186], we can assume that the f-moments of the Yb on 4b sites are systematically polarized according to the $P6_3cm$ antiferromagnetic structure shown in Figure 25(d). The phase transition at T_{Yb} involves the order of the Yb^{3+} moments on 2a sites antiparallel to the 4b moments and a reorientation of the Mn^{3+} spins resulting in the ferrimagnetic order of the f-moments according to the $P6_3cm$ magnetic symmetry. At higher magnetic fields, the flop of the Yb^{3+} moments at 2a positions results in the alignment of all f moments with the external field at $\tilde{T}_N$.

The physical picture of the magnetic orders of Mn^{3+} spins and Yb^{3+} moments on 4b and 2a sites was first proposed by Fabrèges et al. based on a comprehensive study combining magnetization measurements, ^{170}Yb Mössbauer, and neutron scattering experiments. The ordered magnetic moments of Mn, Yb(4b), and Yb(2a) could be separately determined and fit to a mean field model. According to the model, the Yb(4b) moment order below T_N is driven by the molecular field generated by the Mn spins and the Yb(2a) order below

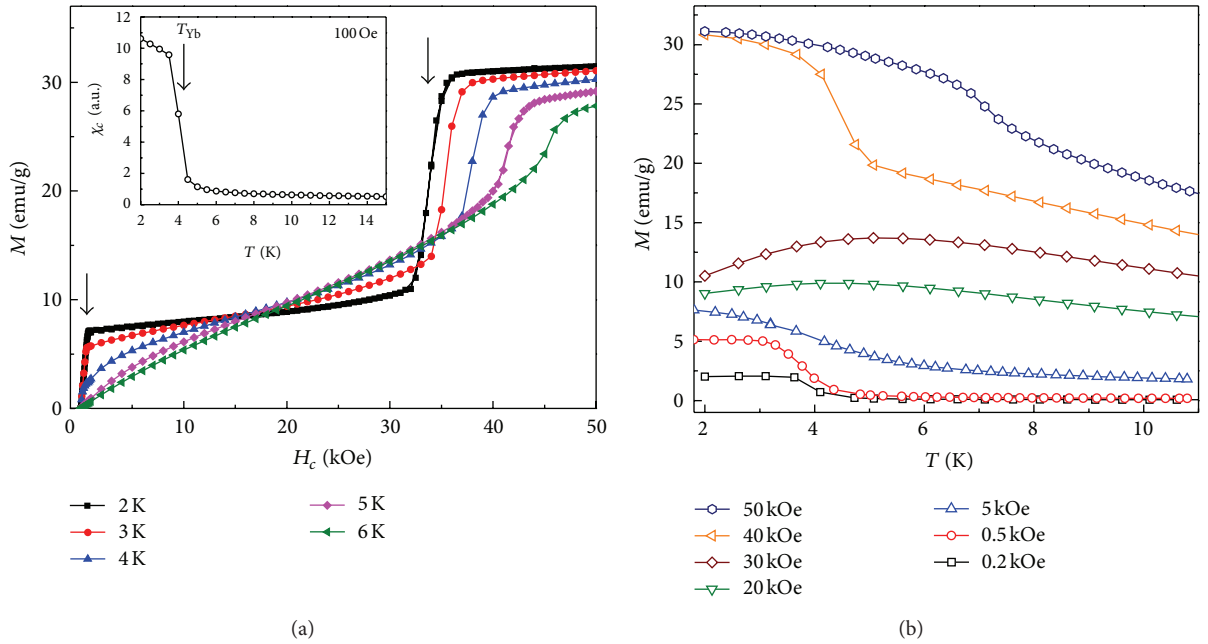

FIGURE 38: (a) Isothermal magnetization of $YbMnO_3$ as function of c-axis fields. The two vertical arrows indicate the two phase transitions. The inset shows the temperature dependence of the susceptibility measured at 100 Oe. The sharp increase at $T_{Yb} = 4$ K is due to the ferrimagnetic order of the Yb^{3+} moments on 2a and 4b crystallographic sites. (b) Temperature dependence of the magnetization in fields up to 50 kOe. The low- and high-field transitions are well defined by sharp increases of $M(T)$.

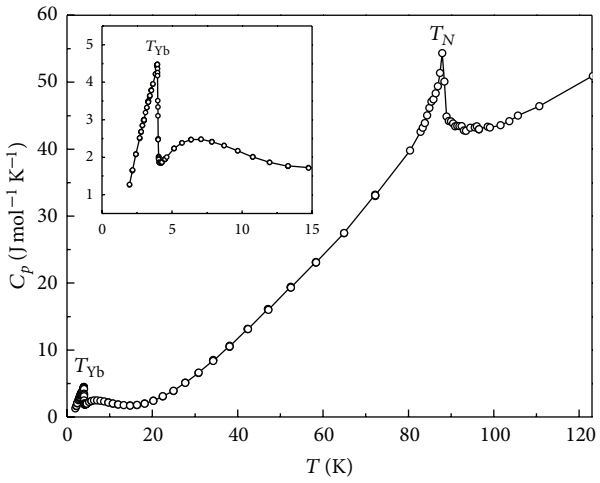

FIGURE 39: Heat capacity of $YbMnO_3$ at zero magnetic field. The λ-shaped anomaly at T_N indicates the second order transition. At about 4 K, the sharp peak (enlarged in the inset) results from the ferrimagnetic order of the Yb^{3+} moments on 2a and 4b sites.

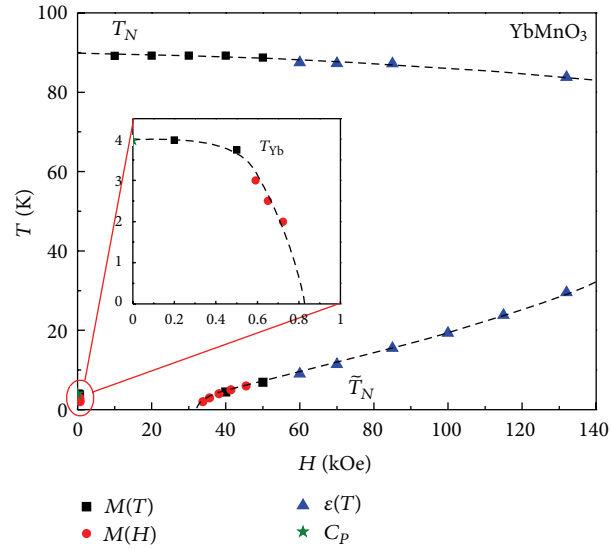

FIGURE 40: Magnetic phase diagram of $YbMnO_3$. The inset shows the low-field phase boundary on an enlarged scale.

T_{Yb} results from the Yb-Yb exchange interactions. The order of Mn spins and rare earth moments at 4b and 2a sites has been studied independently by Salama et al., arriving at similar conclusions [192, 193].

2.5. Metastable Hexagonal $DyMnO_3$. The hexagonal structure of $DyMnO_3$ is metastable and it can be synthesized using special chemical techniques [92, 194]. In the hexagonal form, $DyMnO_3$ is ferroelectric, similar to all other hexagonal manganites. The Dy^{3+} ion is the largest in the series, resulting in the most expanded structure with lattice constants a and c exceeding those of all other hexagonal $RMnO_3$. A reduction of the magnetic exchange couplings between the different ions can be expected and it is not surprising that the Néel temperature of $DyMnO_3$ ($T_N = 57$ K) is the lowest among all $RMnO_3$ [195]. The magnetic properties of $DyMnO_3$ were first

studied by Ivanov et al. [194]. The most notable feature was a sharp peak in the ac magnetic susceptibility observed at $T_{Dy} \approx 6$ K and a remanent magnetization below this temperature, indicating a possibly ferrimagnetic state at low T. The low-temperature ferrimagnetic phase was found to extend to higher temperature in external magnetic fields oriented along the c-axis.

Subsequent studies of the magnetic properties are in qualitative agreement with the original data [111, 195], however, the values for T_N and T_{Dy} scatter among different investigations. Harikrishnan et al. [195] derived $T_N = 57$ K and $T_{Dy} = 3$ K from magnetic and heat capacity data. Nandi et al. [111] found $T_N = 68$ K and $T_{Dy} \approx 8$ K. The differences may be due to small variations in the chemical composition of the samples used by different groups. The magnetic order of the Dy^{3+} moments was studied using X-ray resonant magnetic scattering [111]. The magnetic symmetry in the temperature range between T_N and T_{Dy} was determined as $P6_3\underline{cm}$ (Γ_3), with the Dy^{3+} moments all parallel to the c-axis. It is interesting that this symmetry is different from the magnetic symmetry of $ErMnO_3$, $TmMnO_3$, and $YbMnO_3$, but it coincides with the symmetry of $HoMnO_3$ below the spin reorientation temperature, T_{SR}. For the low-temperature phase, the $P6_3\underline{cm}$ (Γ_2) magnetic symmetry which allows for a ferromagnetic moment was proposed. It should be noted that the X-ray resonant magnetic scattering experiment only determines the magnetic symmetry of the ordered Dy sublattices, with no information about the magnetic structure of the Mn^{3+} spins.

The magnetic symmetry of the Mn sublattice was studied through SHG optical measurements as well as neutron scattering experiments and compared with the magnetic symmetry of the Dy sublattice in the temperature-field phase diagram of $DyMnO_3$ [196]. Interestingly, different magnetic symmetries have been found for Mn and Dy moments in the temperature range between T_N and T_{Dy} in zero magnetic field. The magnetic space group for the Mn^{3+} spins was determined as $P6_3\underline{c}m$ while the space group for the Dy^{3+} moment order was $P6_3\underline{cm}$, confirming the earlier studies [111]. This indicates that the 3d-4f coupling between the order parameters describing the Mn^{3+} spin order and the Dy^{3+} moments is weaker than assumed. To understand the coexistence of two order parameters with different symmetry, Wehrenfennig et al. [196] proposed the coupling between 3d spins and 4f moments to be of the biquadratic form. This biquadratic interaction can trigger the simultaneous order of the Mn^{3+} spin and Dy^{3+} moment systems with different magnetic symmetries. The proposed mechanism would introduce novel physics into the basic understanding of multiferroic hexagonal manganites.

In the low-temperature phase ($T < T_{Dy}$) and in magnetic fields applied along the c-axis the order of the Mn^{3+} spins was found to follow the same magnetic symmetry as the Dy^{3+} moments, namely $P6_3\underline{cm}$. The high-field magnetic symmetry appears reasonable in view of the fact that $P6_3\underline{cm}$ allows for a ferromagnetic moment along the c-axis which is certainly stabilized by the external field.

2.6. $InMnO_3$: A Paraelectric Hexagonal Manganite. $InMnO_3$ was synthesized in 1992 [197] and the structure was determined to be hexagonal with space group $P6_3cm$, similar to other $RMnO_3$ discussed above [89]. First magnetic measurements have shown a clear anomaly at $T_N = 120$ K. The 120 K transition was identified as the onset of magnetic order through neutron scattering experiments. Two more anomalies of the magnetic susceptibility at 40 K, and 15 K, observed at low fields, did disappear in moderate magnetic fields [89, 198, 199]. Based on the temperature dependence of different neutron scattering peaks and the additional anomalies of the susceptibility at lower temperatures, Greedan et al. suggested the possible existence of spin reorientation transitions. However, the intrinsic nature of those low-temperature anomalies has been questioned and attributed to possible impurity phases since high-pressure synthesized samples of $InMnO_3$ did not provide support for additional phase transitions below T_N [200]. A weak ferromagnetic-like hysteresis was reported in field-dependent magnetization measurements at low temperature. The phase transition at 120 K is clearly supported by heat capacity measurements showing a distinct peak at T_N [200, 201]. The low-frequency dielectric constant exhibits a kink at T_N, similar to other hexagonal manganites, which is an indication of the strong interaction of the spins with the lattice.

The existence of ferroelectricity in $InMnO_3$ is a matter of dispute. Based on the structural data derived from neutron scattering experiments [89], Abrahams estimated the ferroelectric transition temperature as $T_c \approx 540$ K [202]. Dielectric and P-E hysteresis measurements have been interpreted as evidence for a ferroelectric transition at 465 K [199]. The origin of the suggested ferroelectric phase in $InMnO_3$ was proposed to be an intra-atomic $4d_{z^2}$-$5p_z$ orbital mixing of In and a covalent bonding ($4d_{z^2}$(In)-$2p_z$(O)) along the c-axis [203]. However, Belik et al. [200, 201] have not found any changes of the dielectric permittivity, the number of phonon excitations, or other quantities sensitive to structural changes at high temperatures up to 900 K, questioning the possible existence of a structural (ferroelectric) phase transition. The relaxor-like property of the P-E hysteresis loop was reproduced and attributed to extrinsic, nonferroelectric effects like high-loss dielectric behavior caused by defect-induced conductivity.

The lattice parameters of $InMnO_3$, as determined from X-ray and neutron scattering experiments [89, 200, 204], deviate significantly from other hexagonal $RMnO_3$. While the lattice parameter of all hexagonal $RMnO_3$, including $ScMnO_3$, are a linear function of the R^{3+} ionic radius, a and c of $InMnO_3$ deviate significantly with a and c found to be clearly smaller and larger, respectively, as expected from the linear dependence [89]. The large c-axis length suggests a reduced magnetic interplane exchange coupling. This effect is further enhanced by frustration effects due to the almost ideal position of the Mn^{3+} ion in the unit cell ($x_{Mn} \approx 1/3$). The two possible exchange paths between Mn^{3+} ions in neighboring planes are therefore almost identical, increasing the magnetic frustration between spins of neighboring planes.

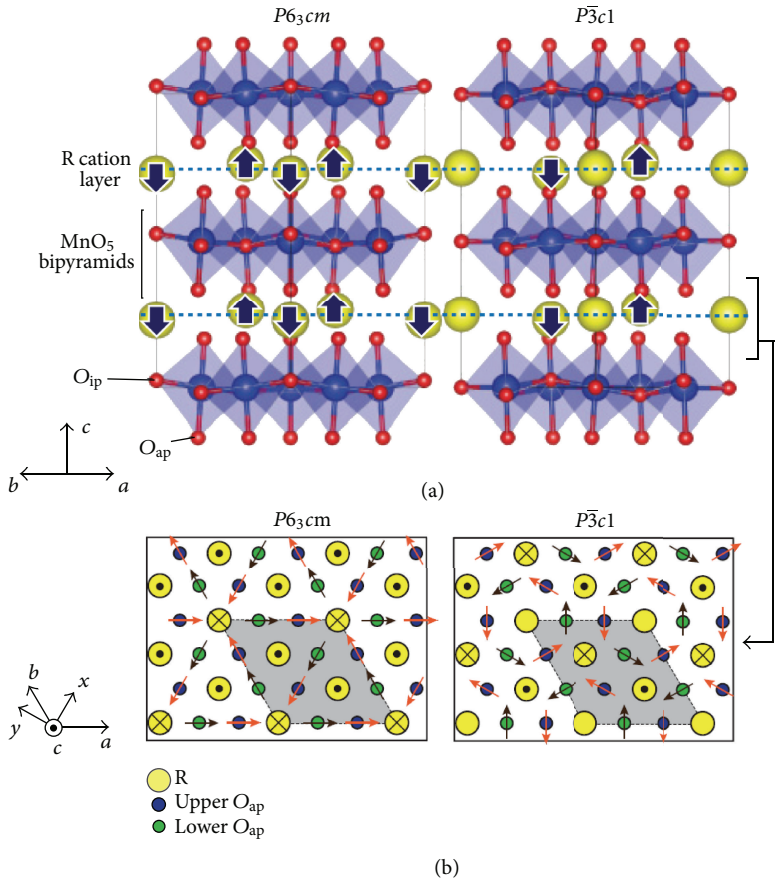

FIGURE 41: Comparison of the two possible structure models of $InMnO_3$, $P6_3cm$ (left) and $P\bar{3}c1$ (right). The fat vertical arrows in (a) show the displacements of the In^{3+} from their ideal positions. (b) represents a sketch of the Mn^{3+} spin order. Reprinted with permission from [205].

In contrast to other hexagonal $RMnO_3$, the magnetic order below T_N causes a doubling of the unit cell along the c-axis [89]. High resolution neutron scattering experiments are consistent with the doubling of the magnetic unit cell, the onset of magnetic order at 120 K, and the absence of any further spin reorientation at lower temperatures [204]. The magnetic symmetry of the ordered Mn^{3+} spins was determined to be either Γ_2 or Γ_4 (Figure 4), with the spins of two subsequent unit cells along the c-axis reversed by 180°. Above T_N, a strong diffuse scattering indicates the presence of a significant amount of two-dimensional spin fluctuations which supports the conjecture that $InMnO_3$ appears to be the most frustrated system among the hexagonal $RMnO_3$ compounds. The 2D short range correlations of the Mn^{3+} spins arise at much higher temperatures, however, 3D long range order is stabilized only at lower temperature by the weak interplane magnetic interactions. The nature of these interactions was discussed by Fabrèges et al. [204] and they were attributed to long-range pseudodipolar interactions stabilizing the magnetic order along the c-axis with the modulation vector $\vec{q} = (0, 0, 1/2)$.

The possible absence of ferroelectricity in $InMnO_3$ seems to be incompatible with the polar space group $P6_3cm$ which was used to fit numerous X-ray diffraction and neutron scattering data. However, Rusakov et al. [201] pointed out that the centrosymmetric, trigonal space group $P\bar{3}c1$ (No. 165) could also be used to fit their X-ray spectra with almost the same R values as the polar group $P6_3cm$. This motivated Kumagai et al. [205] to revisit and study the structure and polarization property of $InMnO_3$ combining X-ray diffraction, piezoelectric force microscopy, and optical SHG measurements with density functional calculations. Based on the calculated lower energy of the $P\bar{3}c1$ structure, the authors concluded that the actual lattice symmetry of $InMnO_3$ is not $P6_3cm$ but rather $P\bar{3}c1$. Furthermore, no evidence for ferroelectricity or ferroelectric domains was found in SHG and piezoelectric force measurements. The two structures under discussion are shown in Figure 41 (Figure 1 in [205]). The main difference between the $P6_3cm$ and $P\bar{3}c1$ structures is the way the MnO_5 bipyramids are tilted from their ideal position and the related displacements of the R^{3+} ions. In $P6_3cm$ symmetry, the R^{3+} ions on different crystallographic sites (2a and 4b) are displaced along the c-axis in opposite directions. The generated dipolar momenta are not compensated yielding a macroscopic polarization (see left column in Figure 41(a)). In the $P\bar{3}c1$ structure, however, one R^{3+} ion remains in the

centrosymmetric 2b position without any displacement along c. The structure has an inversion center and no ferroelectric polarization is allowed. This is shown in the right column of Figure 41(a). The corresponding Mn^{3+} spin orders are shown in Figure 41(b).

With all experimental evidence for a missing polarization it can be concluded that $InMnO_3$ is so far the only paraelectric hexagonal manganite. The possible origin of this "anomaly" was discussed by Kumagai et al. [205] based on the results of band structure calculations. It was concluded that the key to understand the different lattice structures of $InMnO_3$ and other $RMnO_3$ is the degree of covalency of the R-O bond. As a result of the competition between electrostatic energy and R-O covalency, either the $P6_3cm$ structure is in favor (for lower R-O covalency) or, for higher covalency, the $P\bar{3}c1$ structure becomes the stable ground state.

2.7. Symmetry Analysis and Landau Theory. To understand the complex magnetic phase diagrams, phase transitions between different magnetic symmetries, and partially coexisting phases, a group theoretical symmetry analysis was conducted by different authors [95, 106, 206]. The point group has four one-dimensional (labeled A_1, A_2, B_1, and B_2) and two two-dimensional irreducible representations (E_1 and E_2). The magnetic space groups in the ordered phases corresponding to the 1D representations are: $P6_3cm$ (A_1), $P6_3\underline{c}\underline{m}$ (A_2), $P\underline{6}_3c\underline{m}$ (B_1), and $P\underline{6}_3\underline{c}m$ (B_2). The compatible magnetic structures have been discussed above and are shown in Figures 4 and 25. The 2D representations can be disregarded since there is no experimental evidence for any ordered magnetic structure corresponding to E_1 or E_2 in the phase diagrams of all hexagonal $RMnO_3$.

The spin configurations of the Mn^{3+}, R^{3+} (2a), and R^{3+} (4b) can be classified according to the four 1D irreducible representations. The different magnetic structures are discussed in detail in [95] and the corresponding spin configurations of rare earth and manganese moments are listed in Table 1 of [206]. The most general Landau free energy expansion with respect to all order parameters of the Mn^{3+} spins and R^{3+} moments on two crystallographic sites can be very extensive with too many parameters involved. It is also not clear how the different order parameters of Mn-spins and R-moments couple to one another, as demonstrated in the case of $DyMnO_3$ above. Therefore, Munawar and Curnoe limited the free energy expansion to two competing order parameters, defined by the B_2 and A_2 representations [206]. This choice is consistent with experimental results for $ErMnO_3$, $TmMnO_3$, and $YbMnO_3$. The free energy expression was derived in [206]:

$$F = \alpha_2\eta_2^2 + \beta_2\eta_2^4 + \alpha_4\eta_4^2 + \beta_4\eta_4^4 + \gamma_{24}\eta_2^2\eta_4^2 - H_z\left(\rho_1\eta_2 + \rho_2\eta_2^3 + \rho_3\eta_2\eta_4^2\right). \quad (7)$$

η_2 and η_4 are the order parameters corresponding to the A_2 ($P6_3\underline{c}\underline{m}$) and B_2 ($P\underline{6}_3\underline{c}m$) irreducible representations, respectively. α_i, β_i, ρ_i, and γ are the expansion parameters. The first four terms represent the energy of the ordered state for both symmetries, the next term describes the coupling between the two order parameters, and the last term is the energy gain due to the coupling of the magnetic order parameters to the external magnetic field. Minimizing the free energy (7) with respect to the order parameters and assuming proper sets of the expansion coefficients [206] could derive temperature-field phase diagrams showing the main features as observed in experiments [93], for example, the transition from the B_2 phase to the A_2 phase upon increasing magnetic field and the existence of a two-phase region in the phase diagram. With the expansion (7), however, it was assumed that the order of Mn^{3+} spins and R^{3+} moments in a single phase follow the same irreducible representation, unlike the special case of $DyMnO_3$ discussed in the previous section.

The same Landau free energy expression (7) was used to describe the phase diagram of $YbMnO_3$ and the critical scaling of the in plane dielectric constant as a function of temperature and c-axis field [191]. The observed scaling of the magneto-dielectric effect could only be explained by assuming a competition of an antiferromagnetic (B_2) with a ferromagnetic (A_2) state. It was shown that any small magnetic field did induce a ferromagnetic order parameter of A_2 symmetry and the high-field transition is actually from a $B_2 + A_2$ phase mixture into a phase with sole A_2 magnetic symmetry. This model did describe the observed scaling of the dielectric constant. The transition between the mixed ($B_2 + A_2$) phase and the ferromagnetic A_2 phase is second order in the high-temperature range, but it becomes a first order transition at lower temperatures (critical point), close to the maximum field along the phase boundary. The two sections of the phase boundary correspond to the two critical temperatures labeled T_N (2nd order transition) and $\tilde{T}_N$ (1st order), respectively, in Section 2.2.4.

3. Summary

Hexagonal manganites $RMnO_3$ belong to an exceptionally interesting family of type (I) multiferroics with high ferroelectric transition temperatures and frustrated magnetic orders existing at much lower temperature. The complex magnetic system of Mn spins and rare earth moments and the inherent frustration due to the triangular geometry of the magnetic sublattices results in a wealth of physical phenomena, phase transitions between different magnetic orders, and magnetoelectric as well as magnetoelastic effects. The series of compounds includes all $RMnO_3$ with rare earth elements (R) from Dy to Lu and $InMnO_3$, $ScMnO_3$, and $YMnO_3$.

$HoMnO_3$ and $YMnO_3$ have been studied most extensively. $HoMnO_3$ possesses the most complex phase diagram in c-axis magnetic fields with a multitude of different phases clearly separated by the properties of magnetic, thermodynamic, and dielectric properties, although the precise magnetic orders and symmetries of all phases have yet to be explored. The strong interaction between the Mn spins and Ho moments, the Mn-Ho exchange, and the coupling to the lattice and the ferroelectric order parameter, together with the frustration of the magnetic exchange pathways, makes this compound a highly correlated system, the study of which appears to be quite challenging. Bulk magnetic, dielectric,

heat capacity, thermal expansion, and other measurements have contributed to unravel the complex phase diagram and to identify the various phase boundaries. Neutron scattering and second harmonic generation optical measurements have determined the magnetic orders of Mn spins as well as Ho moments in different phases. Combining all studies has helped to arrive at a more complete understanding of the complex interactions of highly frustrated magnetic systems and the origin of the magnetoelectric effects in this class of multiferroics.

$YMnO_3$ appeared interesting because of the missing rare earth magnetic moment which simplifies the magnetic subsystem and should make it easier to study the magnetoelectric interaction of the Mn spin order with the ferroelectricity. Nevertheless, new phenomena have been discovered in the ferroelectric and magnetic domain walls, such as a clamping property which causes a ferroelectric domain boundary always to coincide with a magnetic domain wall. These observations show that magnetoelectric interactions can be particularly strong in domain boundaries of multiferroic compounds.

Among the other hexagonal manganites, several family members exhibit further interesting properties and phenomena. $ScMnO_3$ undergoes an Mn spin reorientation transition well below it's Néel temperature due to the weak in-plane magnetic anisotropy of the Mn spins. $ErMnO_3$, $YbMnO_3$, and $DyMnO_3$, similar to $HoMnO_3$, show low-temperature phases which are determined by a ferromagnetic order of their respective f moments on the two inequivalent rare earth sublattices. The strong f-f exchange interaction is assumed to be the origin of the f-moment alignment and the exchange with the manganese spins than forces the Mn spin system to rotate to be compatible with the same magnetic symmetry. However, hexagonal $DyMnO_3$ was found to adopt different magnetic symmetries below T_N for the Mn spins and Dy moments, respectively, which was not observed in other $RMnO_3$. $InMnO_3$ seems to be the only paramagnetic hexagonal manganite since the originally reported ferroelectricity in this compound was disputed and no evidence of a sizable polarization was found in more detailed experiments.

The wealth of interesting phenomena and the unraveling of novel physics in multiferroic hexagonal manganites is closely related to the simultaneous presence of geometric frustration, particularly of the magnetic system, the coupling and mutual interaction of different magnetic ions, the important role of magnetic anisotropy, mainly controlled by the rare earth ions, and the strong interaction of moments with the lattice and the ferroelectric order parameter. This makes the compound family unique and a perfect subject for further studies. The results are expected to also provide fundamental insight into other complex multiferroics or highly frustrated magnetic systems.

Acknowledgments

This work is supported in part by the US Air Force Office of Scientific Research, the T.L.L. Temple Foundation, the J. J. and R. Moores Endowment, and the State of Texas through the Texas Center for Superconductivity at the University of Houston.

References

[1] W. C. Röntgen, "Ueber die durch Bewegung eines im homogenen electrischen Felde befindlichen Dielectricums hervorgerufene electrodynamische Kraft," *Annalen Der Physik*, vol. 271, pp. 264–270, 1888.

[2] H. A. Wilson, "On the electric effect of rotating a dielectric in a magnetic field," *Philosophical Transactions of the Royal Society A*, vol. 204, pp. 121–137, 1905.

[3] P. Curie, "Sur la symétrie dans les phénomènes physiques. Symétrie d'un champ électrique d'un champ magnétique," *Journal de Physique*, vol. 3, pp. 393–416, 1894.

[4] I. E. Dzyaloshinskii, "On the magneto-electrical effect in antiferromagnets," *Soviet Physics*, vol. 10, pp. 628–629, 1960, *Zhurnal Eksperimental'Noi I Teoreticheskoi Fiziki*, vol. 37, no. 3, pp. 881–882, 1959.

[5] D. N. Astrov, "The magnetoelectric effect in antiferromagnetics," *Soviet Physics*, vol. 11, pp. 708–709, 1960, *Zhurnal Eksperimental'noi i Teoreticheskoi Fiziki*, vol. 38, pp. 984–985, 1960.

[6] V. J. Folen, G. T. Rado, and E. W. Stalder, "Anisotropy of the magnetoelectric effect in Cr_2O_3," *Physical Review Letters*, vol. 6, no. 11, pp. 607–608, 1961.

[7] D. N. Astrov, "Magnetoelectric effect in chromium oxide," *Soviet Physics*, vol. 13, pp. 729–733, 1961, *Zhurnal Eksperimental'noi i Teoreticheskoi Fiziki*, vol. 40, pp. 1035, 1961.

[8] G. T. Rado and V. J. Folen, "Observation of the magnetically induced magnetoelectric effect and evidence for antiferromagnetic domains," *Physical Review Letters*, vol. 7, no. 8, pp. 310–311, 1961.

[9] G. T. Rado, "Mechanism of the magnetoelectric effect in an antiferromagnet," *Physical Review Letters*, vol. 6, pp. 609–610, 1961.

[10] R. M. Hornreich, "Magnetoelectric effect: materials, physical aspects, and applications," *IEEE Transactions on Magnetics*, vol. 8, no. 3, pp. 584–589, 1972.

[11] H. Schmid, "Magnetoelectric effects in insulating magnetic materials," in *Introduction to Complex Mediums for Optics and Electromagnetics*, W. S. Weiglhofer and A. Lakhtakia, Eds., vol. 123, p. 167, SPIE Press Monograph, Bellingham, Wash, USA, 2003.

[12] T. H. O'Dell, "The field invariants in a magneto-electric medium," *Philosophical Magazine*, vol. 8, pp. 411–418, 1963.

[13] W. F. Brown, R. M. Hornreich, and S. Shtrikman, "Upper bound on the magnetoelectric susceptibility," *Physical Review*, vol. 168, no. 2, pp. 574–577, 1968.

[14] E. Ascher and A. G. M. Janner, "Upper bounds on the magnetoelectric susceptibility," *Physics Letters A*, vol. 29, no. 6, p. 295, 1969.

[15] G. T. Rado, J. M. Ferrari, and W. G. Maisch, "Magnetoelectric susceptibility and magnetic symmetry of magnetoelectrically annealed $TbPO_4$," *Physical Review B*, vol. 29, no. 7, pp. 4041–4048, 1984.

[16] J. P. Rivera, "A short review of the magnetoelectric effect and relatedexperimental techniques on single phase (multi-) ferroics," *European Physical Journal B*, vol. 71, pp. 299–313, 2009.

[17] H. G. Kahle, S. Bluck, and A. Kasten, "Simultaneous measurement of magnetic and magneto-electric susceptibility in

$TbPO_4$," *Journal of Magnetism and Magnetic Materials*, vol. 54-57, no. 3, pp. 1327–1328, 1986.

[18] H. Schmid, "Some symmetry aspects of ferroics and single phase multiferroics," *Journal of Physics*, vol. 20, Article ID 434201, 2008.

[19] E. Ascher, "Higher-order magneto-electric effects," *Philosophical Magazine*, vol. 17, no. 145, pp. 149–157, 1968.

[20] J.-P. Rivera, "On definitions, units, measurements, tensor forms of the linear magnetoelectric effect and on a new dynamic method applied to Cr–Cl boracite," *Ferroelectrics*, vol. 161, no. 1, pp. 165–180, 1994.

[21] S. L. Hou and N. Bloembergen, "Paramagnetoelectric effects in $NiSO_4$ $6H_2O$," *Physical Review*, vol. 138, no. 4 A, pp. A1218–A1226, 1965.

[22] T. H. O'Dell, "An induced magneto-electric effect in yttrium iron garnet," *Philosophical Magazine*, vol. 16, no. 141, pp. 487–494, 1967.

[23] J.-P. Rivera and H. Schmid, "Linear and quadratic magnetoelectric (ME) effect in Ni-Cl boracite," *Journal of Applied Physics*, vol. 70, no. 10, pp. 6410–6412, 1991.

[24] K.-C. Liang, W. Zhang, B. Lorenz, Y. Y. Sun, P. S. Halasyamani, and C. W. Chu, "Weak ferromagnetism and internal magnetoelectric effect in $LiFeP_2O_7$," *Physical Review B*, vol. 86, Article ID 094414, 2012.

[25] A. M. Kadomtseva, Y. F. Popov, G. P. Vorob'ev et al., "Magnetoelectric and magnetoelastic properties of rare-earth ferroborates," *Low Temperature Physics*, vol. 36, no. 6, Article ID 004006LTP, pp. 511–521, 2010.

[26] Y. F. Popov, A. P. Pyatakov, A. M. Kadomtseva et al., "Peculiarities in the magnetic, magnetoelectric, and magnetoelastic properties of $SmFe_3(BO_3)_4$ multiferroic," *Journal of Experimental and Theoretical Physics*, vol. 111, no. 2, pp. 199–203, 2010.

[27] A. K. Zvezdin, G. P. Vorob'ev, A. M. Kadomtseva et al., "Magnetoelectric and magnetoelastic interactions in $NdFe_3(BO_3)_4$ multiferroics," *JETP Letters*, vol. 83, no. 11, pp. 509–514, 2006.

[28] K. C. Liang, R. P. Chaudhury, B. Lorenz et al., "Giant magnetoelectric effect in $HoAl_3(BO_3)_4$," *Physical Review B*, vol. 83, no. 18, Article ID 180417, 2011.

[29] R. P. Chaudhury, B. Lorenz, Y. Y. Sun, L. N. Bezmaternykh, V. L. Temerov, and C. W. Chu, "Magnetoelectricity and magnetostriction due to the rare-earth moment in $TmAl_3(BO_3)_4$," *Physical Review B*, vol. 81, Article ID 220402, 4 pages, 2010.

[30] N. A. Hill, "Why are there so few magnetic ferroelectrics?" *Journal of Physical Chemistry B*, vol. 104, pp. 6694–6709, 2000.

[31] E. Ascher, H. Rieder, H. Schmid, and H. Stössel, "Some properties of ferromagnetoelectric Nickel-Iodine boracite, $Ni_3B_7O_{13}I$," *Journal of Applied Physics*, vol. 37, p. 1404, 1966.

[32] G. A. Smolenskii, V. A. Isupov, N. N. Krainik, and A. L. Agranovskaya, "Concerning the coexistence of the ferroelectric and ferrimagnetic states," *Izvestiya Rossijskoj Akademii Nauk. Seriya Fizika Atmosfery i Okeana*, vol. 25, p. 1333, 1961.

[33] V. A. Bokov, I. E. Myl'nikova, and G. A. Smolenskii, "Ferroelectrics and an- tiferromagnetics," *Zhurnal Eksperimental'Noi I Teoreticheskoi Fiziki*, vol. 42, p. 643, 1962.

[34] G. A. Smolenskii and I. E. Chupis, "Ferroelectromagnets," *Soviet Physics Uspekhi*, vol. 25, p. 475, 1982.

[35] H. Schmid, "Multi-ferroic magnetoelectrics," *Ferroelectrics*, vol. 162, p. 317, 1994.

[36] M. Fiebig, "Revival of the magnetoelectric effect ," *Journal of Physics D*, vol. 38, no. 8, article R123, 2005.

[37] T. Kimura, T. Goto, H. Shintani, K. Ishizaka, T. Arima, and Y. Tokura, "Magnetic control of ferroelectric polarization," *Nature*, vol. 426, no. 6962, pp. 55–58, 2003.

[38] F. Bertaut, F. Forrat, and P. Fang, "Les manganites de terres Fares et d'yurtum: une nouvelle classe de ferrotleciriques," *Comptes Rendus de l'Académie des Sciences*, vol. 256, p. 1958, 1963.

[39] H. L. Yakel, W. C. Koehler, E. F. Bertaut, and E. F. Forrat, "On the crystal structure of the manganese(III) trioxides of the heavy lanthanides and yttrium," *Acta Crystallographica*, vol. 16, pp. 957–962, 1963.

[40] M. Fiebig, T. Lottermoser, M. K. Kneip, and M. Bayer, "Correlations between magnetic and electrical orderings in multiferroic manganites," *Journal of Applied Physics*, vol. 99, no. 8, Article ID 08E302, 2006.

[41] F. Yen, C. de la Cruz, B. Lorenz et al., "Magnetic phase diagrams of multiferroic hexagonal $RMnO_3$ (R = Er, Yb, Tm, and Ho)," *Journal of Materials Research*, vol. 22, no. 8, pp. 2163–2173, 2007.

[42] G. A. Smolenskii and V. A. Bokov, "Coexistence of magnetic and electric ordering in crystals," *Journal of Applied Physics*, vol. 35, no. 3, pp. 915–918, 1964.

[43] Z. J. Huang, Y. Cao, Y. Y. Sun, Y. Y. Xue, and C. W. Chu, "Coupling between the ferroelectric and antiferromagnetic orders in $YMnO_3$," *Physical Review B*, vol. 56, no. 5, pp. 2623–2626, 1997.

[44] G. Lawes, A. B. Harris, T. Kimura et al., "Magnetically driven ferroelectric order in $Ni_3V_2O_8$," *Physical Review Letters*, vol. 95, no. 8, Article ID 087205, pp. 1–4, 2005.

[45] A. H. Arkenbout, T. T. M. Palstra, T. Siegrist, and T. Kimura, "Ferroelectricity in the cycloidal spiral magnetic phase of $MnWO_4$," *Physical Review B*, vol. 74, Article ID 184431, 7 pages, 2006.

[46] K. Taniguchi, N. Abe, T. Takenobu, Y. Iwasa, and T. Arima, "Ferroelectric polarization flop in a frustrated magnet $MnWO_4$ induced by a magnetic field," *Physical Review Letters*, vol. 97, Article ID 097203, 4 pages, 2006.

[47] O. Heyer, N. Hollmann, I. Klassen et al., "A new multiferroic material: $MnWO_4$," *Journal of Physics*, vol. 18, no. 39, article no. L01, pp. L471–L475, 2006.

[48] S. Park, Y. J. Vhoi, C. L. Zhang, and S.-W. Cheong, "Ferroelectricity in an S = 1/2 Chain Cuprate," *Physical Review Letters*, vol. 98, no. 5, Article ID 057601, 2007.

[49] T. Kimura, J. C. Lashley, and A. P. Ramirez, "Inversion-symmetry breaking in the noncollinear magnetic phase of the triangular-lattice antiferromagnet $CuFeO_2$," *Physical Review B*, vol. 73, Article ID 220401, 4 pages, 2006.

[50] Y. Yamasaki, S. Miyasaka, Y. Kaneko, J.-P. He, T. Arima, and Y. Tokura, "Magnetic reversal of the ferroelectric polarization in a multiferroic spinel oxide," *Physical Review Letters*, vol. 96, no. 20, Article ID 207204, 2006.

[51] S. W. Cheong and M. Mostovoy, "Multiferroics: a magnetic twist for ferroelectricity," *Nature Materials*, vol. 6, no. 1, pp. 13–20, 2007.

[52] Y. J. Choi, H. T. Yi, S. Lee, Q. Huang, V. Kiryukhin, and S. W. Cheong, "Ferroelectricity in an ising chain magnet," *Physical Review Letters*, vol. 100, Article ID 047601, 4 pages, 2008.

[53] A. Inomata and K. Kohn, "Pyroelectric effect and possible ferroelectric transition of helimagnetic $GdMn_2O_5$, $TbMn_2O_5$ and YMn_2O_5," *Journal of Physics*, vol. 8, no. 15, p. 2673, 1996.

[54] N. Hur, S. Park, P. A. Sharma, S. Guha, and S. W. Cheong, "Colossal magnetodielectric effects in $DyMn_2O_5$," *Physical Review Letters*, vol. 93, no. 10, pp. 1–107207, 2004.

[55] B. Lorenz, Y. Q. Wang, and C. W. Chu, "Ferroelectricity in perovskite $HoMnO_3$ and $YMnO_3$," *Physical Review B*, vol. 76, Article ID 104405, 5 pages, 2007.

[56] Y. S. Chai, Y. S. Oh, L. J. Wang et al., "Intrinsic ferroelectric polarization of orthorhombic manganites with *E*-type spin order," *Physical Review B*, vol. 85, Article ID 184406, 6 pages, 2012.

[57] D. Higashiyama, S. Miyasaka, N. Kida, T. Arima, and Y. Tokura, "Control of the ferroelectric properties of $DyMn_2O_5$ by magnetic fields," *Physical Review B*, vol. 70, no. 17, Article ID 174405, pp. 1–7, 2004.

[58] N. Hur, S. Park, P. A. Sharma, J. S. Ahn, S. Guha, and S. W. Cheong, "Electric polarization reversal and memory in a multiferroic material induced by magnetic fields," *Nature*, vol. 429, no. 6990, pp. 392–395, 2004.

[59] S. Seki, Y. Yamasaki, M. Soda, M. Matsuura, K. Hirota, and Y. Tokura, "Correlation between spin helicity and an electric polarization vector in quantum-spin chain magnet $LiCu_2O_2$," *Physical Review Letters*, vol. 100, Article ID 127201, 4 pages, 2008.

[60] H. Sagayama, K. Taniguchi, N. Abe et al., "Correlation between ferroelectric polarization and sense of helical spin order in multiferroic $MnWO_4$," *Physical Review B*, vol. 77, no. 22, Article ID 220407, 2008.

[61] C. R. Dela Cruz, B. Lorenz, Y. Y. Sun et al., "Pressure-induced enhancement of ferroelectricity in multiferroic RMn_2O_5 (R=Tb,Dy,Ho)," *Physical Review B*, vol. 76, no. 17, Article ID 174106, 2007.

[62] R. P. Chaudhury, C. R. Dela Cruz, B. Lorenz et al., "Pressure-induced polarization reversal in multiferroic YMn_2O_5," *Physical Review B*, vol. 77, no. 22, Article ID 220104, 2008.

[63] C. R. dela Cruz, B. Lorenz, and C. W. Chu, "Tuning ferroelectricity in $DyMn_2O_5$ by pressure and magnetic fields," *Physica B*, vol. 403, no. 5-9, pp. 1331–1335, 2008.

[64] R. P. Chaudhury, F. Yen, C. R. dela Cruz et al., "Pressure-temperature phase diagram of multiferroic $Ni_3V_2O_8$," *Physical Review B*, vol. 75, Article ID 012407, 4 pages, 2007.

[65] S. Seki, Y. Yamasaki, Y. Shiomi, S. Iguchi, Y. Onose, and Y. Tokura, "Impurity-doping-induced ferroelectricity in the frustrated antiferromagnet $CuFeO_2$," *Physical Review B*, vol. 75, no. 10, Article ID 100403, 2007.

[66] S. Kanetsuki, S. Mitsuda, T. Nakajima, D. Anazawa, H. A. Katori, and K. Prokes, "Field-induced ferroelectric state in frustrated magnet $CuFe_{1-x}Al_xO_2$," *Journal of Physics*, vol. 19, no. 14, Article ID 145244, 2007.

[67] R. P. Chaudhury, B. Lorenz, Y. Q. Wang, Y. Y. Sun, and C. W. Chu, "Suppression and recovery of the ferroelectric phase in multiferroic $MnWO_4$," *Physical Review B*, vol. 77, Article ID 104406, 6 pages, 2008.

[68] R. P. Chaudhury, F. Ye, J. A. Fernandez-Baca et al., "Robust ferroelectric state in multiferroic $Mn_{1-x}Zn_xWO_4$," *Physical Review B*, vol. 83, Article ID 014401, 6 pages, 2011.

[69] K. C. Liang, Y. Q. Wang, Y. Y. Sun et al., "The complex multiferroic phase diagram of $Mn_{1-x}Co_xWO_4$," *New Journal of Physics*, vol. 14, no. 14, Article ID 073028, 2012.

[70] W. Prellier, M. P. Singh, and P. Murugavel, "The single-phase multiferroic oxides: from bulk to thin film," *Journal of Physics*, vol. 17, no. 30, pp. R803–R832, 2005.

[71] W. Eerenstein, N. D. Mathur, and J. F. Scott, "Multiferroic and magnetoelectric materials," *Nature*, vol. 442, no. 7104, pp. 759–765, 2006.

[72] Y. Tokura, "Multiferroics-toward strong coupling between magnetization and polarization in a solid ," *Journal of Magnetism and Magnetic Materials*, vol. 310, no. 2, part 2, pp. 1145–1150, 2007.

[73] C. N. R. Rao and C. R. Serrano, "New routes to multiferroics ," *Journal of Materials Chemistry*, vol. 17, pp. 4931–4938, 2007.

[74] G. Lawes and G. Srinivasan, "Introduction to magnetoelectric coupling and multiferroic films," *Journal of Physics D*, vol. 44, no. 24, Article ID 243001, 2011.

[75] J. van den Brink and D. I. Khomskii, "Multiferroicity due to charge ordering," *Journal of Physics*, vol. 20, no. 43, Article ID 434217, 2008.

[76] P. S. Halasyamani and K. R. Poeppelmeier, "Noncentrosymmetric oxides," *Chemistry of Materials*, vol. 10, no. 10, pp. 2753–2769, 1998.

[77] M. Atanasov and D. Reinen, "Density functional studies on the lone pair effect of the trivalent group (V) elements: I. electronic structure, vibronic coupling, and chemical criteria for the occurrence of lone pair distortions in AX_3 Molecules (A=N to Bi; X=H, and F to I)," *The Journal of Physical Chemistry A*, vol. 105, no. 22, pp. 5450–5467, 2001.

[78] R. Seshadri and N. A. Hill, "Visualizing the role of Bi 6s "Lone Pairs" in the off-center distortion in rerromagnetic $BiMnO_3$," *Chemistry of Materials*, vol. 13, no. 9, pp. 2892–2899, 2001.

[79] B. B. Van Aken, T. T. M. Palstra, A. Filippetti, and N. A. Spaldin, "The origin of ferroelectricity in magnetoelectric $YMnO_3$," *Nature Materials*, vol. 3, no. 3, pp. 164–170, 2004.

[80] K. Lukaszewicz and J. Karut-Kalicińska, "X-Ray investigations of the crystal structure and phase transitions of $YMnO_3$," *Ferroelectrics*, vol. 7, no. 1, pp. 81–82, 1974.

[81] G. Nénert, Y. Ren, H. Stokes, and T. T. M. Palstra, "Symmetry changes at the ferroelectric transition in the multiferroic $YMnO_3$," http://arxiv.org/abs/cond-mat/0504546.

[82] G. Nénert, M. Pollet, S. Marinel, G. R. Blake, A. Meetsma, and T. T. M. Palstra, "Experimental evidence for an intermediate phase in the multiferroic $YMnO_3$," *Journal of Physics*, vol. 19, no. 46, Article ID 466212, 2007.

[83] I.-K. Jeong, N. Hur, and T. Proffen J, "High-temperature structural evolution of hexagonal multiferroic $YMnO_3$ and $YbMnO_3$," *Journal of Applied Crystallography*, vol. 40, no. 4, pp. 730–734, 2007.

[84] A. S. Gibbs, K. S. Knight, and P. Lightfoot, "High-temperature phase transitions of hexagonal $YMnO_3$," *Physical Review B*, vol. 83, no. 9, Article ID 094111, 2011.

[85] S. C. Abrahams, "Atomic displacements at and order of all phase transitions in multiferroic $YMnO_3$ and $BaTiO_3$," *Acta Crystallographica Section B*, vol. 65, no. 4, pp. 450–457, 2009.

[86] T. Lonkai, D. G. Tomuta, U. Amann et al., "Development of the high-temperature phase of hexagonal manganites," *Physical Review B*, vol. 69, no. 13, Article ID 134108, 2004.

[87] E. F. Bertaut and M. Mercier, "Structure magnetique de $MnYO_3$," *Physics Letters A*, vol. 5, no. 1, pp. 27–29, 1964.

[88] W. C. Koehler, H. L. Yakel, E. O. Wollan, and J. W. Cable, "A note on the magnetic structures of rare earth manganese oxides," *Physics Letters*, vol. 9, no. 2, pp. 93–95, 1964.

[89] J. E. Greedan, M. Bieringer, J. F. Britten, D. M. Giaquinta, and H. C. zur Loye, "Synthesis, crystal structure, and unusual magnetic properties of $InMnO_3$," *Journal of Solid State Chemistry*, vol. 116, no. 1, pp. 118–130, 1995.

[90] D. G. Tomuta, S. Ramakrishnan, G. J. Niewenhuys, and J. A. Mydosh, "The magnetic susceptibility, specific heat and dielectric constant of hexagonal $YMnO_3$, $LuMnO_3$ and $ScMnO_3$," *Journal of Physics*, vol. 13, no. 20, pp. 4543–4552, 2001.

[91] T. Katsufuji, M. Masaki, A. Machida et al., "Crystal structure and magnetic properties of hexagonal $RMnO_3$ (R = Y, Lu, and Sc) and the effect of doping," *Physical Review B*, vol. 66, no. 13, Article ID 134434, pp. 1344341–1344348, 2002.

[92] N. Kamegashira, H. Satoh, and S. Ashizuka, "Synthesis and crystal structure of hexagonal $DYMnO_3$," *Materials Science Forum*, vol. 449-452, no. II, pp. 1045–1048, 2004.

[93] M. Fiebig, T. Lottermoser, and R. V. Pisarev, "Spin-rotation phenomena and magnetic phase diagrams of hexagonal $RMnO_3$," *Journal of Applied Physics*, vol. 93, no. 10, pp. 8194–8196, 2003.

[94] X. Fabrèges, I. Mirebeau, P. Bonville et al., "Magnetic order in $YbMnO_3$ studied by neutron diffraction and Mössbauer spectroscopy," *Physical Review B*, vol. 78, no. 21, Article ID 214422, 2008.

[95] A. Muñoz, J. A. Alonśo, M. J. Martínez-Lope, M. T. Casáis, J. L. Martínez, and M. T. Fernández-Díaz, "Magnetic structure of hexagonal, $RMnO_3$ (R = Y, Sc): thermal evolution from neutron powder diffraction data," *Physical Review B*, vol. 62, no. 14, pp. 9498–9510, 2000.

[96] J. Park, U. Kong, A. Pirogov et al., "Neutron-diffraction studies of $YMnO_3$," *Applied Physics A*, vol. 74, no. I, pp. S796–S798, 2002.

[97] J. Reif, C. Rau, and E. Matthias, "Influence of magnetism on second harmonic generation," *Physical Review Letters*, vol. 71, no. 12, pp. 1931–1934, 1993.

[98] V. V. Pavlov, R. V. Pisarev, A. Kirilyuk, and T. Rasing, "Observation of a transversal nonlinear magneto-optical effect in thin magnetic garnet films," *Physical Review Letters*, vol. 78, no. 10, pp. 2004–2007, 1997.

[99] D. Fröhlich, St. Leute, V. V. Pavlov, and R. V. Pisarev, "Nonlinear optical spectroscopy of the two-order-parameter compound $YMnO_3$," *Physical Review Letters*, vol. 81, no. 15, pp. 3239–3242, 1998.

[100] M. Fiebig, D. Fröhlich, K. Kohn et al., "Determination of the magnetic symmetry of hexagonal manganites by second harmonic generation," *Physical Review Letters*, vol. 84, no. 24, pp. 5620–5623, 2000.

[101] T. Iizuka-Sakano, E. Hanamura, and Y. Tanabe, "Second-harmonic-generation spectra of the hexagonal manganites $RMnO_3$," *Journal of Physics*, vol. 13, no. 13, pp. 3031–3055, 2001.

[102] M. Fiebig, C. Degenhardt, and R. V. Pisarev, "Interaction of frustrated magnetic sublattices in E$RMnO_3$," *Physical Review Letters*, vol. 88, no. 2, Article ID 027203, pp. 272031–272034, 2002.

[103] T. Lonkai, D. Hohlwein, J. Ihringer, and W. Prandl, "The magnetic structures of $YMnO_3$-δ and $HoMnO_3$," *Applied Physics A*, vol. 74, no. I, pp. S843–S845, 2002.

[104] N. Iwata, "Dielectric anomalies at magnetic transitions of hexagonal rare earth manganese oxides $RMnO_3$," *Journal of the Physical Society of Japan*, vol. 67, no. 9, pp. 3318–3319, 1998.

[105] H. Sugie, N. Iwata, and K. Kohn, "Magnetic ordering of rare earth ions and magnetic-electric interaction of hexagonal $RMnO_3$ (R = Ho, Er, Yb or Lu)," *Journal of the Physical Society of Japan*, vol. 71, no. 6, pp. 1558–1564, 2002.

[106] A. Muñoz, J. A. Alonso, and M. J. Martínez-Lope, "Evolution of the magnetic structure of hexagonal $HoMnO_3$ from neutron powder diffraction data," *Chemistry of Materials*, vol. 13, pp. 1497–1505, 2001.

[107] P. J. Brown and T. Chatterji, "Neutron diffraction and polarimetric study of the magnetic and crystal structures of $HoMnO_3$ and $YMnO_3$," *Journal of Physics*, vol. 18, no. 44, pp. 10085–10096, 2006.

[108] O. P. Vajk, M. Kenzelmann, J. W. Lynn, S. B. Kim, and S.-W. Cheong, "Magnetic order and spin dynamics in ferroelectric $HoMnO_3$," *Physical Review Letters*, vol. 94, no. 8, Article ID 087601, 2005.

[109] M. Fiebig, C. Degenhardt, and R. V. Pisarev, "Magnetic phase diagram of $HoMnO_3$," *Journal of Applied Physics*, vol. 91, no. 10, p. 8867, 2002.

[110] M. Fiebig, T. Lottermoser, T. Lonkai, A. V. Goltsev, and R. V. Pisarev, "Magnetoelectric effects in multiferroic manganites," *Journal of Magnetism and Magnetic Materials*, vol. 290-291, pp. 883–890, 2005.

[111] S. Nandi, A. Kreyssig, L. Tan et al., "Nature of Ho magnetism in multiferroic $HoMnO_3$," *Physical Review Letters*, vol. 100, no. 21, Article ID 217201, 2008.

[112] S. G. Condran and M. L. Plumer, "A model of magnetic order in hexagonal $HoMnO_3$," *Journal of Physics*, vol. 22, no. 16, Article ID 162201, 2010.

[113] B. Lorenz, A. P. Litvinchuk, M. M. Gospodinov, and C. W. Chu, "Field-induced reentrant novel phase and a ferroelectric-magnetic order coupling in $HoMnO_3$," *Physical Review Letters*, vol. 92, no. 8, pp. 872041–872044, 2004.

[114] F. Yen, C. R. dela Cruz, B. Lorenz et al., "Low-temperature dielectric anomalies in $HoMnO_3$: the complex phase diagram," *Physical Review B*, vol. 71, Article ID 180407, 4 pages, 2005.

[115] P. A. Sharma, J. S. Ahn, N. Hur et al., "Thermal conductivity of geometrically frustrated, ferroelectric $YMnO_3$: extraordinary spin-phonon interactions," *Physical Review Letters*, vol. 93, no. 17, pp. 1–177202, 2004.

[116] H. D. Zhou, J. C. Denyszyn, and J. B. Goodenough, "Effect of Ga doping on the multiferroic properties of $RMn_{1-x}Ga_xO_3$ (R=Ho,Y)," *Physical Review B*, vol. 72, no. 22, Article ID 224401, 2005.

[117] H. D. Zhou, J. Lu, R. Vasic et al., "Relief of frustration through spin disorder in multiferroic $Ho_{1-x}Y_xMnO_3$," *Physical Review B*, vol. 75, no. 13, Article ID 132406, 2007.

[118] R. Vasic, H. D. Zhou, E. Jobiliong, C. R. Wiebe, and J. S. Brooks, "Probing multiferroicity and spin-spin interactions via dielectric measurements on Y-doped $HoMnO_3$ in high magnetic fields," *Physical Review B*, vol. 75, no. 1, Article ID 014436, 2007.

[119] H. D. Zhou, R. Vasic, J. Lu, J. S. Brooks, and C. R. Wiebe, "The effect of Er doping on the multiferroics of $Ho_{1-x}Er_xMnO_3$," *Journal of Physics*, vol. 20, no. 3, Article ID 035211, 2008.

[120] N. Hur, I. K. Jeong, M. F. Hundley, S. B. Kim, and S. W. Cheong, "Giant magnetoelectric effect in multiferroic $HoMnO_3$ with a high ferroelectric transition temperature," *Physical Review B*, vol. 79, Article ID 134120, 2009.

[121] B. Lorenz, F. Yen, M. M. Gospodinov, and C. W. Chu, "Field-induced phases in $HoMnO_3$ at low temperatures," *Physical Review B*, vol. 71, Article ID 014438, 9 pages, 2005.

[122] V. Skumryev, M. D. Kuz'Min, M. Gospodinov, and J. Fontcuberta, "Anisotropic paramagnetic response of hexagonal R MnO_3," *Physical Review B*, vol. 79, no. 21, Article ID 212414, 2009.

[123] H. D. Zhou, J. A. Janik, B. W. Vogt et al., "Specific heat of geometrically frustrated and multiferroic RMn_{1-x} Gax O_3 (R = Ho,Y)," *Physical Review B*, vol. 74, no. 9, Article ID 094426, 2006.

[124] A. Midya, S. N. Das, P. Mandal, S. Pandya, and V. Ganesan, "Anisotropic magnetic properties and giant magnetocaloric effect in antiferromagnetic $R\mathrm{MnO}_3$ crystals (R=Dy, Tb, Ho, and Yb)," *Physical Review B*, vol. 84, Article ID 235127, 10 pages, 2011.

[125] P. Liu, X. L. Wang, Z. X. Cheng, Y. Du, and H. Kimura, "Structural, dielectric, antiferromagnetic, and thermal properties of the frustrated hexagonal $\mathrm{Ho}_{1-x}\mathrm{Er}_x\mathrm{MnO}_3$ manganites," *Physical Review B*, vol. 83, Article ID 144404, 8 pages, 2011.

[126] A. Oleaga, A. Salazar, D. Prabhakaran, J. G. Cheng, and J. S. Zhou, "Critical behavior of the paramagnetic to antiferromagnetic transition in orthorhombic and hexagonal phases of $R\mathrm{MnO}_3$ (R=Sm, Tb, Dy, Ho, Er, Tm, Yb, Lu, Y) ," *Physical Review B*, vol. 85, Article ID 184425, 8 pages, 2012.

[127] C. R. dela Cruz, F. Yen, B. Lorenz et al., "Strong spin-lattice coupling in multiferroic HoMnO_3: thermal expansion anomalies and pressure effect ," *Physical Review B*, vol. 71, Article ID 060407, 4 pages, 2005.

[128] A. P. Litvinchuk, M. N. Iliev, V. N. Popov, and M. M. Gospodinov, "Raman and infrared-active phonons in hexagonal HoMnO_3 single crystals: Magnetic ordering effects," *Journal of Physics*, vol. 16, no. 6, pp. 809–819, 2004.

[129] A. B. Souchkov, J. R. Simpson, M. Quijada et al., "Exchange interaction effects on the optical properties of LuMnO_3," *Physical Review Letters*, vol. 91, no. 2, pp. 027203/1–027203/4, 2003.

[130] X. Fabréges, S. Petit, I. Mirebeau et al., "Spin-lattice coupling, frustration, and magnetic order in multiferroic $R\mathrm{MnO}_3$," *Physical Review Letters*, vol. 103, Article ID 067204, 4 pages, 2009.

[131] T. A. Tyson, T. Wu, K. H. Ahn, S. B. Kim, and S. W. Cheong, "Local spin-coupled distortions in multiferroic hexagonal HoMnO_3," *Physical Review B*, vol. 81, Article ID 054101, 7 pages, 2010.

[132] M. Poirier, J. C. Lemyre, P. O. Lahaie, L. Pinsard-Gaudart, and A. Revcolevschi, "Enhanced magnetoelastic coupling in hexagonal multiferroic HoMnO_3," *Physical Review B*, vol. 83, no. 5, Article ID 054418, 2011.

[133] T. Lottermoser and M. Fiebig, "Magnetoelectric behavior of domain walls in multiferroic HoMnO_3," *Physical Review B*, vol. 70, no. 22, Article ID 220407, 2004.

[134] H. J. Lewtas, T. Lancaster, P. J. Baker, S. J. Blundell, D. Prabhakaran, and F. L. Pratt, "Local magnetism and magnetoelectric effect in HoMnO_3 studied with muon-spin relaxation," *Physical Review B*, vol. 81, no. 1, Article ID 014402, 2010.

[135] J. C. Lemyre and M. Poirier, "Microwave investigation of the phase diagram of hexagonal multiferroic HoMnO_3," *Physical Review B*, vol. 79, Article ID 094423, 6 pages, 2009.

[136] O. P. Vajk, M. Kenzelmann, J. W. Lynn, S. B. Kim, and S. W. Cheong, "Neutron-scattering studies of magnetism in multiferroic HoMnO_3," *Journal of Applied Physics*, vol. 99, no. 8, Article ID 08E301, 2006.

[137] S. Lee, A. Pirogov, M. Kang et al., "Giant magneto-elastic coupling in multiferroic hexagonal manganites," *Nature*, vol. 451, pp. 805–808, 2008.

[138] T. Chatterji, B. Ouladdiaf, P. F. Henry, and D. Bhattacharya, "Magnetoelastic effects in multiferroic YMnO_3," *Journal of Physics: Condensed Matter*, vol. 24, Article ID 336003, 2012.

[139] T. Lottermoser, T. Lonkai, U. Amann, D. Hohlwein, J. Ihringer, and M. Fiebig, "Magnetic phase control by an electric field," *Nature*, vol. 430, no. 6999, pp. 541–544, 2004.

[140] B. G. Ueland, J. W. Lynn, M. Laver, Y. J. Choi, and S. W. Cheong, "Origin of electric-field-induced magnetization in multiferroic HoMnO_3," *Physical Review Letters*, vol. 104, Article ID 147204, 14 pages, 2010.

[141] C. J. Fennie and K. M. Rabe, "Ferroelectric transition in YMnO_3 from first principles," *Physical Review B*, vol. 72, Article ID 100103, 2005.

[142] M. Stengel, C. J. Fennie, and P. Ghosez, "Electrical properties of improper ferroelectrics from first principles," *Physical Review B*, vol. 86, no. 9, Article ID 094112, 9 pages, 2012.

[143] D.-Y. Cho, J.-Y. Kim, B.-G. Park et al., "Ferroelectricity driven by y d0-ness with rehybridization in YMnO_3," *Physical Review Letters*, vol. 98, no. 21, Article ID 217601, 2007.

[144] T. Katsufuji, S. Mori, M. Masaki, Y. Moritomo, N. Yamamoto, and H. Takagi, "Dielectric and magnetic anomalies and spin frustration in hexagonal $R\mathrm{MnO}_3$ (R=Y, Yb, and Lu)," *Physical Review B*, vol. 64, no. 10, Article ID 104419, pp. 1044191–1044196, 2001.

[145] B. B. V. Aken, J. W. G. Bos, R. A. de Groot, and T. T. M. Palstra, "Quantum 120-degrees model on pyrochlore lattice: orbital ordering in $\mathrm{MnV}_2\mathrm{O}_4$l," *Physical Review B*, vol. 63, Article ID 125127, 2001.

[146] Y. Aikawa, T. Katsufuji, T. Arima, and K. Kato, "Effect of Mn trimerization on the magnetic and dielectric properties of hexagonal YMnO_3," *Physical Review B*, vol. 71, Article ID 184418, 2005.

[147] T. Lonkai, D. G. Tomuta, J. U. Hoffmann, R. Schneider, D. Hohlwein, and J. Ihringer, "Magnetic two-dimensional short-range order in hexagonal manganites," *Journal of Applied Physics*, vol. 93, no. 10, pp. 8191–8193, 2003.

[148] J. Park, J. G. Park, G. S. Jeon et al., "Magnetic ordering and spin-liquid state of YMnO_3," *Physical Review B*, vol. 68, no. 10, Article ID 104426, 6 pages, 2003.

[149] A. Dixit, A. E. Smith, M. A. Subramanian, and G. Lawes, "Suppression of multiferroic order in hexagonal YMn_{1-x} Inx O_3 ceramics," *Solid State Communications*, vol. 150, no. 15-16, pp. 746–750, 2010.

[150] A. K. Singh, S. Patnaik, S. D. Kaushik, and V. Siruguri, "Dominance of magnetoelastic coupling in hexagonal multiferroic YMnO_3," *Physical Review B*, vol. 81, Article ID 184406, 2010.

[151] E. F. Bertaut, R. Pauthenet, and M. Mercier, "Sur des proprietes magnetiques du manganite d'yttrium," *Physics Letters*, vol. 18, no. 1, p. 13, 1965.

[152] D. P. Kozlenko, S. E. Kichanov, S. Lee, J. G. Park, and B. N. Savenko, "Pressure-induced spin fluctuations and spin reorientation in hexagonal manganites," *Journal of Physics*, vol. 19, no. 15, Article ID 156228, 2007.

[153] M. Janoschek, B. Roessli, L. Keller, S. N. Gvasaliya, K. Conder, and E. Pomjakushina, "Reduction of the ordered magnetic moment in YMnO_3 with hydrostatic pressure," *Journal of Physics*, vol. 17, no. 42, pp. L425–L430, 2005.

[154] S. Petit, F. Moussa, M. Hennion, S. Pailhés, L. Pinsard-Gaudart, and A. Ivanov, "Spin phonon coupling in hexagonal multiferroic YMnO_3," *Physical Review Letters*, vol. 99, no. 26, Article ID 266604, 2007.

[155] T. J. Sato, S. H. Lee, T. Katsufuji et al., "Unconventional spin fluctuations in the hexagonal antiferromagnet YMnO_3," *Physical Review B*, vol. 68, no. 1, Article ID 014432, pp. 144321–144325, 2003.

[156] T. Chatterji, S. Ghosh, A. Singh, L. P. Regnault, and M. Rheinstädter, "Spin dynamics of YMnO_3 studied via inelastic neutron scattering and the anisotropic Hubbard model," *Physical Review B*, vol. 76, Article ID 144406, 2007.

[157] F. Demmel and T. Chatterji, "Persistent spin waves above the Néel temperature in YMnO_3," *Physical Review B*, vol. 76, Article ID 212402, 4 pages, 2007.

[158] M. Tachibana, J. Yamazaki, H. Kawaij, and T. Atake, "Heat capacity and critical behavior of hexagonal $YMnO_3$," *Physical Review B*, vol. 72, Article ID 064434, 5 pages, 2005.

[159] S. Lee, A. Pirogov, J. H. Han, J. G. Park, A. Hoshikawa, and T. Kamiyama, "Direct observation of a coupling between spin, lattice and electric dipole moment in multiferroic $YMnO_3$," *Physical Review B*, vol. 71, Article ID 180413, 4 pages, 2005.

[160] M. Poirier, F. Laliberté, L. Pinsard-Gaudart, and A. Revcolevschi, "Magnetoelastic coupling in hexagonal multiferroic $YMnO_3$ using uktrasound measurements," *Physical Review B*, vol. 76, Article ID 174426, 2007.

[161] A. Pimenov, A. A. Mukhin, V. Y. Ivanov, V. D. Travkin, A. M. Balbashov, and A. Loidl, "Possible evidence for electromagnons in multiferroic manganites," *Nature Physics*, vol. 2, no. 2, pp. 97–100, 2006.

[162] D. Senff, P. Link, K. Hradil et al., "Magnetic excitations in multiferroic $TbMnO_3$: evidence for a hybridized soft mode," *Physical Review Letters*, vol. 98, no. 13, Article ID 137206, 2007.

[163] H. Fukumura, S. Matsui, H. Harima et al., "Raman scattering studies on multiferroic $YMnO_3$," *Journal of Physics*, vol. 19, no. 36, Article ID 365239, 2007.

[164] M. Zaghrioui, V. T. Phuoc, R. A. Souza, and M. Gervais, "Polarized reflectivity and lattice dynamics calculation of multiferroic $YMnO_3$," *Physical Review B*, vol. 78, Article ID 184305, 2008.

[165] J. Vermette, S. Jandl, A. A. Mukhin et al., "Raman study of the antiferromagnetic phase transitions in hexagonal $YMnCO_3$ and $LuMnO_3$," *Journal of Physics*, vol. 22, no. 35, Article ID 356002, 2010.

[166] J. Vermette, S. Jandl, and M. M. Gospodinov, "Raman study of spin-phonon coupling in E$RMnO_3$," *Journal of Physics*, vol. 20, no. 42, Article ID 425219, 2008.

[167] M. Fiebig, D. Fröhlich, B. B. Krichevtsov, and R. V. Pisarev, "Second harmonic generation and magnetic-dipole-electric-dipole interference in antiferromagnetic Cr_2O_3," *Physical Review Letters*, vol. 73, no. 15, pp. 2127–2130, 1994.

[168] M. Fiebig, D. Fröhlich, G. Sluyterman, and R. V. Pisarev, "Domain topography of antiferromagnetic Cr_2O_3 by second harmonic generation," *Applied Physics Letters*, vol. 66, no. 21, article 2906, 3 pages, 1995.

[169] M. Fiebig, D. Fröhlich, S. Leute, and R. V. Pisarev, "Second harmonic spectroscopy and control of domain size in antiferromagnetic $YMnO_3$," *Journal of Applied Physics*, vol. 83, no. 11, pp. 6560–6562, 1998.

[170] M. Fiebig, T. Lottermoser, D. Fröhlich, A. V. Goltsev, and R. V. Pisarev, "Observation of coupled magnetic and electric domains," *Nature*, vol. 419, no. 6909, pp. 818–820, 2002.

[171] M. Fiebig, D. Fröhlich, S. Leute, and R. V. Pisarev, "Topography of antiferromagnetic domains using second harmonic generation with an external reference," *Applied Physics B*, vol. 66, no. 3, pp. 265–270, 1998.

[172] S. Leute, T. Lottermoser, and D. Fröhlich, "Nonlinear spatially resolved phase spectroscopy," *Optics Letters*, vol. 24, no. 21, pp. 1520–1522, 1999.

[173] E. Hanamura, K. Hagita, and Y. Tanabe, "Clamping of ferroelectric and antiferromagnetic order parameters of $YMnO_3$," *Journal of Physics*, vol. 15, no. 3, pp. L103–L109, 2003.

[174] A. V. Goltsev, R. V. Pisarev, T. Lottermoser, and M. Fiebig, "Structure and interaction of antiferromagnetic domain walls in hexagonal $YMnO_3$," *Physical Review Letters*, vol. 90, no. 17, Article ID 177204, 4 pages, 2003.

[175] M. Fiebig, A. V. Goltsev, T. Lottermoser, and R. V. Pisarev, "Structure and interaction of domain walls in $YMnO_3$," *Journal of Magnetism and Magnetic Materials*, vol. 272-276, no. I, pp. 353–354, 2004.

[176] H. J. Lewtas, A. T. Boothroyd, M. Rotter et al., "Magnetic excitations in multiferroic $LuMnO_3$ studied by inelastic neutron scattering," *Physical Review B*, vol. 82, no. 18, Article ID 184420, 7 pages, 2010.

[177] K. Uusi-Esko, J. Malm, N. Imamura, H. Yamauchi, and M. Karppinen, "Characterization of $R$$MnO_3$ (R = Sc, Y, Dy-Lu): High-pressure synthesized metastable perovskites and their hexagonal precursor phases," *Materials Chemistry and Physics*, vol. 112, no. 3, pp. 1029–1034, 2008.

[178] H. W. Xu, J. Iwasaki, T. Shimizu, H. Satoh, and N. Kamegashira, "Structure, magnetic susceptibility and heat capacity of $ScMnO_3$," *Journal of Alloys and Compounds*, vol. 221, no. 1-2, pp. 274–279, 1995.

[179] M. Bieringer and J. E. Greedan, "Magnetic structure and spin reorientation transition in $ScMnO_3$," *Journal of Solid State Chemistry*, vol. 143, no. 1, pp. 132–139, 1999.

[180] M. Fiebig, D. Fröhlich, T. Lottermoser, and R. V. Pisarev, "Photoinduced instability of the magnetic structure of hexagonal $ScMnO_3$," *Physical Review B*, vol. 65, no. 22, Article ID 224421, 6 pages, 2002.

[181] E. Galstyan, B. Lorenz, K. S. Nartyrosyan et al., "Magnetic hysteretic phenomena in multiferroic $HoMnO_3$ single crystals and polycrystals with nano- and micrometer particle size," *Journal of Physics*, vol. 20, no. 32, Article ID 325241, 2008.

[182] B. B. Van Aken and T. T. M. Palstra, "Influence of magnetic on ferroelectric ordering in $LuMnO_3$," *Physical Review B*, vol. 69, no. 13, Article ID 134113, 2004.

[183] M. Bieringer, J. E. Greedan, and A. S. Wills, "Investigation of magnetic structure evolution in the substitutional solid solution $ScxLu_{1-x}MnO_3$," *Applied Physics A*, vol. 74, pp. S601–S603, 2002.

[184] M. Fiebig, D. Fröhlich, T. Lottermoser, and K. Kohn, "Spin-angle topography of hexagonal manganites by magnetic second-harmonic generation," *Applied Physics Letters*, vol. 77, no. 26, p. 4401, 2000.

[185] M. C. Sekhar, S. Lee, G. Choi, C. Lee, and J. G. Park, "Doping effects of hexagonal manganites $Er_{1-x}Y_xMnO_3$ with triangular spin structure," *Physical Review B*, vol. 72, no. 1, Article ID 014402, 6 pages, 2005.

[186] D. Meier, H. Ryll, K. Kiefer et al., "Mutual induction of magnetic 3d and 4f order in multiferroic hexagonal E$RMnO_3$," *Physical Review B*, vol. 86, no. 18, Article ID 184415, 8 pages.

[187] J. Park, U. Kong, S. I. Choi, J. G. Park, C. Lee, and W. Jo, "Magnetic structure studies of E$RMnO_3$," *Applied Physics A*, vol. 74, no. I, pp. S802–S804, 2002.

[188] E. C. Standard, T. Stanislavchuk, A. A. Sirenko, N. Lee, and S. W. Cheong, "Magnons and crystal-field transitions in hexagonal $R$$MnO_3$ (R = Er, Tm, Yb, Lu) single crystals ," *Physical Review B*, vol. 85, no. 14, Article ID 144422, 11 pages, 2012.

[189] H. A. Salama and G. A. Stewart, "Exchange-induced Tm magnetism in multiferroic h-$TmMnO_3$," *Journal of Physics*, vol. 21, no. 38, Article ID 386001, 2009.

[190] J.-S. Zhou, J. B. Goodenough, J. M. Gallardo-Amores, E. Morán, M. A. Alario-Franco, and R. Caudillo, "Hexagonal versus perovskite phase of manganite $R$$MnO_3$ (R=Y, Ho, Er, Tm, Yb, Lu)," *Physical Review B*, vol. 74, no. 1, Article ID 014422, 7 pages, 2006.

[191] U. Adem, M. Mostovoy, N. Bellido, A. A. Nugroho, C. Simon, and T. T. M. Palstra, "Scaling behavior of the magnetocapacitance of $YbMnO_3$," *Journal of Physics*, vol. 21, no. 49, Article ID 496002, 2009.

[192] H. A. Salama, G. A. Stewart, D. H. Ryan, M. Elouneg-Jamroz, and A. V. J. Edge, "A Mössbauer spectroscopy investigation of *h*-$YbMnO_3$," *Journal of Physics*, vol. 20, no. 25, Article ID 255213, 2008.

[193] H. A. Salama, C. J. Voyer, D. H. Ryan, and G. A. Stewart, "Magnetic order of the rare earth sublattice in *h*-$YbMnO_3$," *Journal of Applied Physics*, vol. 105, no. 7, Article ID 07E110, 3 pages, 2009.

[194] V. Y. Ivanov, A. A. Mukhin, A. S. Prokhorov, A. M. Balbashov, and L. D. Iskhakova, "Magnetic properties and phase transitions in hexagonal $DYMnO_3$ single crystals," *Physics of the Solid State*, vol. 48, no. 9, pp. 1726–1729, 2006.

[195] S. Harikrishnan, S. Rößler, C. M. N. Kumar et al., "Phase transitions and rare-earth magnetism in hexagonal and orthorhombic $DyMnO_3$ single crystals," *Journal of Physics*, vol. 21, no. 9, Article ID 096002, 2009.

[196] C. Wehrenfennig, D. Meier, T. Lottermoser et al., "Incompatible magnetic order in multiferroic hexagonal $DYMnO_3$," *Physical Review B*, vol. 82, no. 10, Article ID 100414, 2010.

[197] D. M. Giaquinta and H. C. zur Loye, "Indium manganese trioxide: a new transition metal oxide with an unusual ABO_3 structure," *Journal of the American Chemical Society*, vol. 114, no. 27, pp. 10952–10953, 1992.

[198] G. V. Vajenine, R. Hoffmann, and H. C. Zur Loye, "The electronic structures and magnetic properties of one-dimensional ABO_6 chains in Sr_3ABO_6 (A = Co, Ni; B = Pt, Ir) and two-dimensional MO_3 sheets in $InMO_3$ (M = Fe, Mn)," *Chemical Physics*, vol. 204, no. 2-3, pp. 469–478, 1996.

[199] C. R. Serrao, S. B. Krupanidhi, J. Bhattacharjee, U. V. Waghmare, A. K. Kundu, and C. N. R. Rao, "$InMnO_3$: a biferroic," *Journal of Applied Physics*, vol. 100, no. 7, Article ID 076104, 2006.

[200] A. A. Belik, S. Kamba, M. Savinov et al., "Magnetic and dielectric properties of hexagonal $InMnO_3$," *Physical Review B*, vol. 79, no. 5, Article ID 054411, 2009.

[201] D. A. Rusakov, A. A. Belik, S. Kamba et al., "Structural evolution and properties of solid solutions of hexagonal InMnO3 and InGaO3," *Inorganic Chemistry*, vol. 50, no. 8, pp. 3559–3566, 2011.

[202] S. C. Abrahams, "Ferroelectricity and structure in the $YMnO_3$ family," *Acta Crystallographica*, vol. 57, pp. 485–490, 2001.

[203] M. A. Oak, J. H. Lee, H. M. Jang, J. S. Goh, H. J. Choi, and J. F. Scott, "*4d-5p* Orbital mixing and asymmetric in *4d–O 2p* hybridization in $InMnO_3$: a new bonding mechanism for hexagonal ferroelectricity," *Physical Review Letters*, vol. 106, no. 4, Article ID 047601, 4 pages, 2011.

[204] X. Fabréges, I. Mirebeau, S. Petit, P. Bonville, and A. A. Belik, "Frustration-driven magnetic order in hexagonal $InMnO_3$," *Physical Review B*, vol. 84, Article ID 054455, 2011.

[205] Y. Kumagai, A. Belik, M. Lilienblum, N. Leo, M. Fiebig, and N. A. Spaldin, "Observation of persistent centrosymmetricity in the hexagonal manganite family," *Physical Review B*, vol. 85, no. 17, Article ID 174422, 7 pages, 2012.

[206] I. Munawar and S. H. Curnoe, "Theory of magnetic phases of hexagonal rare earth manganites," *Journal of Physics*, vol. 18, no. 42, article no. 004, pp. 9575–9583, 2006.